UNIVERSITY OF TROMSØ UIT

FACULTY OF SCIENCE AND TECHNOLOGY
DEPARTMENT OF GEOLOGY

Geological setting and origin of a gold-mineralized zone at Myrefjellet, Mauken, Troms.

Arne Mikalsen Alnes

GEO-3900 Master's Thesis in Geology

May 2013

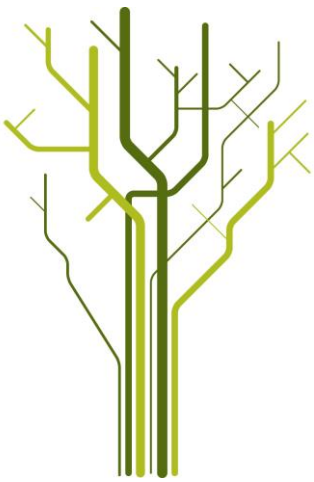

Abstract

In 2008 Scandinavian Highlands discovered a gold mineralization within the Mauken basement window. The Mauken basement window is a thought to be an eastward continuation of the West Troms Basement Complex which is a series of rocks with an age span from Neoarchaean to Paleoproterozic. The mineralization found in a steeply dipping NW-SE striking shear zone and is hosted in a meta-sedimentary unit.

The rock which hosts the mineralization is metamorphosed under greenschist facies conditions. The protolith for the mineralization has not been determined and could be of magmatic or of sedimentary origin, which the rocks surrounding the mineralization are. Surrounding the mineralization is a halo of sericitization, but the rock is also influenced by chloritization and local carbonatization. The mineral assemblage of the mineralization is dominated by quartz, micas, and carbonates. The gold mineralization is closely linked to the formation of arsenopyrite, since most of the gold is found as inclusions in arsenopyrite grains.

The deposit is likely to have been formed in relation to the Svecofennian orogeny and could be classified as an orogenic gold deposit.

Acknowledgement

I wish to thank my supervisor Kåre Kullerud at University of Tromsø and Mikkel Vognsen at Scandinavian Highlands for help and guidance with my master thesis. Thanks to Scandinavian Highlands for giving me access to their geological data and drill cores and the museum of natural science in Oslo for giving me access the SEM.

I also would like to thank NGU for supporting this work and especially Jan Sverre Sandstad and Terje Bjerkegård for tips and feedback.

Tanks to all my fellow students at “brakka” for good advices and encouragement through the whole master process, it would have been boring without you.

And Ingebjørg for always being there and reading through the text. Looking forward to our future together!

Tromsø, May 2013

Arne Alnes

TABLE OF CONTENT

1. Introduction

Purpose of study

In 2008 Scandinavian Highlands discovered a gold mineralization in Mauken, Northern Norway. The discovery was made after several seasons of reconnaissance and prospecting in the area. The mineralization is situated in a regional steeply dipping NW-SE trending shear zone, forming a 4-8 meter wide mineralized zone, which can be traced on for more than 1800 meters.

The shear zone was drilled by surface diamond drilling in the fall 2010 and the core material from this campaign is the basis for the thesis. The aim of this thesis will be to describe the mineralization based on visual core logging, XRF data, thin section studies and Scanning Electron Microscope analysis.

This will be done in order to understand and interpret the formation of the mineralization. Which is the dominant alteration type? And what is the origin of the formation?

Localization of the study area

The Mauken Mountain is located in the municipality of Målselv and is situated 70 km south of Tromsø (Figure 1.1). The actual mineralized zone is located 500-600 meters absl. and has several good outcropping showings. The zone of mineralization is located in a metasedimentary unit within a steeply dipping NW-SE trending shear zone, and can be traced for 1800 meter along strike (unpublished data from Scandinavian Highlands).

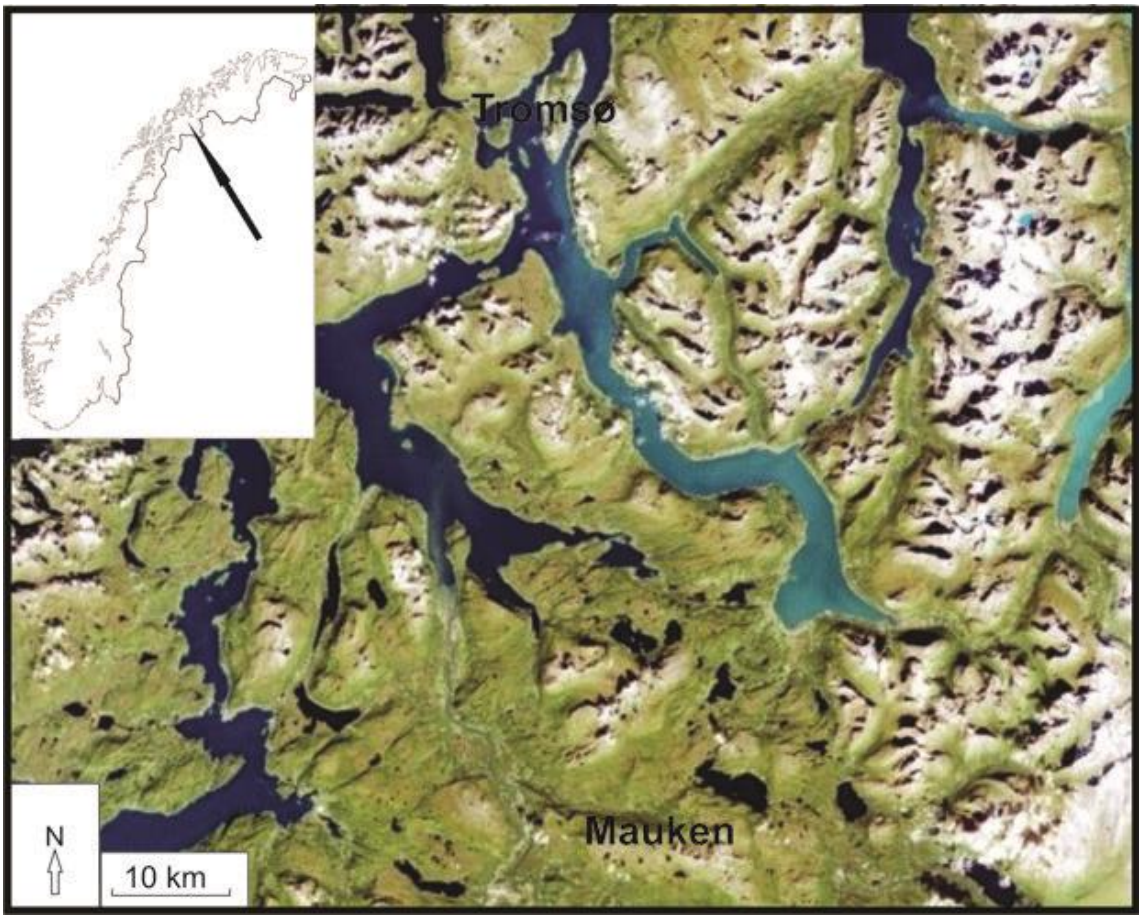

Figure 1.1: Map showing the location of Mauken. Taken from (www.norgeibilder.no, 2012)

Regional geology

The studied rocks occur within the Mauken Window, which is a basement window occurring within the North-Norwegian Caledonides. The Precambrian rock of the basement window is inferred to be a westward continuation of the Baltic shield, which covers most of Sweden, Finland and the northwestern parts of Russia (Bergh et al., 2010).

The evolution of the shield spans over hundreds of million years and has several important orogenic periods. These periods can be summed up as: the Saamian orogeny (3.1-2.9 Ga), the Lopian orogeny (2.9-2.6 Ga), the Svecofennian domain (2.0-1.75 Ga), the Gothian orogeny (1.75-1.5 Ga), the Hallandian `orogeny` (1.5-1.4 Ga), and the Sveconorwegian orogeny (1.25-0.9 Ga) (Gaál and Gorbatschev, 1987). The period between 2.6 Ga and 2.0 Ga was characterized by events of sedimentation and magmatism, due to rifting of the Archaean craton (Weihed et al., 2005). Within the shield there is an observed geochronological zonation with the youngest rocks in the southwest and the oldest one in northeast (Gaál and Gorbatschev, 1987). This zonation divides the shield into three domains: the Archaean Domain, the Svecofennian Domain and the Southwest Scandinavian Domain (Gaál and Gorbatschev, 1987). Mauken is a part of the Svecofennian Domain.

The remnants of the Baltic shield found in Northern Norway are dominantly found in eastern Finnmark and in tectonic windows, such as the Mauken basement window. In the Troms region, the Baltic shield is exposed on in the West Troms Basement Complex (WTBC), and it is likely that Mauken forms an eastern extension of these basement rocks. The WTBC stretches from Senja in the south to Vanna in the north. The age of these rocks spans from Neoarchaean to Paleoproterozic (Bergh et. al 2010). The WTBC contains several belts of metasupracrustal rocks including the Archaean Ringvassøya greenstone belt. The age of this belt has been determined to be 2.85-2.83Ga (Motuza, 2001, Kullerud, 2006). The Ringvassøya belts age is significantly higher than its “neighbors” in northern Norway. The Karasjok Greenstone Belt has been dated to a Sm-Nd age of 2085 +/- 85 Ma (Krill, 1985) and the Kautokeino belt is assumed to have a similar age (Krill, 1985).

The rocks in-between Mauken and the Precambrian islands of western Troms belong to the Caledonides, which is a series of nappes from the collision between Laurentia and Baltica in Late Silurian to Early Devonian time (Roberts, 2003).

The age of the Mauken basement window has not been determined, but a minimum age can be established. The rocks of the basement window have been intruded by granitoids which has an age of 1706 +/- 15 and 1768 +/- 49 Ma (Norges geologiske undersøkelse, 2012)

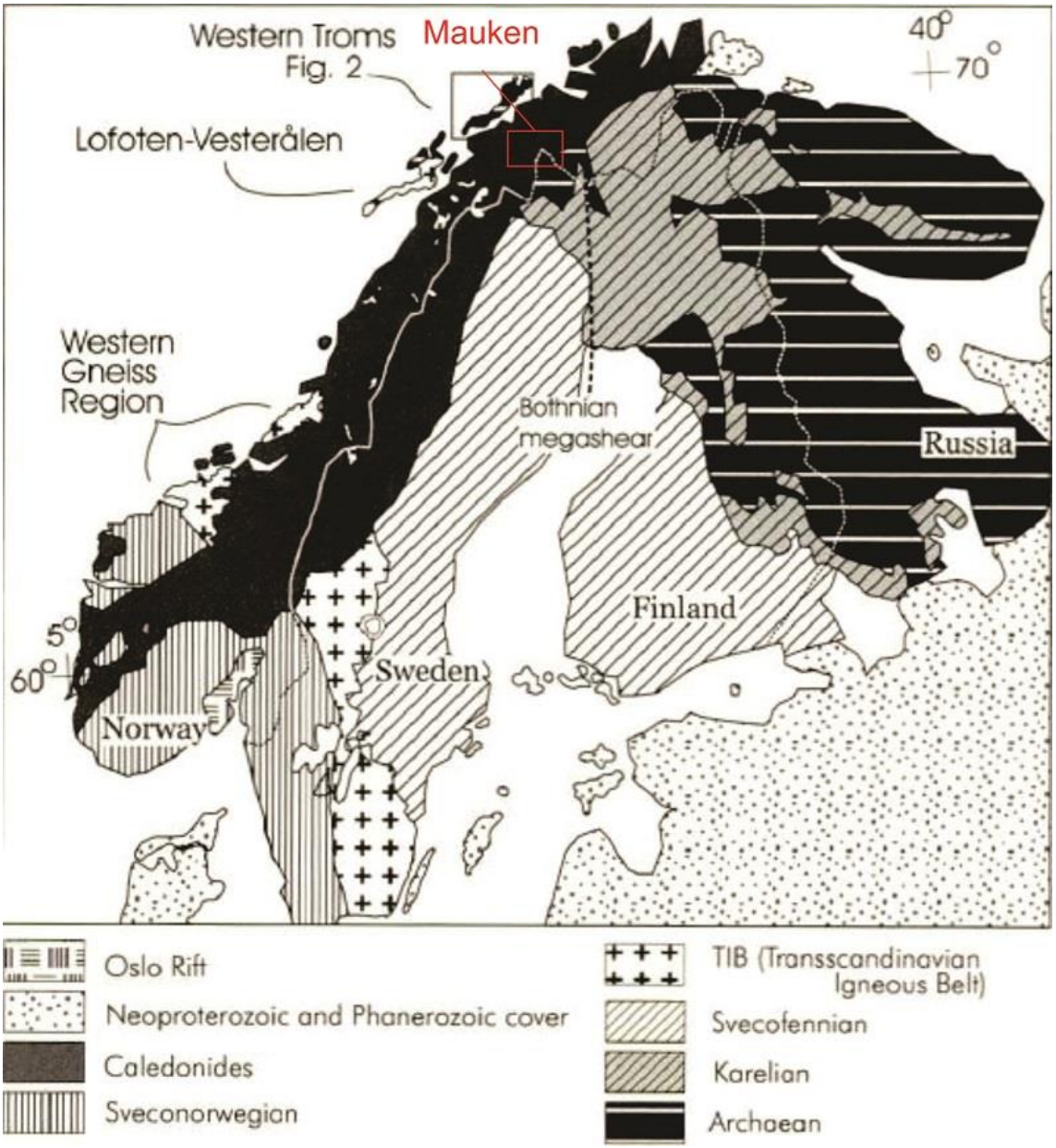

Figure 1.2: Map of the most important components in the Baltic shield. Modified after (Corfu et al., 2003)

Previous work

The Mauken basement window is an area which has not been described recently, prior to Scandinavian Highlands' activities in the area. The latest and most comprehensive work was done by Landmark (1967) and followed by Berthelsen (1967) who published his work around two geophysical anomalies in the area the same year.

The publication of Landmark (1967) was a description of the geological map "Målselv" (1959).Here Landmark describes Mauken as a "basement *window of Precambrian rocks exposed beneath the Caledonian nappes in Målselv*". He reported that there were two main units of Precambrian rocks. These two units Landmark referred to as the Mauken amphibolite and the Andsfjellet granodiorite.

The Mauken amphibolite is described by Landmark as a uniform steeply dipping layer striking NW-SE. The thickness of the layer varying between 1200 m and 3000 m and the principal minerals are hornblende, micas and zoisite.

The Andsfjellet granodiorite is described as a unit with several different textures, but it has more or less the same mineral assemblages which consist of quartz, acid plagioclase and microcline. The texture which is most extensive is a medium grained massive rock with a weakly developed foliation.

Berthelsen (1967) described the two geophysical anomalies, the Mauken window and the Divielva window. Berthelsen (1967) describes 4 major units of basement rocks in Mauken: Myrefjell formation (*metavulcanics with intermixed and intercalated metasediments*), Aurevatn formation (*feldspatic and micaceous quartzites, subordinate calcareous rocks, sericite, and chlorite schists*), Øverbygd crystalline complex (*intrusive granodiorite, gneiss, and migmatite, metabasaltic rocks, and gabbro*), and the Kampen granodiorite (*massive to foliated granodiorite with a few relics of gneiss*).

The Myrefjell formation of Berthelsen is the same unit as the Mauken amphibolite of Landmark.

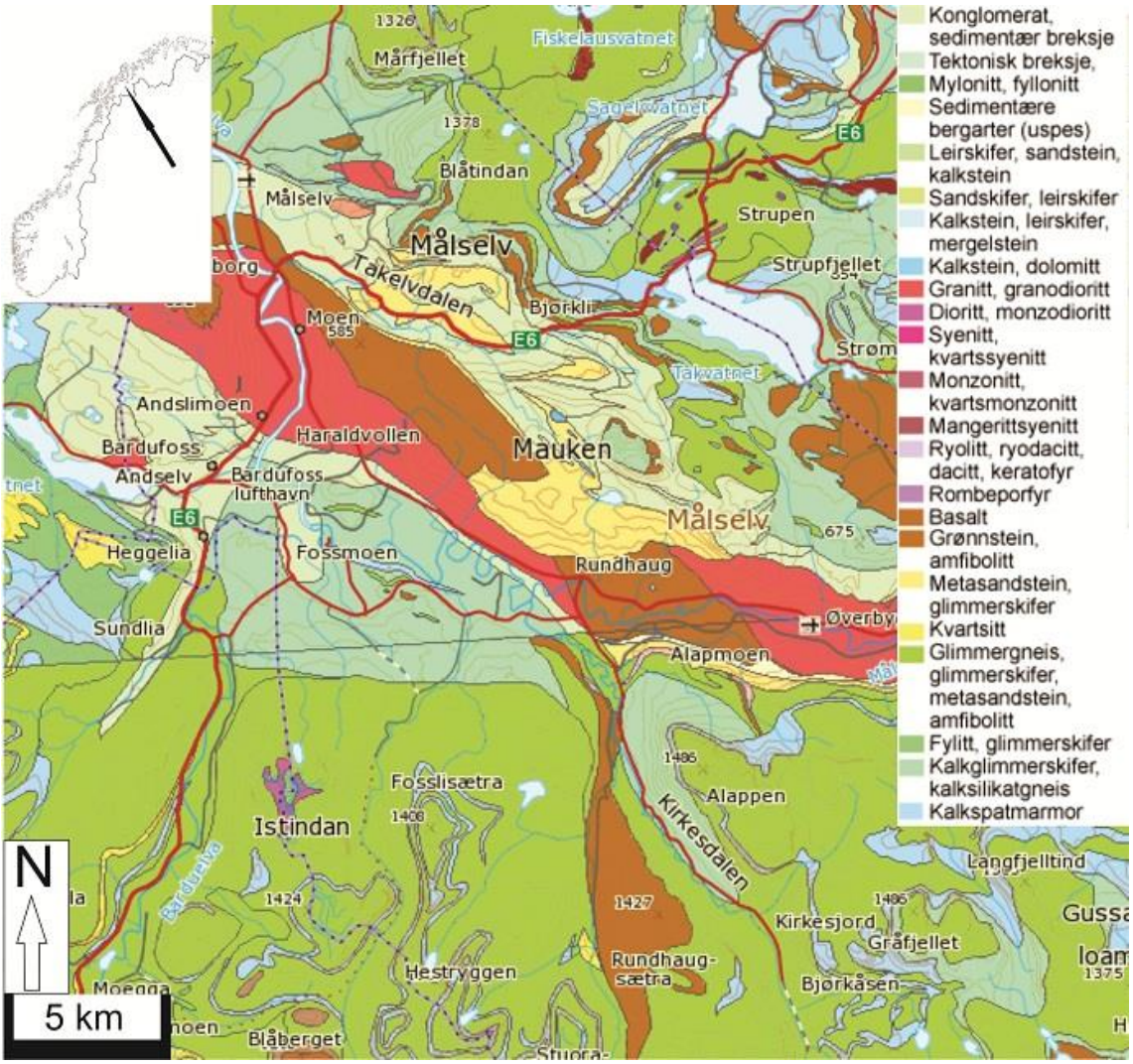

Figure 1.3: Geological map of the Mauken window and surrounding rocks. The rocks of the Mauken window are the ones in the center of the map (shown in red, brown, and yellow colors). The map is based on Tromsø 1:250000 (Zwaan et al., 1998) and Narvik 1:250000 (Gustavson, 1974), taken from (ngu.no).

According to the geological map of NGU (figure 1.3) the Mauken basement window is characterized by granites/granodiorite, basalts, greenstone/amphibolite, and meta-sedimentary rocks. The mineralization is located to a meta-sandstone on the boundary of a basaltic unit.

In figure 1.4 is a more detailed map from Mauken which shows the location of the mineralization and its host rocks. The map shows that the mineralization is placed in an area which holds several different units. The area is dominated by rusty schist and a greenschist with carbonate breccia.

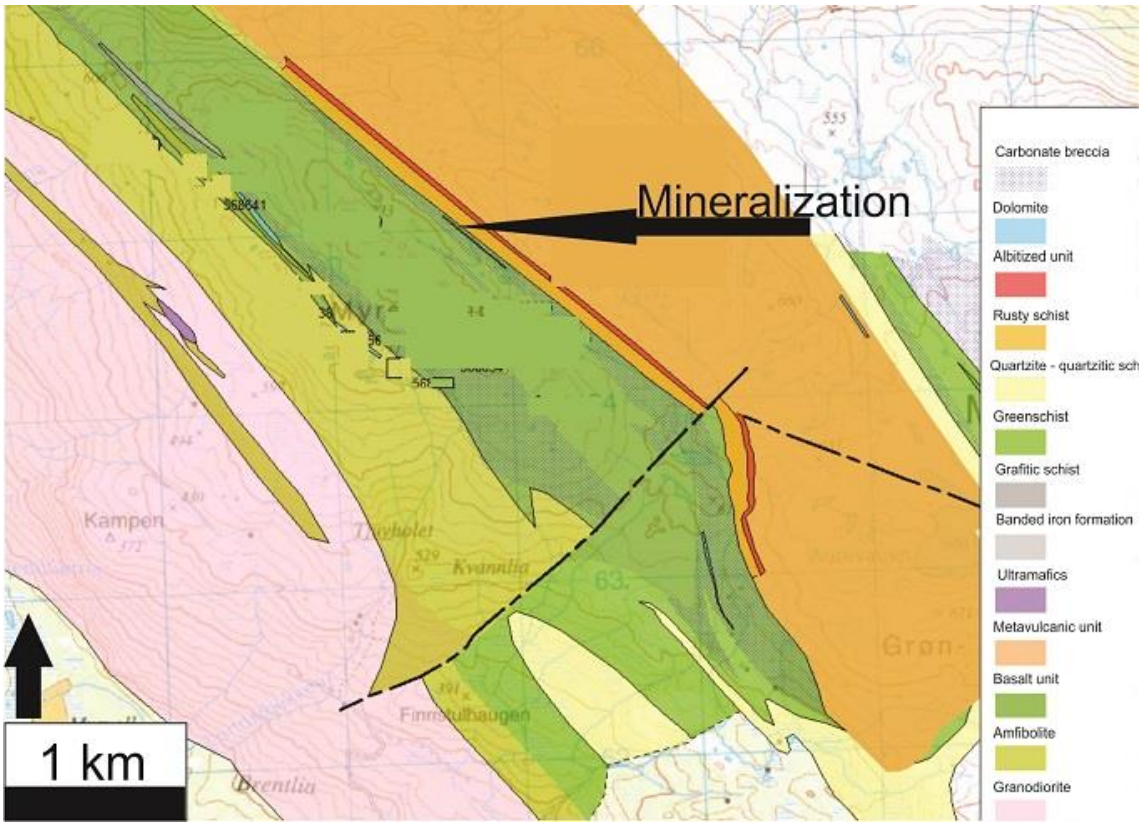

Figure 1.4: Geological map of from Mauken (Myrefjell) and surrounding rocks (Vognsen, written communication, 2012).

Geophysical surveys

During the summer of 2011 NGU carried out an airborne survey of the Mauken area. This was a part of the MINN program which aims to get a better overview of the mineral recourses in Northern Norway. The program is carried out by NGU and is given a 100 million NOK budget over a period of 4 years. The results from the Mauken survey were published in a NGU report from 2012 (Rodionov et. al 2012) . Some of the results from the report are shown in figure 1.5. The mineralization is located in an area with high a magnetic signal. The exact location is on the Northeastern boundary of this unit with high magnetic properties. The area also has high resistivity, but it is a bit lower than its surroundings.

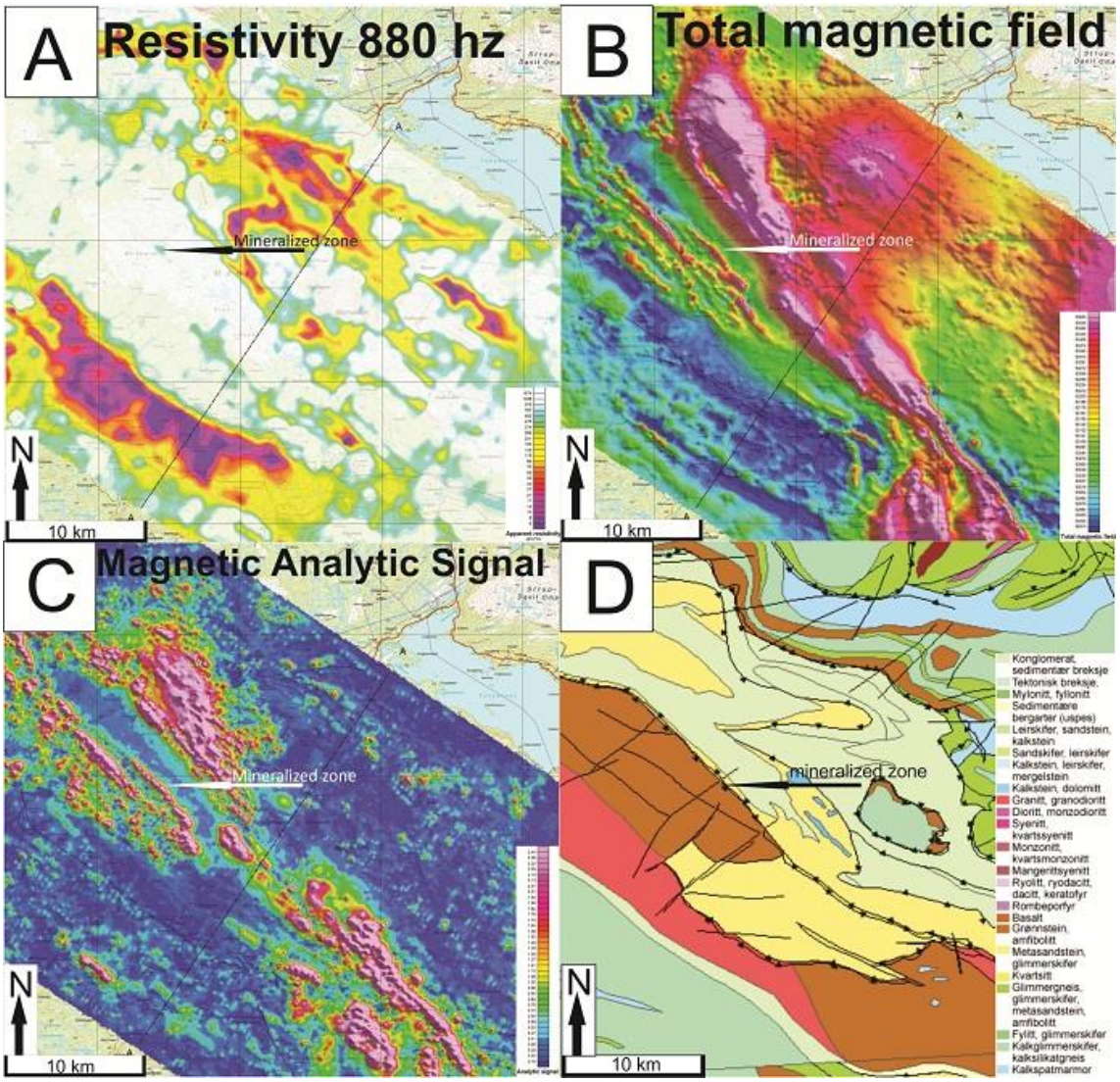

Figure 1.5: A, B, and C show some results from the geophysical survey done by NGU the summer of 2011 (Rodionov et. al 2012). Figure D shows a geological map (ngu.no) of the same area.

Gold in the Fennoscandian shield

The Mauken Au mineralization is one out of several Au mineralizations known in the Fennoscandian shield. Most of the ores deposits in the shield were formed during a specific time period. “With few exceptions, all major ore deposits formed in specific tectonic settings between 2.06 and 1.78 Ga and thus a strong geodynamic control on ore deposit formation is suggested” (Weihed et al., 2005).

The Suurikuusikko deposit in Northern Finland is Europe's biggest gold mine with reserves close to one million ounces (Airo and Mertanen, 2008). This deposit is situated within the Central Lapland greenstone belt (CLGB) which has a Palaeoproterozoic age and the Au mineralization is closely associated with arsenopyrite and pyrite (Kojonen and Johanson, 1999). The Central Lapland greenstone belt is known to host numerous Au-mineralizations, although not in same size as Suurikuusikko. The belt stretches from Lapland (Finland) and into Northern Norway. The Norwegian continuation of CLGB is represented by the Karasjok greenstone belt and the Kautokeino greenstone belt (Gaál and Gorbatschev, 1987). The Kautokeino greenstone belt hosts several Au mineralizations within shear zones (Ettner et al., 1993). The best known would be the Bidjovagge Au and Cu mineralization which has high Au values associated to late quartz-carbonate veins holding tellurides (Bjørlykke et al., 1987).

In the West Troms Basement complex (which Mauken is a thought continuation of) several greenstone belts are situated. The Ringvassøya greenstone belt is one of them and hosts several Au mineralizations (Sandstad and Nilsson 1997) , but the age of this belt is significantly higher than the greenstone belts of central Lapland. In addition none of the discoveries made in the WTBC has been put into production.

Other well know gold mineralization in the Baltic Shield is the Aitik Cu-Au-As mineralization, (which is ore related to an intrusion related deposit dated to around 1890 Ma) (Wanhainen et.al 2006) and the Björkdal deposit. The Björkdal deposit is situated in the Skellefte district in Sweden and the mineralization is hosted by a quartz-monzodioritic intrusion (Billström et al., 2009). The Björkdal deposit is the biggest Au mineralization in the district with a tonnage of 20 Mt with 2.5 g/t Au (Weihed et al., 2003).

2. Methods

Core logging

In February 2011, core number 1 from the Au mineralization was logged in the Scandinavian Highlands premises close to Copenhagen. The first 80 meters of the core was logged and mapped for different lithologies, veins, fractures, and mineralized zones. The most interesting parts from the core were sampled, and brought back to Tromsø for preparation of thin sections and XRF-analysis.

X-ray fluorescence (XRF)

For major and trace element analysis, a Bruker S8 Tiger XRF at the Department of Geology, UiT, was used. To get the samples ready for analysis there were several steps. First the samples were cut and then crushed in a "Retsch ® type BB2/A jaw crusher". Then the samples were crushed into fine powder in a swing mill. For analysis of the major elements, the rock powder was mixed together with Li-tetraborate ($Li_2B_4O_7$) in the ratio of 1:7 (0,6000 g of rock powder and 4,2000 g of Li-tetraborate). After the weighing procedure, the samples were molten in platinum crucibles at temperatures around 1200^{o}C. Then the samples were cooled down in platinum molds. Two parallels of the major elements were made, in order to control that the samples had been prepared properly.
The procedure for preparing the samples for trace element analysis started with weighing up 9,0 g of rock powder and mixing it with 9 wax pills in a mortar. The wax pills were of the type POLYSIUS PORLAB® Mahlhilfe. After the mixing, the final step was to place the sample material in a cylindrical shaped container and pressed with a piston into pills. When the pills were removed from the piston they were ready for the XRF-machine.

In addition to the XRF analyses a data set of ICP analysis was made available for this study.

Microscopy

26 thin sections where prepared, all thin sections with corresponding XRF-analysis. The thin sections were cut and polished at the University of Tromsø. The thin sections were studied using a “Leitz Laoborlux 11 Pl S” polarization microscope. The silicates were studied by using both cross polarized (XPL) and plane polarized light (PPL). The opaque phases were studied by using reflected light.

SEM

To identify the opaque minerals a Scanning Electron Microscope (SEM) was used. This was done at the Museum of Natural History in Oslo. The microscope was a Hitachi S 3600N Scanning Electron Microscope. The detector was a Bruker 127 ev xflash detector 5030. During the SEM analysis a program to detect chemical variations in a selected area of the thin section was used. This was done to detect chemical zonations within a mineral grain.

Abbreviations

The following abbreviations have been used in the thesis. The mineral abbreviations are from Kretz (1983).

Minerals

Apy - arsenopyrite

Bt - biotite

Cal - calcite

Chl- chlorite

Grt - garnet

Ms - muscovite

Py - pyrite

Qts - quartz

Rt - rutile

Ttn - titanite

Tur – tourmaline

Zo - zoisite

Others

PPL - plane polarized light

XPL - cross polarized light

3. Petrography and mineralogy of the studied rock

Description of the outcrop

In figure 3.1, pictures from the outcrop and a rock with a fresh surface from the mineralization are shown. The outcrop from the mineralized zone is heavily weathered and shows a rusty color. On the right side of the picture from the outcrop, veins going horizontally and showing a higher relief are seen. These veins consist of quartz which weathers less than the host rock. In the picture from the fresh surface, the weathered (rusty) zone which surrounds the whole rock, is clearly seen . The rock is very fine grained so identification of different minerals is difficult. The minerals identified at the outcrop were quarts and sulfides. Arsenopyrites can be seen as needle shaped silvery crystals on the fresh surface. The crystals are oriented vertically on the picture.

The other elements which the rock consist of will be described in the chapter “thin section description”.

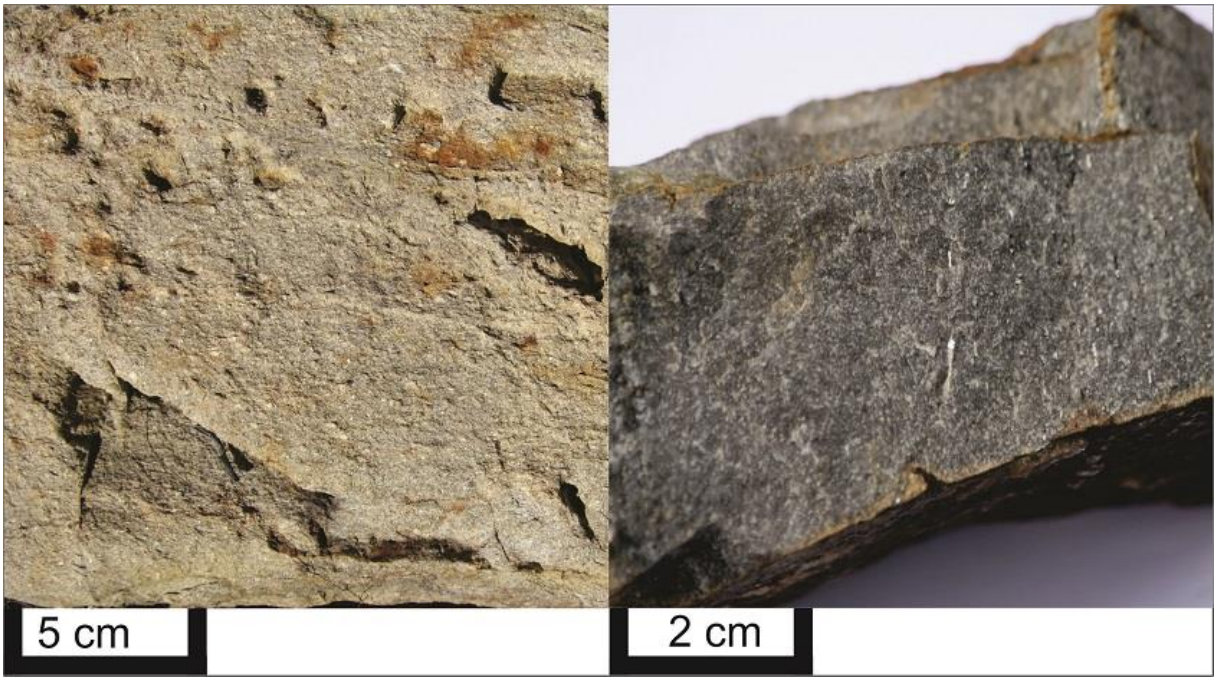

Figure 3.1: Pictures from the outcrop of the mineralization. The image to the left shows the weathered outcrop, while the image to the right shows a fresh surface from the rock.

Description of the drill core (core number 1)

This description is based on the core mapping done in Denmark at the Scandinavian Highlands premises in February 2012.

From the surface and down the first 25m is dominated by a laminated sedimentary rock. The different laminae are mm to cm thick and consist of quartz and micas. The core more or less consists of a very fine grained rock, and therefore a more thoroughly description of the mineralogy is given in the thin section description. The rock is affected by local brittle deformation; this deformation is characterized by veining and fractures filled by quartz and/or carbonates (see figure 3.9 and 3.10). In addition, at 18.8 meters depth, several big red garnets (1-6 mm) can be observed, the big garnets are only observed at this depth (see figure 3.2).

Figure 3.2: Core piece from 18.70 m to 18.80 m. The rock is dominated by fine grained quartz and micas with laminated texture. Pale red garnets are circled in red. Note the striation from the core saw going from the bottom left corner towards the upper right corner.

The next meter shows a gradual transition to a finer laminated rock. This rock interval consists of finer laminae with a thickness of a few mm. The laminae consist of a light layer of quartz and a dark layer of sulfide rich material (see Figure 3.3).

Figure 3.3: Core piece from 28.15 m to 28.80 m. the rock is dominated by fine grained quarts and micas and shows a laminated texture. The yellow/golden stripes are fine grained pyrite.

This unit (25 m-28.9m) ends at 28.9 m where a sharp contact appears. This contact is clearly seen as a quartz vein cutting through all structures in the drill core (Figure 3.4). This contact/quartz-vein distinguishes itself from other veins by being thicker and is clearly seen in the whole width of the core.

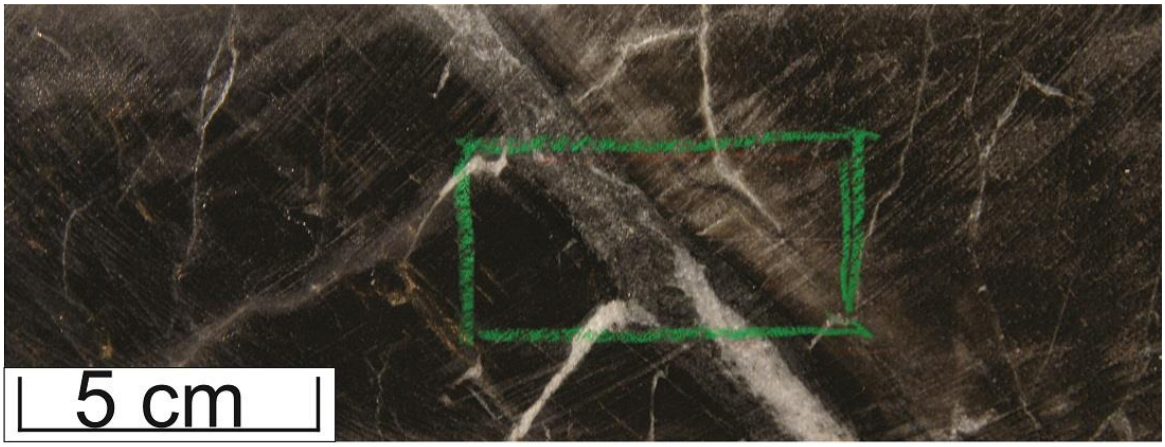

Figure 3.4: Core piece from 28.80 m to 28.95 m. The green square in the middle of the figure is the outline for the thin section. The big vein in the figure is filled by quartz and might be a contact zone between to lithologies.

At 28.9 m the Au mineralized zone starts; this is a 6.3 m wide zone with a varied rock. In general the rock is steel gray, fine grained and contains a lot of euhedral arsenopyrite (Figure 3.5) showing preferred orientation growth. The Au mineralized zone contains a lot of veins of both quartz and carbonates. The carbonates appear to be youngest since they cut through all structures and even the quartz veins.

Figure 3.5: Core piece from 29.50 m to 29.65 m. The figure is from the part of the core which has the highest content of Au and As. This is clearly seen as numerous arsenopyrites (silver to whitish needles). The green square in the middle of the figure is the outline for the thin section.

Within the Au mineralized zone there are some areas which are heavily influenced by carbonitization. Especially at 32.4 meters and 34.05 meters depth the rock is heavily influenced (Figure 3.6). The protolith of the mineralized zone could either be a sedimentary rock or an ingenious intrusion. This will be discussed further in a chapter to come.

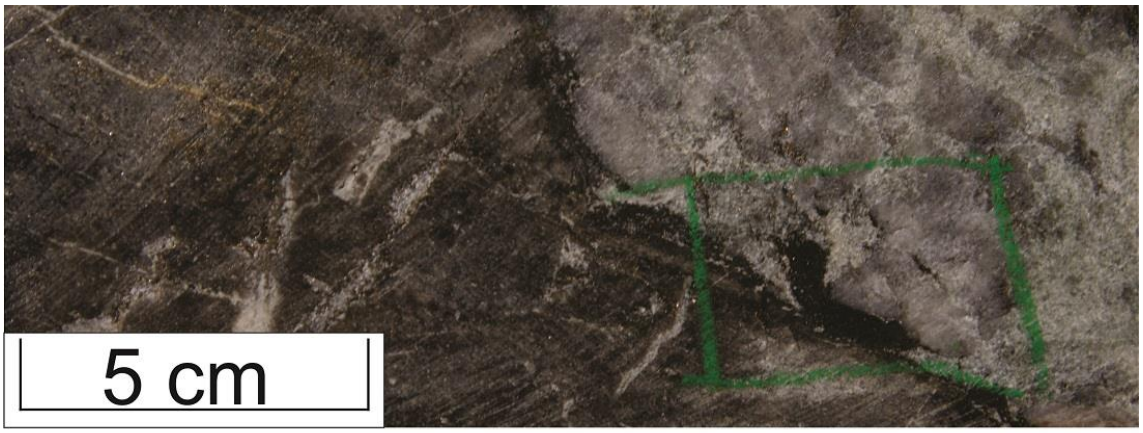

Figure 3.6: Core piece from 34.05 m to 34.20 m. This section of the core is heavily altered by carbonitization and can be seen as a total replacement of the original mineral assemblage by carbonates (white mineral). The green square in the middle of the figure is the outline for the thin section.

The interval from 35.2 to 40.4 m is similar to the interval straight below the mineralization and consists of mm to cm thick laminae. At 40.4 m there is a relative sharp contact similar to the one above the mineralization. This contact is also emphasized by a quartz vein (Figure 3.7).

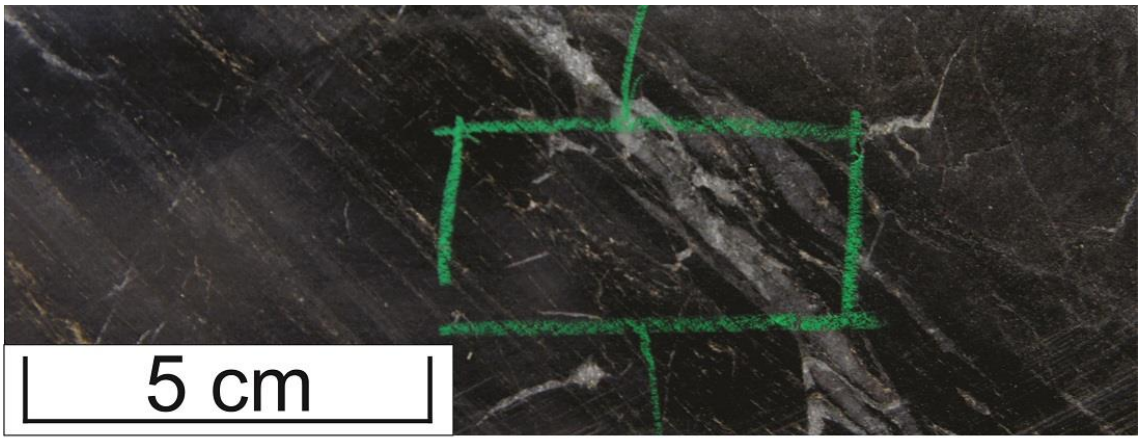

Figure 3.7: Core piece from 40.40 m to 40.55 m. The figure shows a quartz vein which cuts through the whole width of the core and might be a contact between two lithologies. The green square in the middle of the figure is the outline for the thin section.

The rest of the drill core (down to 80 meters) is a grey fine-grained rock. It alternates between being foliated and banded and contains porphyroblasts of quartz.

Thin section description

The petrology and mineralogy of all the samples from the mineralized zone and unmineralized zone are mostly the same. The samples contain micas and quarts as the principle minerals. Most of the samples also contain carbonates and these are present in veins. There are also veins present which hold quarts. Other important minerals that are present are chlorite, garnet, tourmaline, rutile, titanite, pyrite, and arsenopyrite. In table 3.1, you can see a list of all the thin sections and their content of the six most common minerals.

In general the rock is fine grained and shows a steep to sub vertical foliation in most of the samples. This foliation has the same orientation throughout the drill core. In addition there seems to be several phases of mineral crystallization, this is due to the appearance of different grain size and veining.

	quartz	biotite	muscovite	calsite	opaque	chlorite
568968	55	35	10	10	2	3
568969	20	40	5	2	30	0
568970	45	25	2	20	3	3
568971	30	20	1	10	5	0
568972	45	25	2	10	5	3
568973	50	30	1	10	2	3
568974	55	25	5	0	3	0
568975	30	45	3	5	8	3
568976	30	30	20	5	8	1
568977	30	25	25	0	5	0
568978	35	20	20	0	10	0
568979	50	20	25	0	8	0
568980	50	15	10	20	2	2
568981	40	20	4	30	8	0
568982	45	30	15	0	7	0
568983	50	30	10	3	4	0
568984	60	20	10	3	4	0
568985	50	25	6	15	3	5
568986	60	20	15	4	9	0
568987	50	25	20	10	4	5
568988	50	20	20	5	8	2
568989	30	10	25	25	15	6
568990	65	20	2	3	1	6
568991	50	25	10	0	2	0
568992	60	20	2	10	0	10
568993	55	25	1	10	3	10

Table 3.1: The table shows the approximate percentage of mineral content in thin sections

Description of minerals

Quartz is colorless in PPL and has no cleavage, low relief, and birefringence. It appears in two different ways. The most prominent one is where it occurs in the matrix with micas (Figure 3.8). In the matrix the quarts grains are (<0.25 mm) and anhedral. The second appearance is in veins (Figure 3.9) and aggregates (Figure 3.12). The size here is significantly larger (0.25-2 mm). The grains both show undulating and straight extinction. Quartz is the most abundant mineral in the thin sections.

White mica is colorless in PPL and has a low relief. It has high birefringence and show straight extinction. The grains are anhedral and size varies a lot, from (<0.1 mm) (Figure 3.8) in the matrix to some bigger grains (0.25-1 mm).

Biotite is brown in PPL and has a low relief. It appears in a wide range of sizes and has high birefringence third to fourth order. It has anhedral to subhedral grains.

Calcite is the dominating carbonate in the samples. It appears only in veins (Figure 3.9) and aggregates (Figure 3.14), and therefore is thought to have a secondary origin. In PPL calcite is colorless and shows a high relief. It has extreme high birefringence and shows pastel colors in XPL. The crystals are anhedral in general and some of them show twining, both one and two sets.

Chlorite is colorless to light green in PPL and has a low relief. It shows pleochroism and has interference colors from blue to black (Figure 3.10). Most of the chlorite is focused as a rim around the calcite-veins.

Garnet is colorless in PPL and shows a high relief. It is isotropic and sub to anhedral. The grains are < 1 mm except one sample which has several large grains (1-6 mm in sample 90). In this sample all the grains are heavily altered (Figure 3.13).

Tourmaline is green in PPL and show strong pleochroism (Figure 3.15). The grains are 0.1-0.25 mm and subhedral. When tourmaline occurs in a thin section it appears in clusters of several grains.

Rutile shows a deep red color in PPL and an extreme high relief. It often appears as inclusions in titanite (Figure 3.10) or rims on sulfides. It has an anhedral shape and size is 0.1-0.25mm.

Titanite is colorless to grey in PPL and has a high relief. It often appears as a rim around rutile, this rim is seen as a mushy grey mineral presumed to be titanite (Figure 3.10).

Pyrite is opaque and is the dominant sulfide in the samples. It is anhedral and appears as small individual grains (Figure 3.11) and big veins and or aggregates (Figure 3.15). In reflected light pyrite is yellow dull colored.

Arsenopyrite is opaque and has euhedral rhombus grains and is the second most common sulfide in the samples. In reflected light arsenopyrite is whitish and shiny (Figure 3.11).

Plagioclase has not been identified in any of my samples, which could be due to the small grain size. The absence of twining can also be a reason why it has not been found in the samples.

The next pages will show thin section pictures and SEM images from some selected samples. The samples are chosen because they show a difference in mineralogy.

General trends in the drill core

First the general trends in the drill core will be described, and then some specific thin sections will be more thoroughly described.

Almost every sample shows a foliation to some extent (figure 3.8). This is showed as a lamination between quarts and micas (mostly biotite). The foliation is consistent in all samples. Most of the samples also show veining (figure 3.9), and there are two types of veins: quartz and calcite. The calcite veins often truncate the quartz veins. The calcite veins also cuts through the foliation of the samples, while the quartz veins both cuts and follows the foliation.

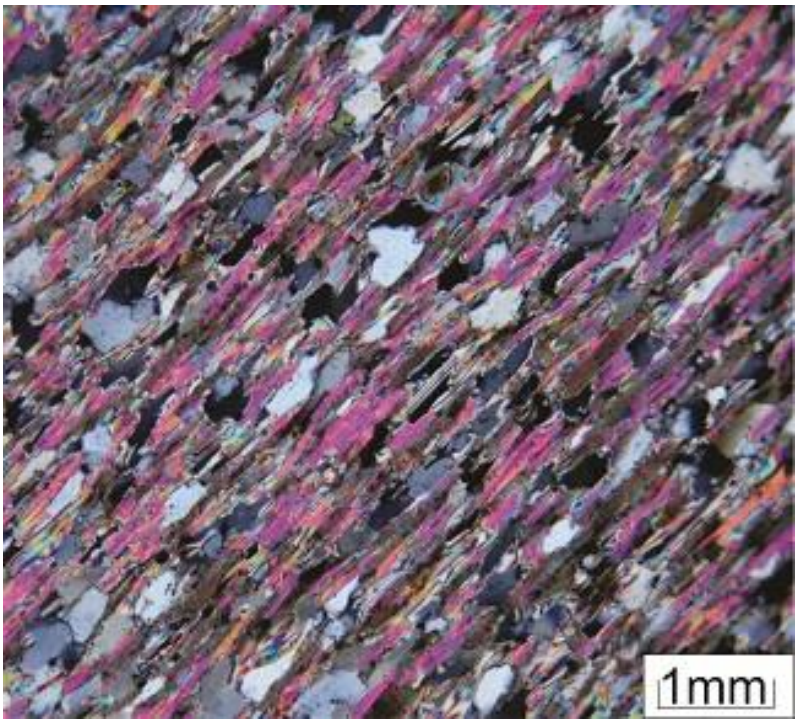

Figure 3.8: The picture shows the foliation in sample 91. The dull colored mineral is quartz while the magenta colored is biotite. The picture is taken in cross polarized light.

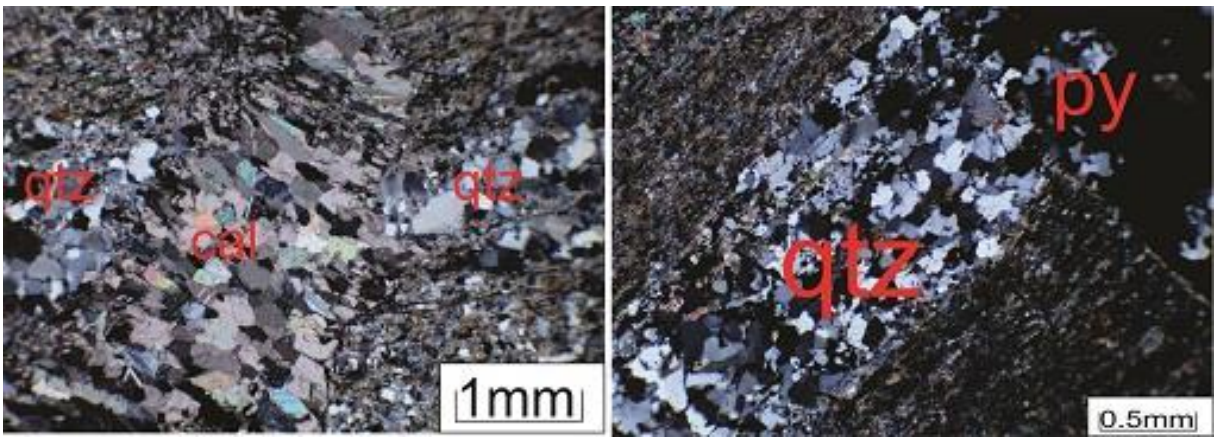

Figure 3.9: Images from thin sections, both taken in cross polarized light. The image to the left shows a calcite vein truncating a quartz vein in sample 92. To the right is a quartz vein which seems to stop in a big pyrite assemblage. The vein is following the foliation of the sample. The matrix around the vein is made up of quartz and biotite.

When chlorite occurs in the sample, it is usually seen as a rim on calcite veins (figure 3.10). The size of this rim has a great variation, from 0.25 mm to a couple of millimeters.

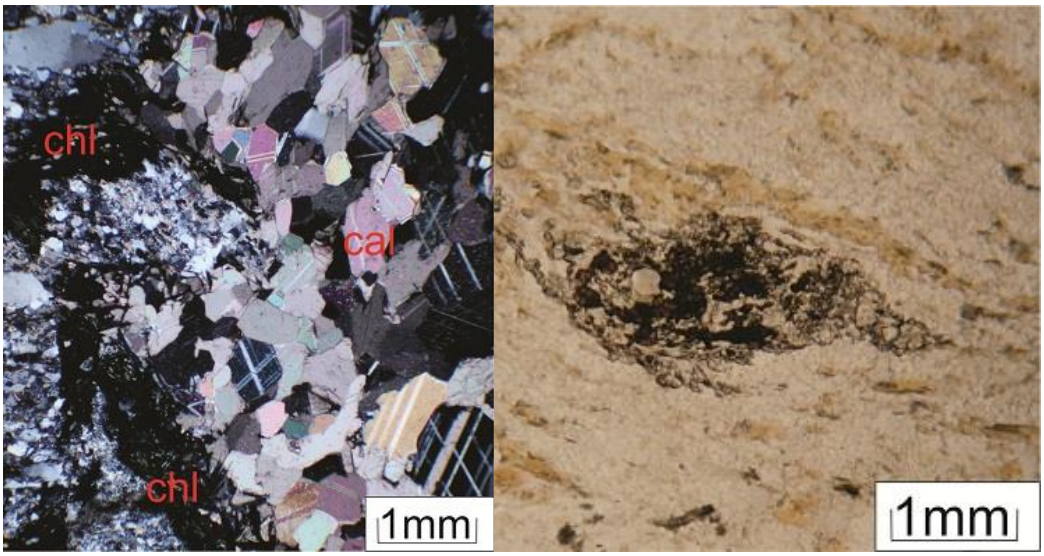

Figure 3.10: The image to the left is taken in cross polarized light and shows a chlorite calcite association. All of the black mineral to the left of the calcite is chlorite. The image to the right is taken in plain polarized light and shows a rutile titanite association. The black-reddish mineral in the center is rutile while the grey mushy mineral which surrounds is titanite.

Rutile and titanite have a close connection in the samples since they often appear together. Rutile is in most cases in the center while titanite lies around it like a halo (figure 3.10). Both minerals also appear independently of each other. Titanite is common as an independent grain, while rutile is more common as a rim on pyrite.

Sample 86

This sample is the one with the highest As values (10468 PPM) from the core and without doubt the sample with the highest concentration of arsenopyrite. This concentration of arsenopyrite explains the As anomaly. The grains of arsenopyrite show rhombohedral shape and are mostly oriented the same way (figure 3.11). A chemical analysis from an arsenopyrite in sample 86 is given in table 3.2.

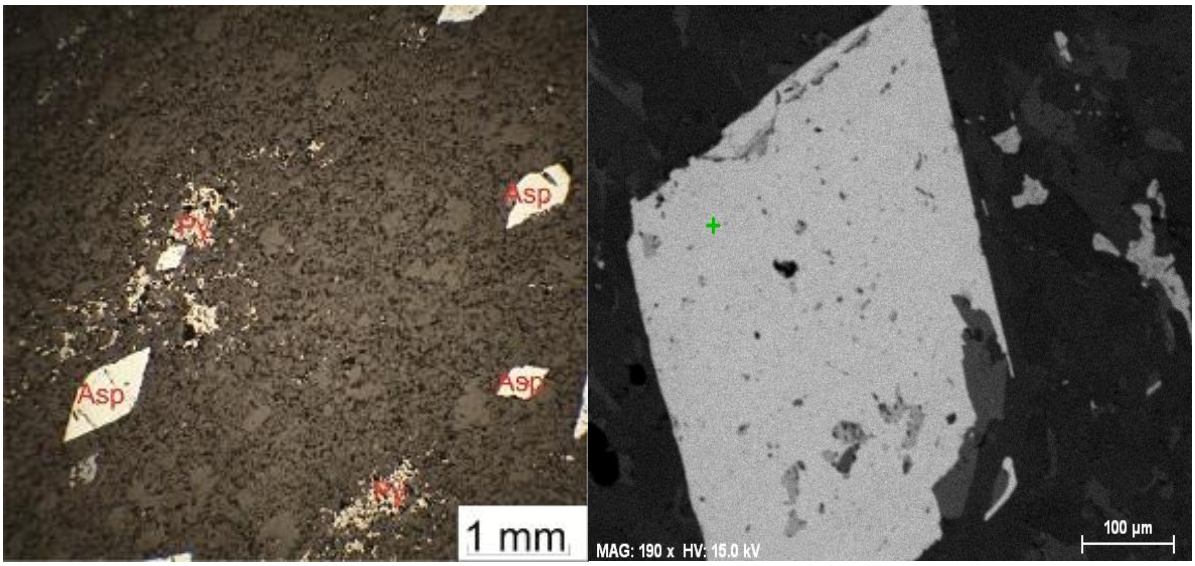

Figure 3.11: The picture to the right shows a Back-scatter electron image of. The green cross marks point for geochemical analysis in Table 3.2. The picture to the left shows arsenopyrites and pyrite in reflected light. Both pictures are from sample 86.

	S	Fe	As
Wt. %	17,11	34,21	48,68
At. %	30,61	32,65	36,73

Table 3.2: The table showing weight percent and atomic percent from geochemical analysis in sample 86. Analysis is from the green cross in the right picture from figure 3.11.

Sample 80 and 81

These two samples are dealt with together since they show a lot of similarities. They are the samples with the highest values of Ca and lowest values of Al. This is clearly seen in the thin sections since they have a great amount of carbonates. Another characteristic is the grain size; the size in the sections is much larger. The reason for this is that there are lesser amounts of fine grained quartz. The rocks mostly consist of coarser grained quarts (>1mm) and calcite (figure 3.12). In addition there are some aggregates of fine grained mica, mostly biotite, but also some muscovite.

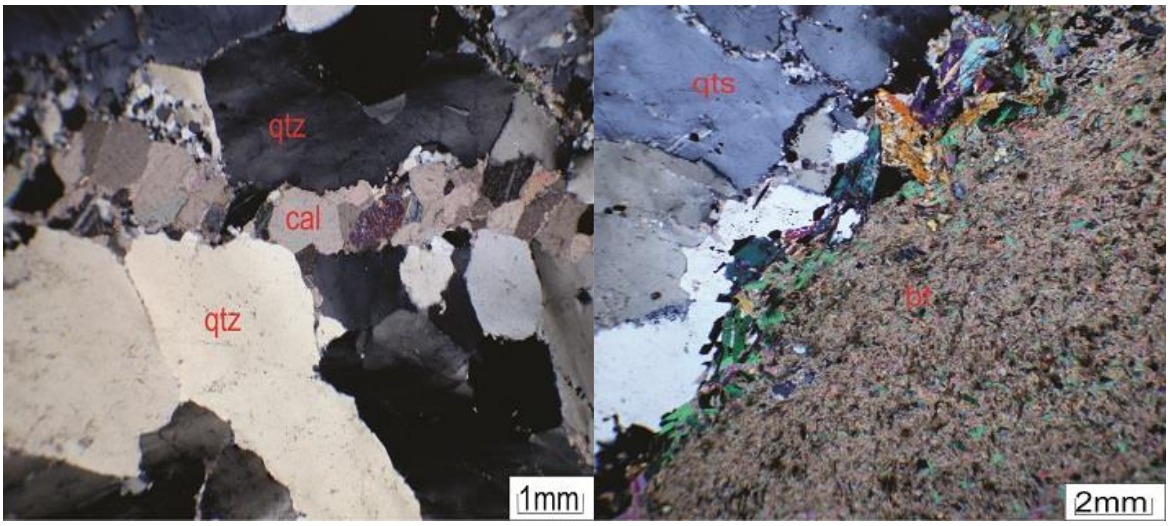

Figure 3.12: Pictures from sample 81 taken in cross polarized light. The image to the left shows an aggregate of quartz with a truncating calcite vein. To the right is an aggregate of primarily biotite, Notice the green mineral (muscovite) between the quartz and biotite

Sample 90

This sample contains several big garnets which are not seen in any other thin section. The garnets are from a couple of mm up to 6 mm on their longest axis (figure 3.13). They all have spherical shapes and seem heavily altered. The rest of the sample is characterized by fine grained mica and quarts (< 0.1mm) with some calcite veins.

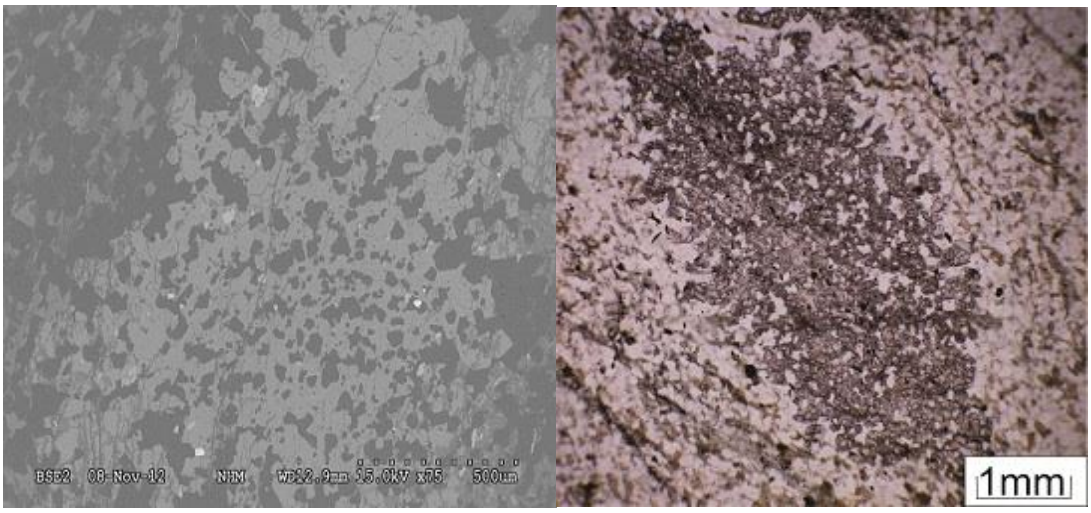

Figure 3.13: Images of garnet from sample 90. The image to left is taken with SEM, the image to the right is taken in plane polarized light.

Sample 89

The sample is dominated by fine grained muscovite which acts as the matrix of the rock. This section is the undoubtedly the most muscovite rich sample, even though some of the samples above and in the upper part of the mineralization contain a bit. Other important minerals in the sample are calcite, pyrite, chlorite, and quartz (figure 3.14).

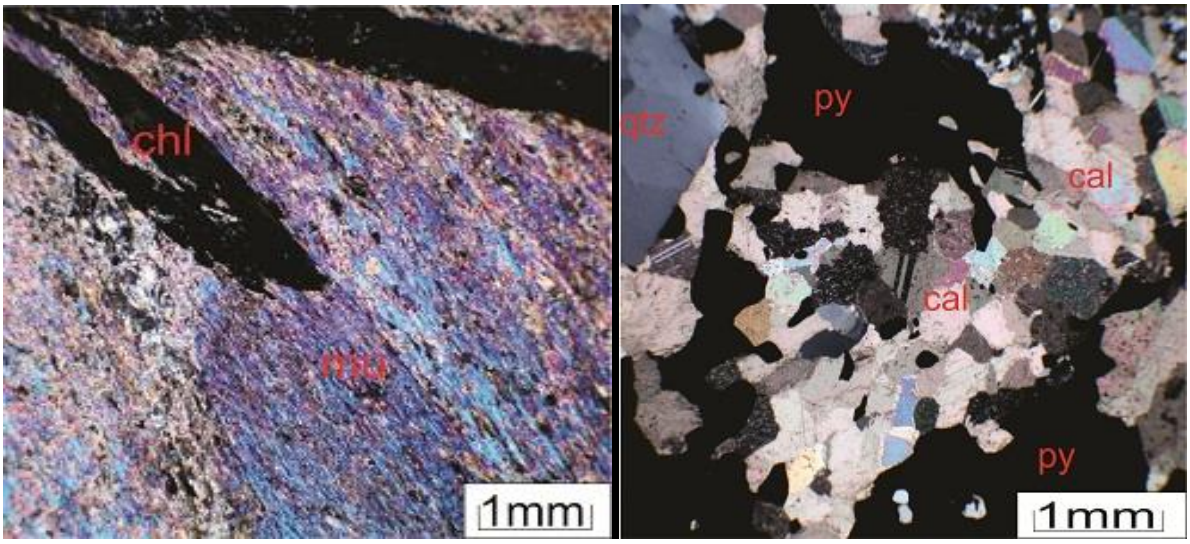

Figure 3.14: Thin section pictures from sample 89, both pictures are taken in cross polarized light. To the left is an image of the muscovite matrix which dominates the sample + a chlorite vein. To the right is an image of a calcite, pyrite, and quartz assemblage.

Sample 69

This is the sample which contains the most sulfides, 30 percent of the whole thin section. There is an aggregate/vein which runs through the whole thin section, 4 cm long and half a centimeter thick (figure 3.15). This assemblage also has several branches. The sulfides are entirely made up of pyrite. This is also the sample which has the most tourmaline. The tourmaline crystals are typically 0.25 mm big and appear together in clusters alongside/in cracks (figure 3.15).

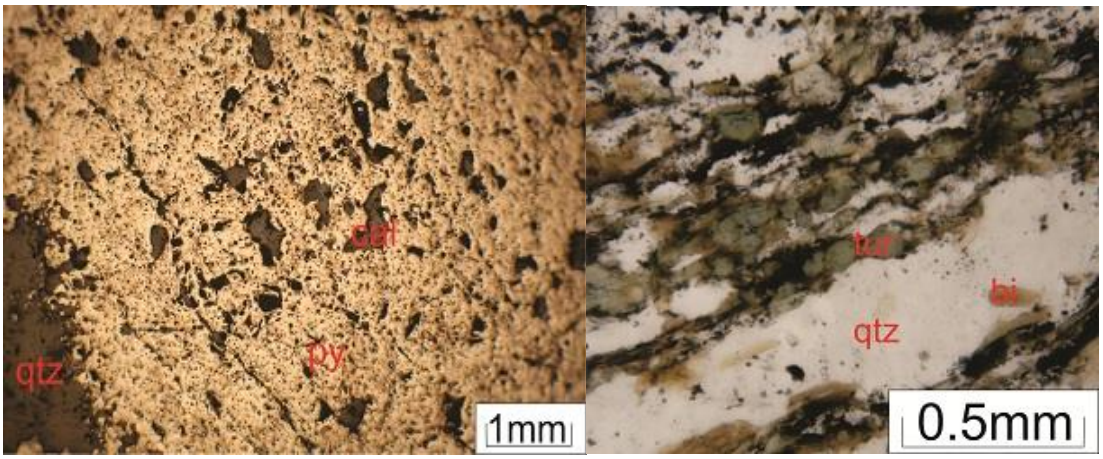

Figure 3.15: Thin section pictures from sample 69. The image to the left is from the pyrite vein in the sample and taken with reflected light. The image to the right show the appearance of tourmaline, taken in plane polarized light

SEM analysis

During the SEM analysis the focus was to identify different opaque phases, so very few analyses were done on the silicates. The analysis done will be presented here and some selected analyses are presented in the section above.

The phases which were identified with some extent were pyrite, arsenopyrite, magnetite, and chalcopyrite. In addition some rare minerals were identified, and these minerals were only identified from one of the samples. An overwhelming part of the opaque minerals turned out to be pyrite, at least 90-95 percent. An example is given in figure 3.16.

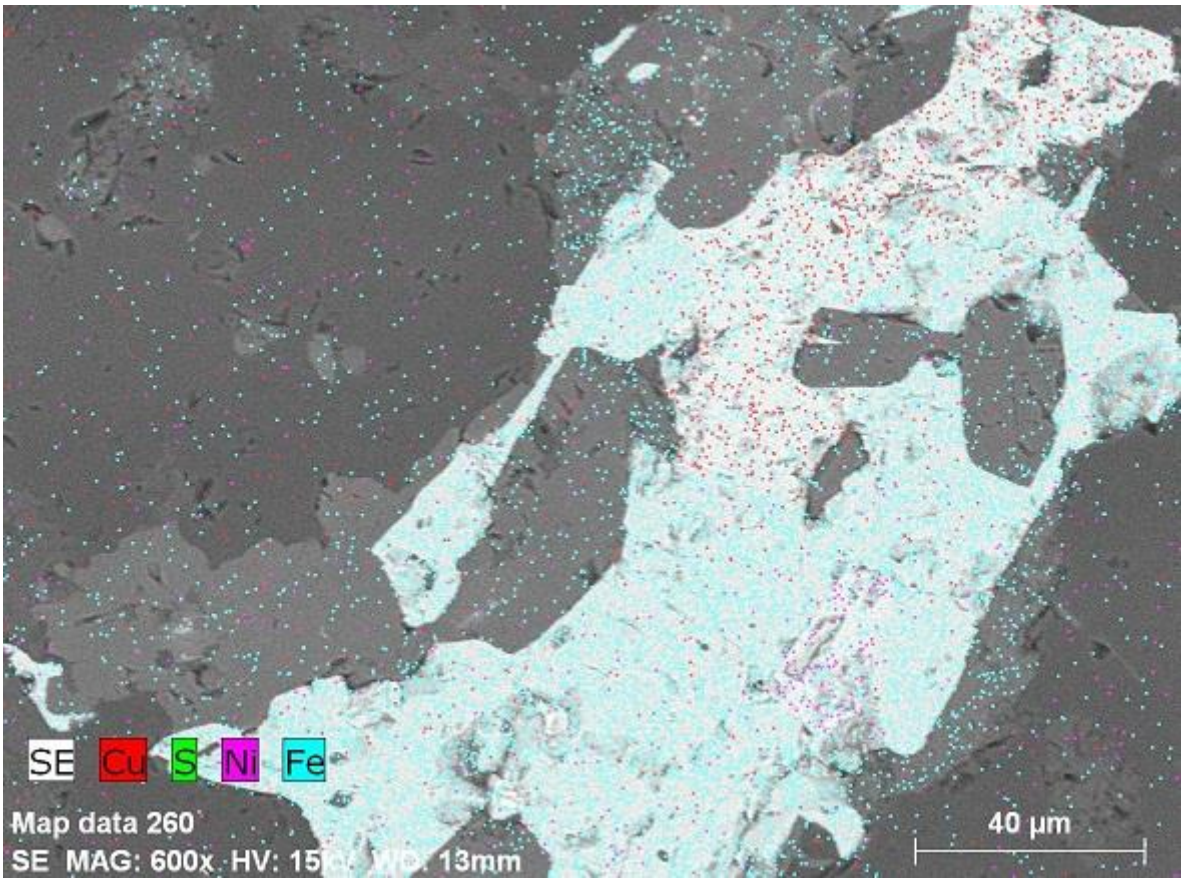

Figure 3.16: Secondary electron image of pyrite and chalcopyrite combined with element maps. The red part is chalcopyrite, while the turquoise is pyrite.

The rare minerals which were identified were consisting of Bi, Sb, Ni, Te, S, Fe, and Ag. The minerals were a cluster which consisted of different minerals which were dominated by various elements. This was evident even on the SEM image (Figure 3.18), but was really clear when the analysis for different elements was done (Figure 3.17).

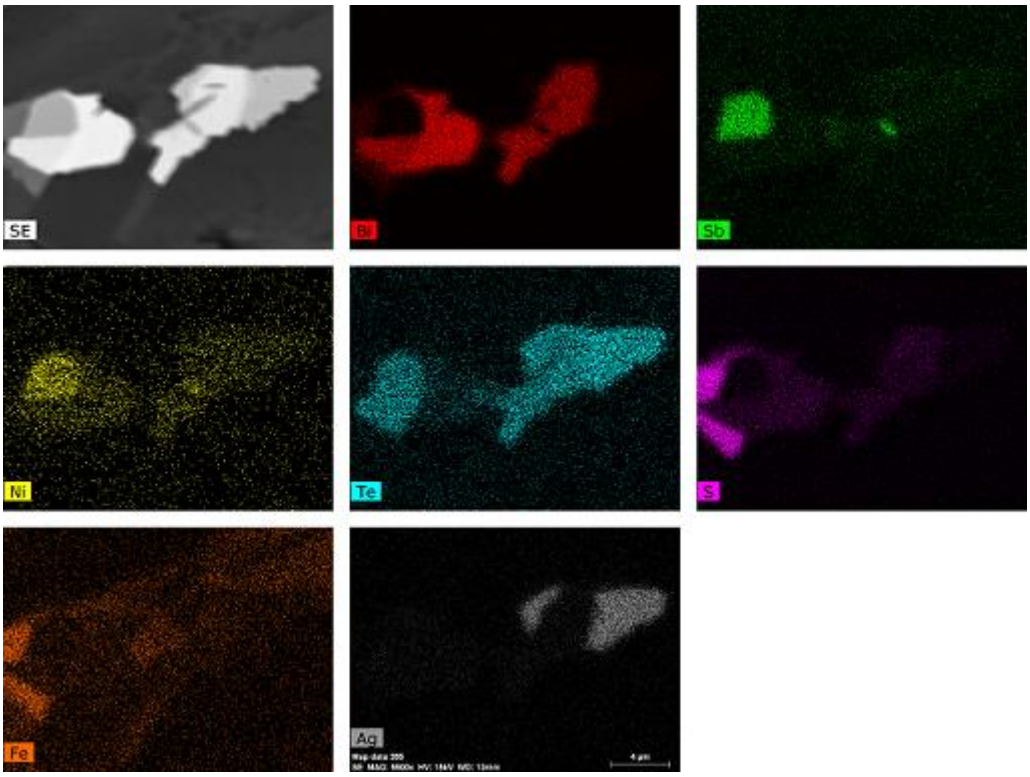

Figure 3.17: Element maps of the concentration for selected elements. The picture on the upper left is the SEM image.

The mineral shown in the figure above on the SEM image is actually a group of mineral as seen on the element maps. The different minerals and which elements they consist of can be seen in the figure below (figure 3.18).

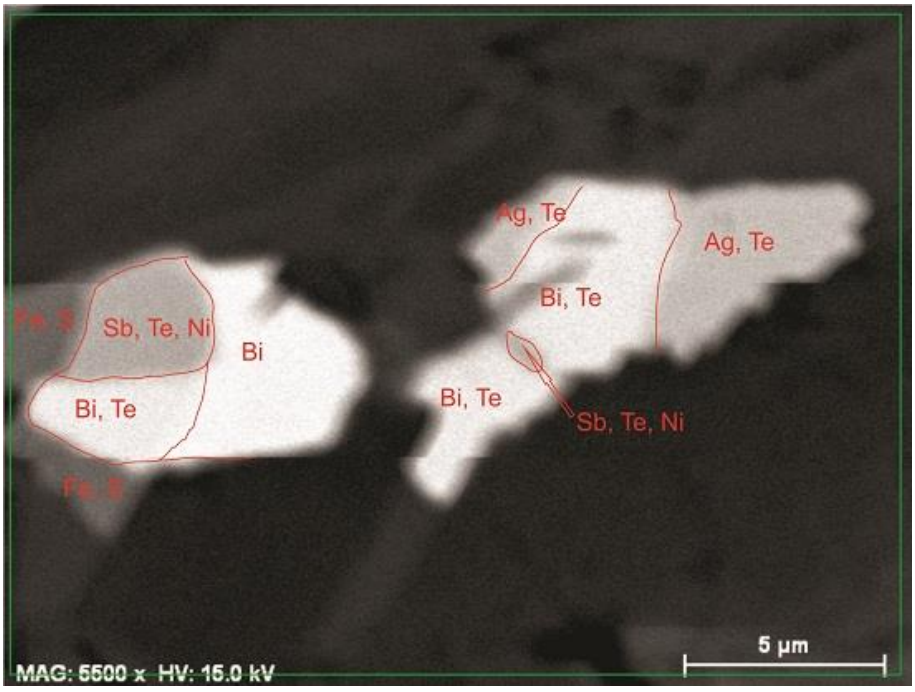

Figure 3.18: Back scatter image whit boundaries for the different minerals.

The different minerals in figure 3.18 have the following chemical composition: The Fe and S mineral is pyrite. The Bi and Te mineral is an unnamed Bi- Telluride (Bi_3Te_2). The Ag and Te mineral is hessite (Ag_2Te), and the Sb, Te and Ni mineral have not been analyzed for mineral composition. The zone which only contains Bi, is native Bi. The names of minerals are taken from www.mindat.org after calculating the structural formula based on SEM-analysis.

In my SEM analysis I could not identify any Au grains or minerals, but previous investigations done by Scandinavian Highlands could on the other hand identify Au grains. The Au was mainly situated in arsenopyrite as inclusions (Figure 3.19), but also found in pyrite as inclusions. The Au grains were concentrated in the center of the arsenopyrite, while the outer rim of the grains was completely free of Au.

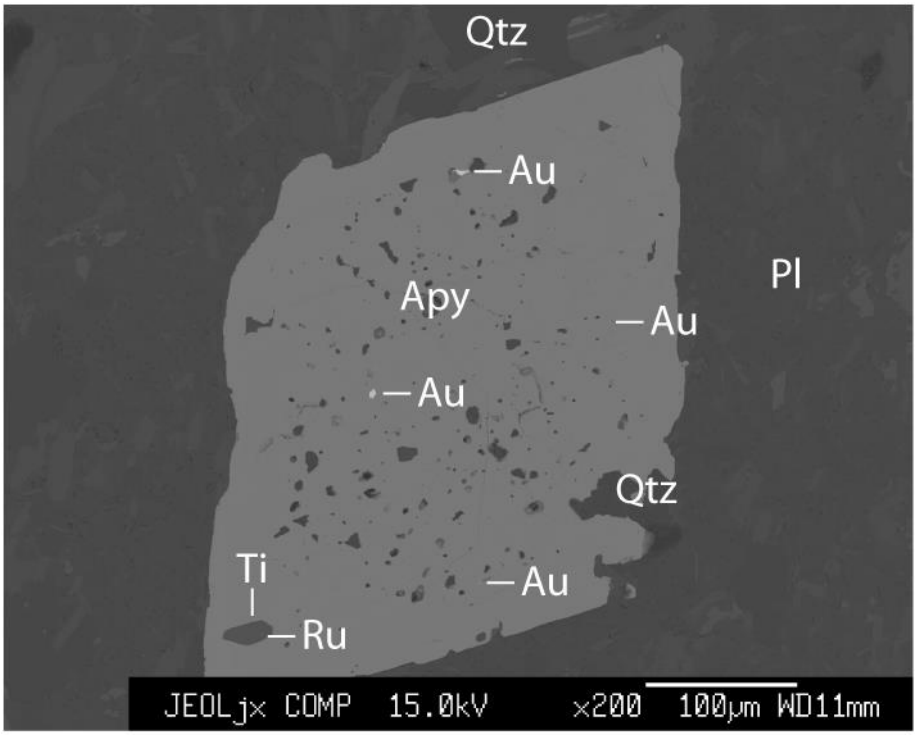

Figure 3.19: Back scatter image showing an arsenopyrite with Au inclusions (Vognsen, written communication, 2012).

4. Geochemistry of the rock

In this part, the description of the XRF-analysis and ICP-MS analysis and will be given. The values from the major element analysis are an average from the two parallels that were made. When the sample numbers from the XRF-analysis are noted, only the last two numbers will be given. For example sample 568968 will be referred to as sample 68.

The zone of mineralization starts at 28.85 meters and ends at 36.50 and is based on Au values from the ICP- MS data. This will be substantiated later in the thesis. The data from the geochemical analysis were interpreted with the help of Rollinson (1993).

Major element geochemistry

XRF data

The data from the major element analysis is given in appendix 1 and the variation for the different elements towards depth is shown in figure 4.1. When using the diagrams in Figure 4.1, one has to take into consideration that the sampling concentration for the mineralized zone (28-36m) is higher than for the rest of the core. For the XRF-plots the density of samples are higher in the mineralized zone and in the ICP- MS plots the intervals of each sample is smaller, which gives more data points per meter. This gives an impression that the mineralized zone varies more than it does.

The silica content of the rock lies between 46 -71 % with an average of 59.8 %. 24 out of 26 samples are in the interval of 54-64 %. The highest value for SiO_2 is found in sample 89 at 26.35 meters depth which is straight above the mineralization; this sample also has a low Al value. Al_2O_3 has a great variation and the lowest value is 2.88 % while the highest is 17.03 %. 23 out of 26 samples are in the range of 12-17 % with an average for all samples of 13.8 %. The samples with the lowest concentration of Al_2O_3 (sample 80 and 81) are the samples with the highest values of CaO (15 and 12 %). The values of CaO are in the range from 1.16 to 15.65 % with an average of 4.48 %. The spikes of CaO correlate with the spikes of MnO. The

values of MnO vary between 0.04 and 0.24 %. Fe_2O_3 has an average of 6.19 and varies between 3.34 and 10.09 %. Fe_2O_3 and S (which are not showed in the diagram) have a similar development in the core. The same is also valid for the development of MgO. The values for Na_2O and K_2O have a spike straight before and straight after the mineralized zone. This spike is also evident for Al_2O_3.

XRF-analysis was also done for the following trace elements Ag, As, Ba, Bi, Ce, Co, Cu, Cr, Cs, Ga, La, Nb, Ni, Pb, Rb, S, Sc, Sb, Se, Sn, Sr, Th, V, Y, Zn, and Zr. These results are presented in appendix 1. Most of these elements have a very low concentration throughout the drill core. The only trace element analyzed that has a significant variation, is As. As is enriched in the mineralized zone and has spikes in the top and the bottom of the mineralized zone. This will be presented more thoroughly later.

The minimum, maximum and average concentrations of the major elements are shown in table 4.1.

	SiO_2 (%)	Al_2O_3 (%)	TiO_2 (%)	Fe_2O_3 (%)	MnO (%)
average	59,81	13,82	0,75	6,19	0,09
max	71,24	17,03	1,02	10,09	0,24
min	46,56	2,88	0,13	3,34	0,04
	MgO (%)	CaO (%)	Na_2O (%)	K_2O (%)	
average	2,83	4,48	1,82	3,25	
max	5,77	15,65	3,42	4,82	
min	1,6	1,16	0,04	0,72	

Table 4.1: Minimum, maximum and average values from the XRF data.

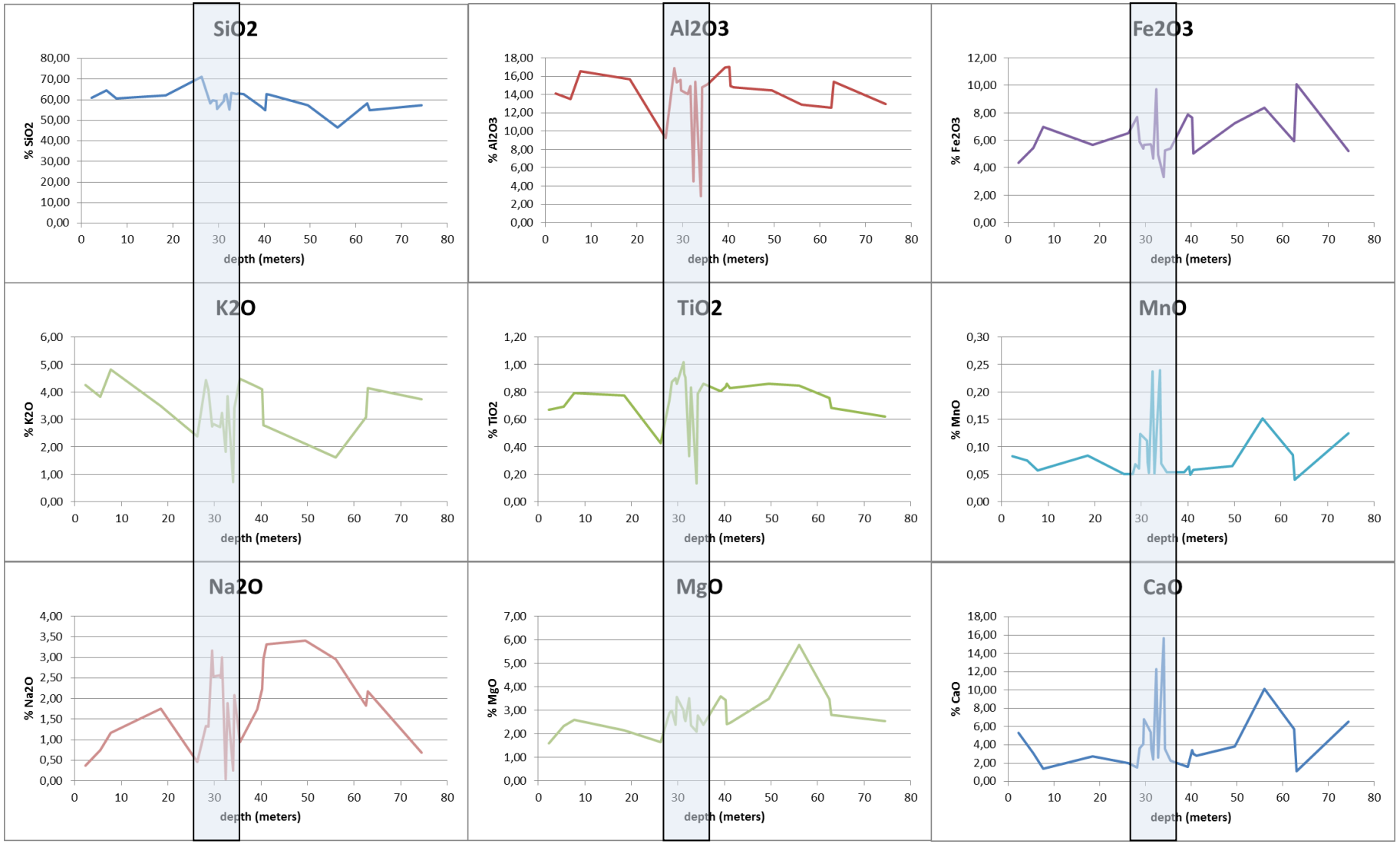

Figure 4.1: The variation of selected major element in the drill core (XRF analysis). The shaded area is the part of the core which hosts the Au mineralization.

ICP-MS data

The data from the major element analysis is given in appendix 2 and the variation for the different elements towards depth is shown in figure 4.2. In the ICP-MS data, Si was not analyzed for and S is instead shown in figure 4.2. The data for the XRF analysis is given as oxides, while the data for the ICP-MS is given as element concentration and that is mainly why the concentration for the elements vary between the data sets.

The trend seen in figure 4.1 where the elements seem to vary more in the mineralized zone than the rest of the drill core, is not seen in the ICP-Ms plot. It is more a widespread variation throughout the whole core.

Al varies from 2.88 to 17.03 Wt. % Al_2O_3 in the XRF data (figure 4.1), but only varies between 5.81 and 9.13 Wt. % Al in the ICP-MS data (figure 4.2). This might be due to the sampling intervals, the XRF data is from an interval of +/- 10 cm while most of the data points from the ICP-MS data are from an interval of 1 m or 0.5 m. So small local variations, will not give as big an impact on the ICP-MS plot as in the XRF plot. This is also clearly seen in the diagrams for Ca. Ca is also an element which shows great variations throughout the whole drill core, and this is also seen for the alkalis (Na and K).

Mn and Ca seem to have a correlated variation through the drill core and this will be followed up in the section about Harker coefficients.

In the mineralized zone there are some interesting features that could be seen. There is general enrichment of S in the whole mineralized zone. There is a decrease in the Na and Ca contents just above and below the mineralization and an enrichment of K in the same area.

The minimum, maximum and average values are shown in table 4.2.

	S (%)	Al (%)	Ti (%)	Fe (%)	Mn (PPM)
Average	0,42	7,85	0,45	4,86	595,43
Max	2,12	9,13	0,54	6,94	1300
Min	0,02	5,81	0,31	3,34	267

	Mg (%)	Ca (%)	Na (%)	K (%)	
Average	2	2,56	1,72	2,57	
Max	3,58	5,22	3,79	4,55	
Min	1,12	0,52	0,46	0,72	

Table 4.2: Minimum, maximum and average values from the ICP-MS data.

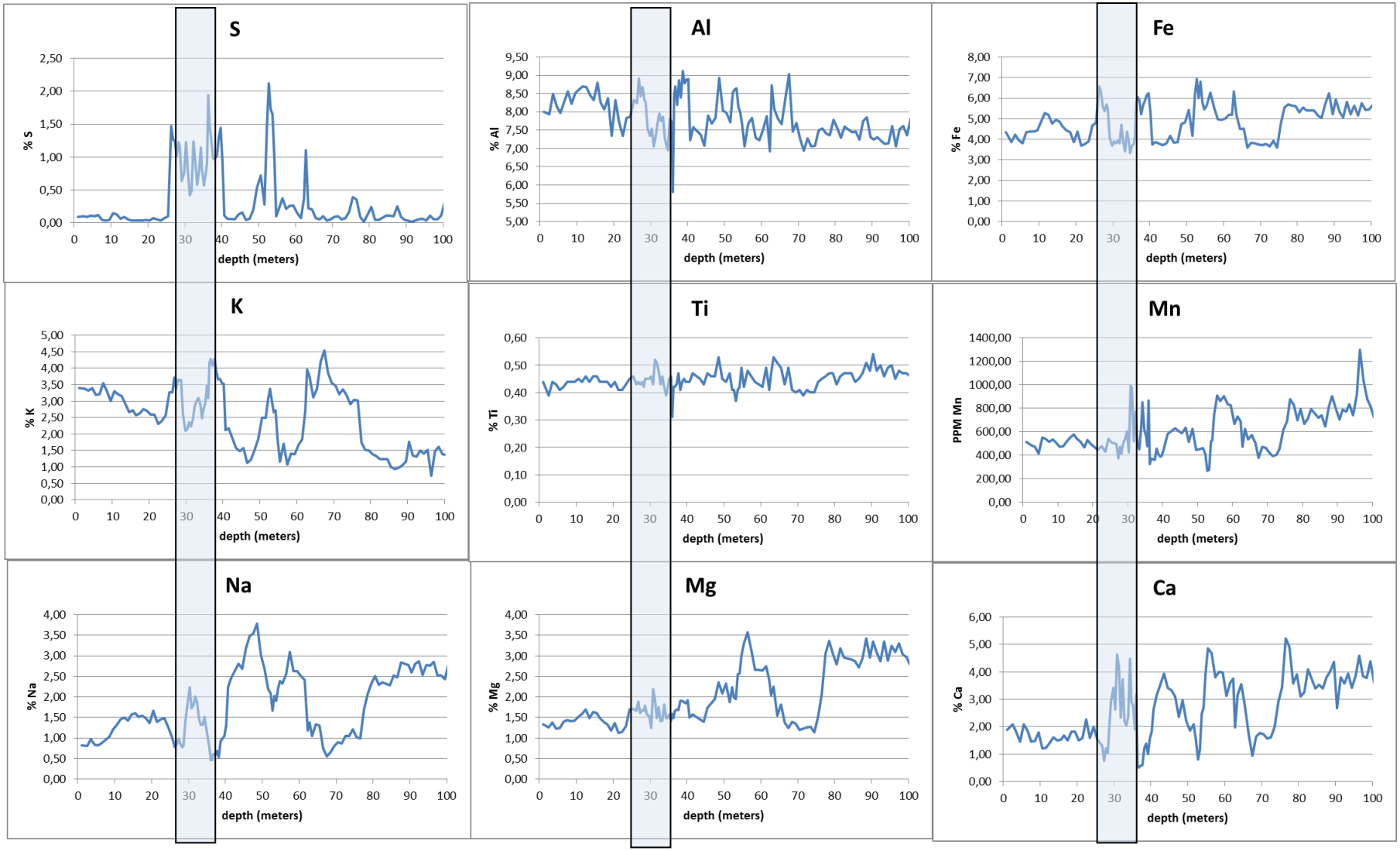

Figure 4.2: The variation of selected major element in the drill core (ICP-MS analysis). The shaded area is the part of the core which hosts the Au mineralization.

Trace element geochemistry

The data from the trace element analysis is given in appendix 1 (XRF) and appendix 2 (ICP-MS), and the variation for the different elements towards the depth shown in figure 4.3. Only the results from the ICP-MS trace elements analysis are reviewed here and only selected elements are shown in figure 4.3. Trace element plots of Au and As will be described later in a separate chapter.

All elements presented in figure 4.3 show a variation throughout the drill core except Ag and Sb. Ag has one zone of enrichment and this is the zone of the mineralization. The enrichment seems great in the diagram, but the values for Ag never exceed 0.8 PPM (table 4.3). Still, there is a clear trend of enrichment in the mineralized zone. Sb is also an element which has a clear enrichment in the mineralized zone, but it also has some small spikes further down the drill core.

P is an element which is enriched in the mineralized zone and some zones further down the drill core. The mineralized zone is the first zone of enrichment for P.

Typical base metals such as Zn, Cu, and Pb do not show any enrichment in the mineralized zone and show generally low values. Pb has a spike in the mineralized zone, but it does not show a general enrichment in the zone.

	Ag (PPM)	Cu (PPM)	P (PPM)	Pb (PPM)	Sb (PPM)	Zn (PPM)
Max	0,80	282,00	1510,00	32,00	33,00	181,00
Min	0,25	15,00	480,00	6,00	2,50	48,00
Average	0,28	70,17	844,41	14,35	6,46	106,53

Table 4.3: Minimum, maximum and average values from the ICP-MS data.

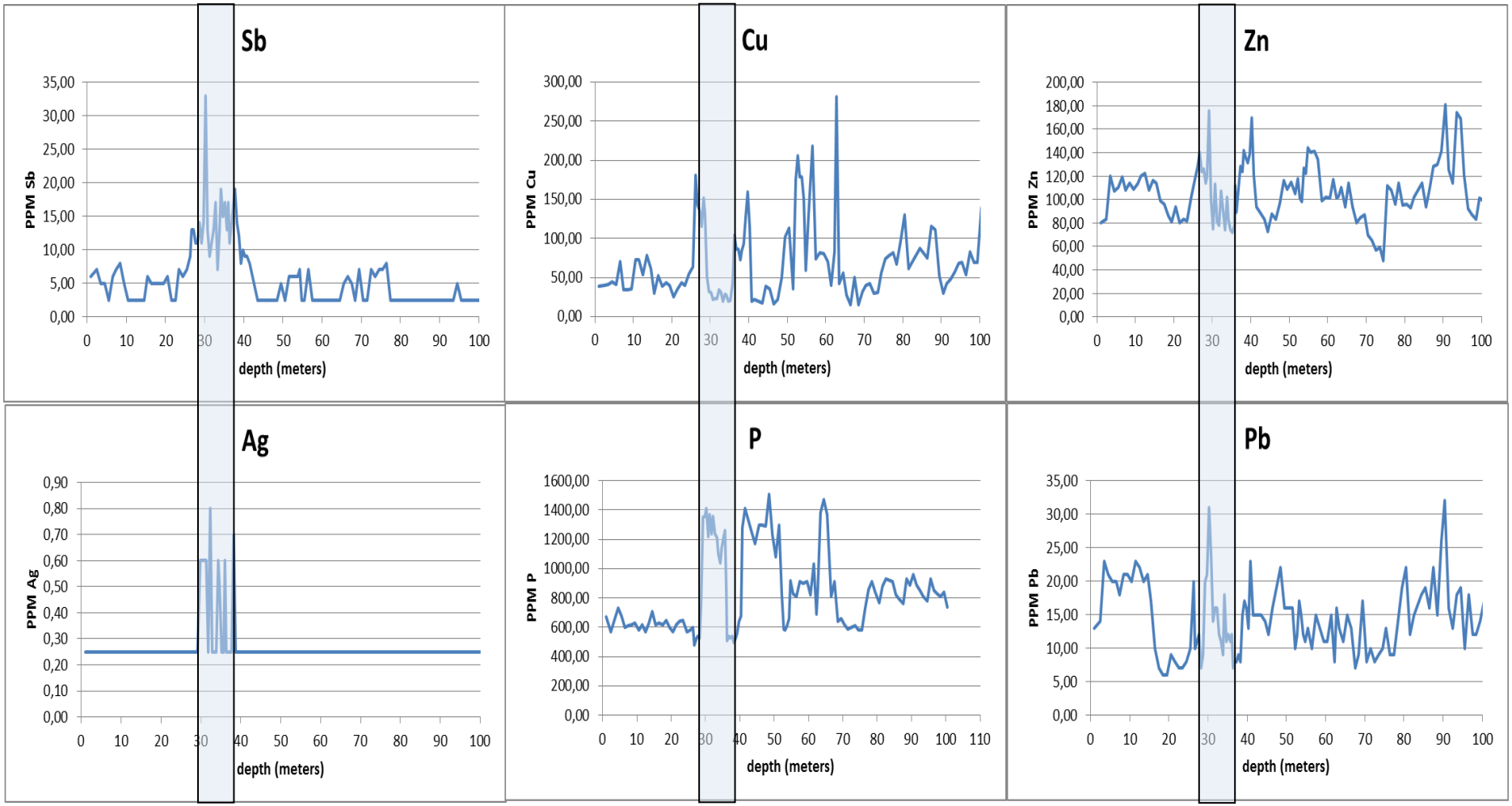

Figure 4.3: The variation of selected trace element in the drill core (ICP-MS analysis). The shaded area is the part of the core which hosts the Au mineralization.

Geochemical Plots

The descriptions of the geochemical trends are based on the XRF-analysis done at the University of Tromsø and the ICP-MS analysis.

Harker Diagrams and Correlation Coefficient

To identify mobile and immobile elements, Harker-diagrams were created, in addition to the correlation coefficients that were calculated. The coefficients are shown in Table 4.4; the ones with the highest coefficient are shown in yellow. This was done to measure the strength of a relationship between two variables, and the Pearson product-moment correlation coefficient has been used. The coefficient (r) varies between +1 and -1. There is a strong relationship if the r value is close to 1 and a strong negative relationship if the value is close to -1. The r value is defined as:

$$r = \frac{covariance\ (x, y)}{\sqrt{[variance\ (x) * variance\ (y)]}}$$

Shown below are some selected Harker-diagrams (Figure 4.2). The diagrams are selected after the calculation of the correlation coefficients.

In Table 4.1 all the correlation coefficients are plotted, the ones in yellow are shown as Harker diagrams in Figure 4.4. The values are calculated from the values from the XRF-analysis found in appendix 1.

Most of the elements show no correlation, but some show a weak correlation (table 4.4). The elements showing correlation are: Al vs. Mn, Ca, Ti, and Pb, Si vs. Mg, Mn vs. Ca, Cu vs. Se, and As vs. Bi. But when you take a closer look at the Harker diagrams, the trend for most of the plots shows something different. The diagrams have outliers which give a wrong impression of the correlation coefficient. When it has one or two outliers it can give the impression of a correlation, when it really is more of a coincident. This is especially evident

in Figure 4.4 for Cu vs. Se and As vs. Bi. The only ones showing a correlation are Si vs. Mg and Mn vs. Ca, whereas the only two elements showing a strong correlation, are Mn vs. Ca. The coefficient is high (0.97) and the data points are more scattered around the trend line. In addition the coefficient calculated with the ICP-MS data is high (0.89) (table 4.5).

Some selected correlation coefficients from the ICP- MS data are shown in table 4.5 and Figure 4.5; they are calculated from the values found in appendix 2. For the ICP- MS data there are several elements which correlate well, especially As vs. Au. The elements show a strong positive correlation (0.99). This correlation is also evident when the element concentration is plotted against the depth of the drill core (Figure 4.5). There is also a positive correlation between Fe-Co, K-Be, Mg-Cr, Mn-Ca, Ni-Mg, Ni-Fe, Ni-Cr, Ni-Co, V-Ni, V-Fe, and V-Co. There is a negative correlation between Na-K and Ca-Be. Something peculiar about the correlation between Na-K, is that it isn't viewable in the XRF-data. But if sample 568980 and 568981 is removed from the data, a correlation appears (a negative correlation of -0.78). The reason why these two samples could be removed is that they are heavily influenced by carbonate veining. The samples contain between 20 and 30 percent carbonate.

When reviewing the Harker plots together with the correlation coefficient for the ICP-MS data, it is clear that the high correlation coefficient is valid and not based on single outliers, like in most of the XRF plots. So the high correlation coefficients in table 4.5 are more reliable than the high number in table 4.4. The reason for this is likely to come from the numerical basis. The XRF data set is based on 26 data points, while the ICP-MS data set is based on 118 data points.

	SiO2	TiO2	Al2O3	Fe2O3	MnO	MgO	CaO	Na2O	K2O	P2O5	Ag	Cu	As	Bi	Sb	Se	S	Zn	Pb	Sn
SiO2	1,00																			
TiO2	-0,17	1,00																		
Al2O3	-0,11	0,85	1,00																	
Fe2O3	-0,59	-0,04	0,06	1,00																
MnO	-0,32	-0,65	-0,84	0,02	1,00															
MgO	-0,85	0,25	0,05	0,56	0,27	1,00														
CaO	-0,33	-0,61	-0,82	-0,08	0,97	0,29	1,00													
Na2O	-0,26	0,73	0,52	0,02	-0,39	0,37	-0,29	1,00												
K2O	0,08	0,41	0,74	0,09	-0,67	-0,25	-0,74	-0,15	1,00											
P2O5	-0,02	0,57	0,18	-0,15	-0,08	0,12	-0,07	0,53	-0,14	1,00										
Ag	0,21	-0,44	-0,27	-0,05	0,09	-0,15	0,09	-0,26	-0,03	-0,52	1,00									
Cu	-0,30	-0,10	0,06	0,59	-0,15	0,10	-0,16	0,07	0,11	-0,28	0,09	1,00								
As	-0,02	0,16	0,10	-0,12	-0,07	-0,09	0,00	0,28	-0,12	0,28	-0,21	-0,06	1,00							
Bi	-0,05	0,14	0,08	-0,04	-0,04	0,01	0,01	0,32	-0,16	0,33	-0,17	-0,03	0,93	1,00						
Sb	0,41	-0,17	-0,16	-0,27	-0,06	-0,33	-0,05	0,06	-0,13	0,16	0,44	-0,04	0,12	0,30	1,00					
Se	-0,22	-0,08	0,10	0,50	-0,18	-0,01	-0,20	0,07	0,18	-0,23	0,10	0,95	-0,06	-0,02	0,06	1,00				
S	-0,13	-0,42	-0,40	0,55	0,27	0,04	0,18	-0,24	-0,17	0,02	-0,02	0,57	0,13	0,23	0,06	0,48	1,00			
Zn	-0,44	0,10	0,16	0,49	-0,01	0,45	-0,04	0,15	0,07	-0,01	0,20	0,16	0,13	0,19	-0,01	0,00	0,31	1,00		
Pb	0,19	-0,79	-0,81	-0,26	0,67	-0,20	0,70	-0,43	-0,60	-0,40	0,45	-0,07	-0,05	-0,09	0,13	-0,05	0,14	-0,22	1,00	
Sn	-0,30	0,14	0,03	0,22	0,08	0,23	0,09	0,04	0,03	0,05	-0,18	0,23	0,18	0,15	-0,13	0,27	0,19	0,12	-0,06	1,00

Table 4.4: Table showing correlation coefficients for XRF-analysis, high values marked in yellow.

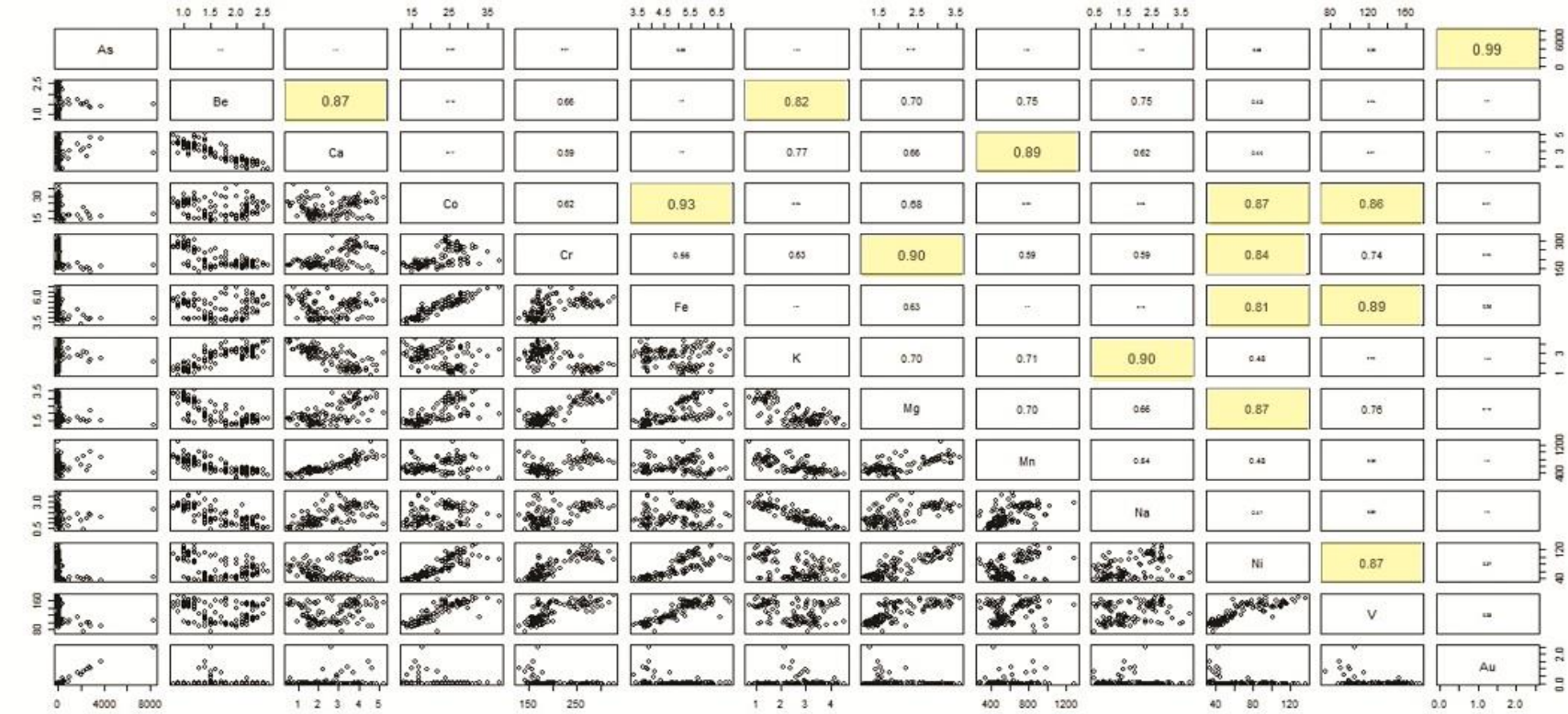

Table 4.5: Selected elements with corresponding correlation coefficients and Harker diagrams from ICP-MS data. High coefficients are marked in yellow. Note that the coefficients in the diagram do not discriminate between positive and negative coefficients. Some selected plots are highlighted in figure 4.3.

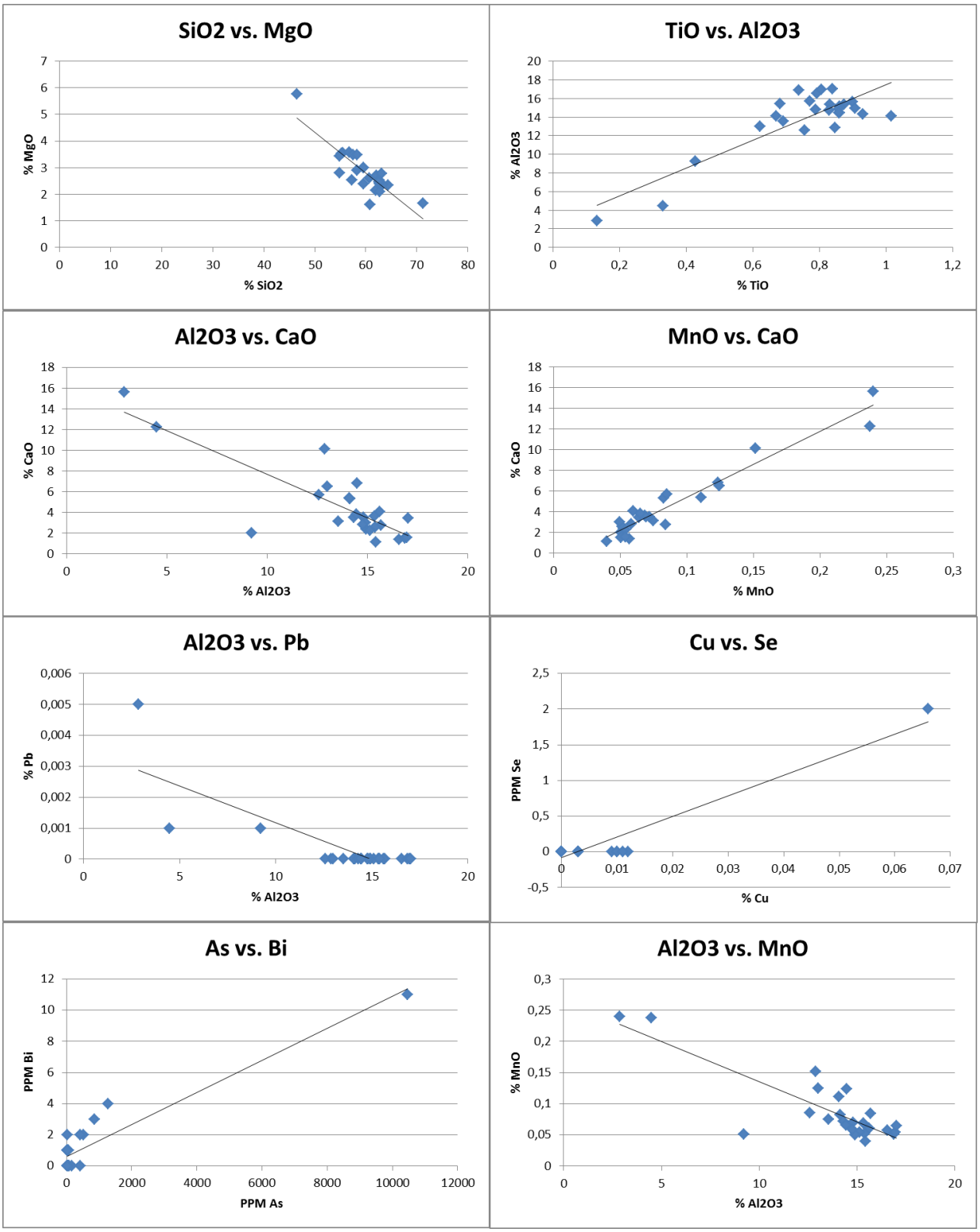

Figure 4.4: Harker plots from XRF data.

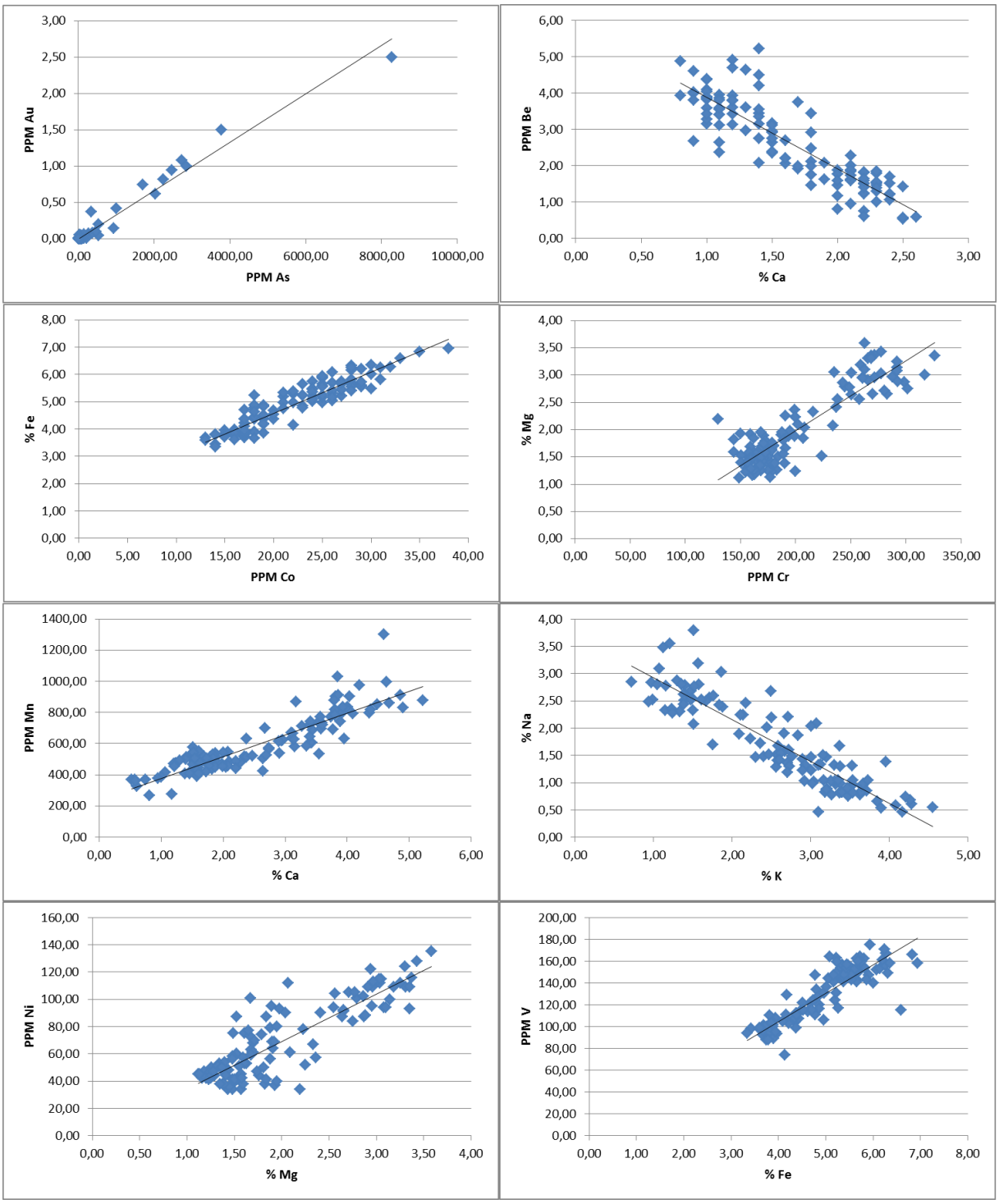

Figure 4.5: Harker plots from ICP-MS data.

Variations in Au and As of the mineralization

When the results from the ICP-MS data are plotted in a binary plot with the depth of the drill core on the x-axis and the different elements plotted along the y-axis, an Au mineralization is revealed (Figure 4.6). The mineralization starts at 28.85 m and ends at 36.50 m. The peak value of Au is 2.5 PPM over an interval of half a meter. The average Au value in the mineralized zone is 0.67 ppm over 8.65 meters. The highest Au values are found in the upper part of the mineralization.

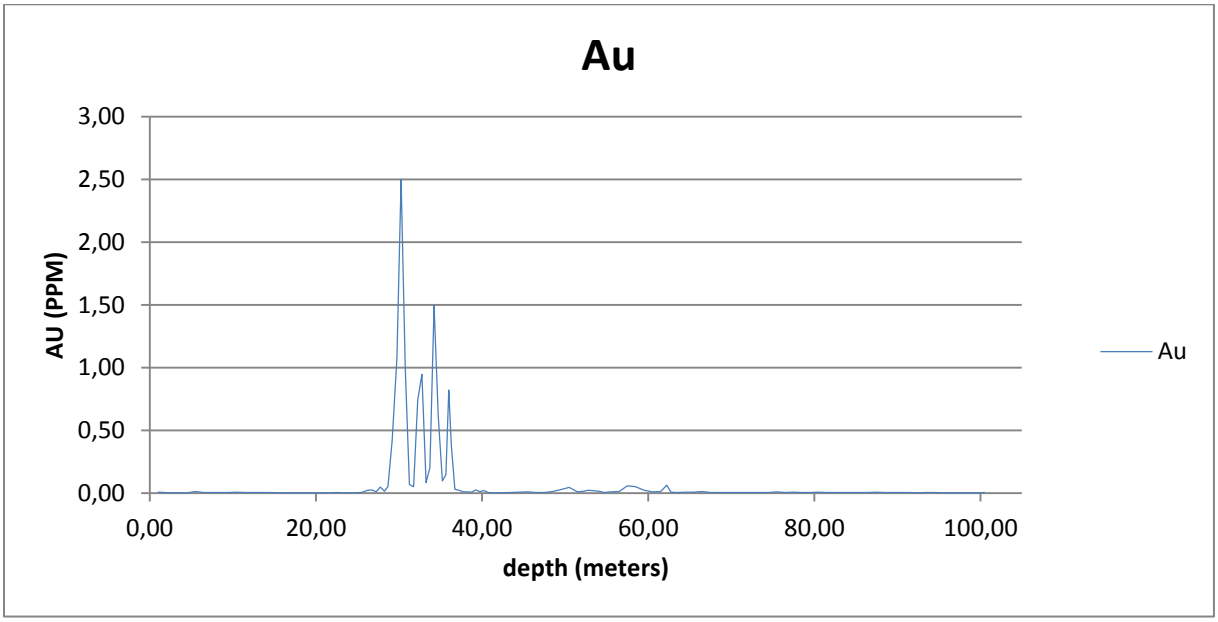

Figure 4.6: Diagram illustrating the trend for Au downwards the drill core.

Arsenic shows a similar trend as Au, it has elevated values in the same interval as Au. They also follow each other in the rest of the drill core (Figure 4.7). This would infer that there is a connection between the two.

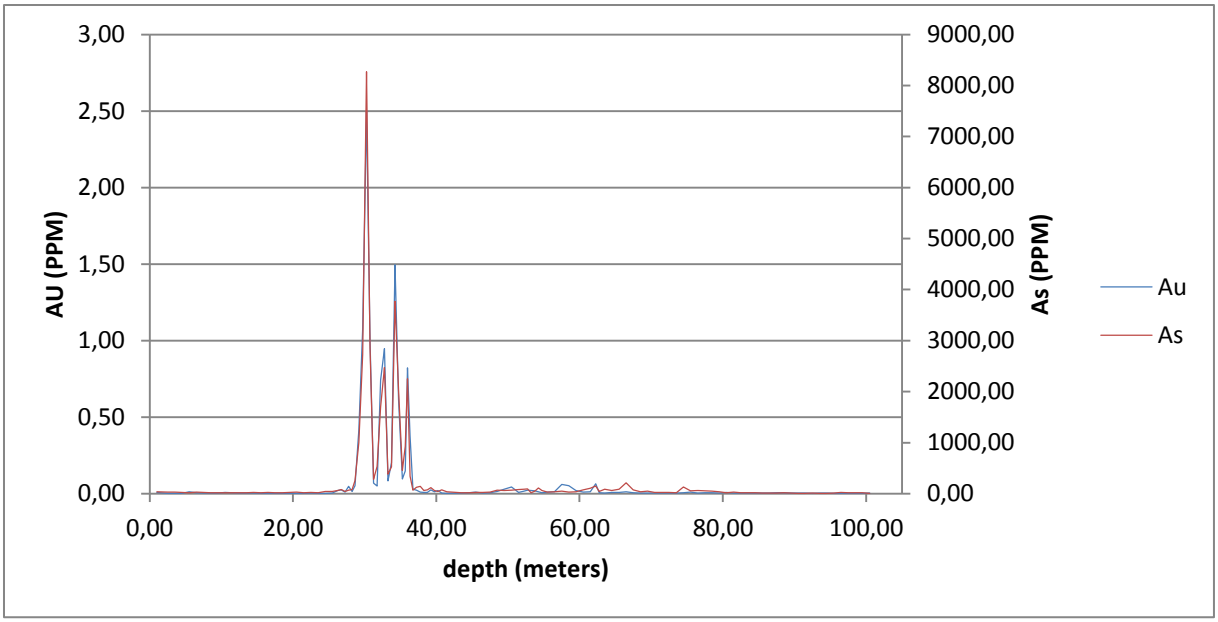

Figure 4.7: Diagram illustrating the trend for As and Au downwards the drill core.

When plotting the XRF-data, they show a similar trend (Figure 4.8). The elevated values of As starts at 29.5 and ends at 35.5 meters. The difference in start and endpoint for the zone of elevated As values is due to the difference in sampling interval. The average As value through the Zone is 1430 ppm for the XRF-data and 1909 ppm for the ICP-data.

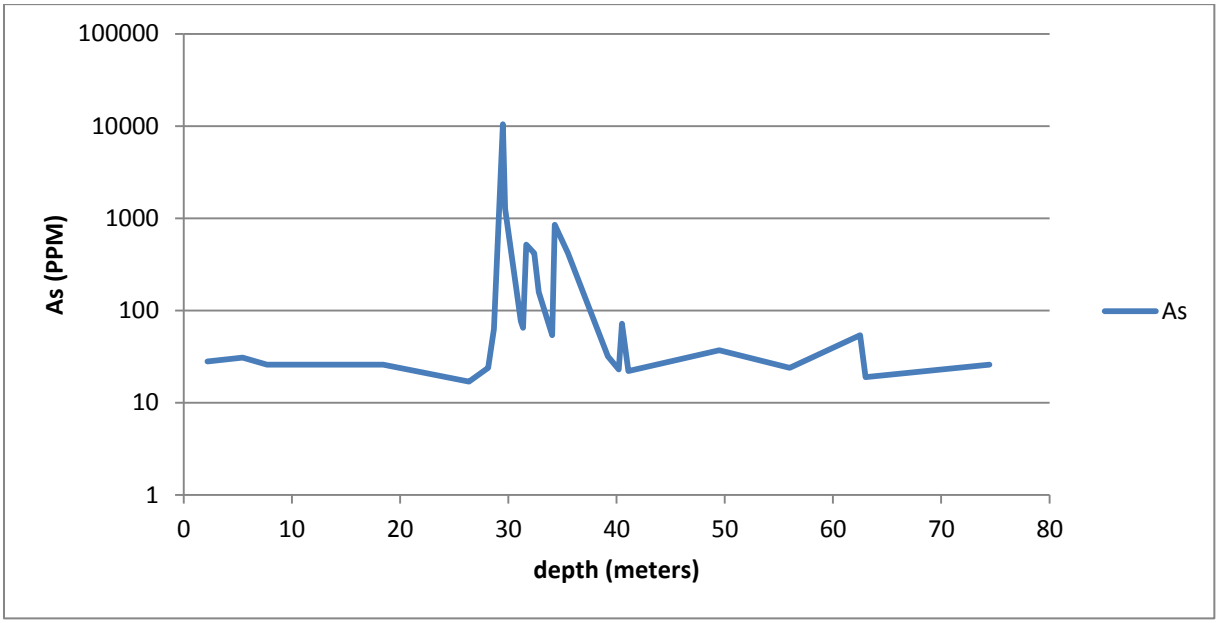

Figure 4.8: Diagram illustrating the trend for As downwards the drill core

5. Discussion

Metamorphic evolution

From the observations made during the drill core mapping and thin section investigation, it is likely that the whole drill core has been influenced by the latest deformational event. This is shown as the foliation of the drill core is consistent throughout the core and the mineral assemblage is also more or less consistent in the whole drill core.

The only minerals which show an atypical appearance (for the drill core) is arsenopyrite, which is closely connected to the concentration of Au and only appears in the Au mineralized zone. Based on these observations it is likely that the whole drill core has been metamorphosed at the same metamorphic facies.

Barrow (1893) discovered that different mineral assemblages appeared with different metamorphic grade. This leads to the term Barrowian zones and according to them, the rocks of the drill core fit best into the Garnet zone. The Garnet zone consists of the following minerals: quartz, muscovite, biotite, garnet, and sodic plagioclase. In my investigations of the thin sections, I have not been able to identify any plagioclase, whereas the previous SEM investigations done by Scandinavian Highlands did. This classification of rocks is designed for classification of pelitic rocks.

The minerals assemblage of the drill core mainly is: quartz, biotite, muscovite, carbonates, chlorite, and sulfides. This assemblage would infer a metamorphic facies of greenschist (e.g. Blatt et. al 2006). The greenschist facies is placed within a relatively small temperature range (300-450°C), and low to intermediate pressure (e.g. Bucher and Frey (1994)).

So these findings infer that the rocks of the drill core were metamorphosed at low to intermediate pressure and temperatures from 300 to 450 °C. In addition this suggests that all possible different lithologies were present in the latest metamorphic event.

Element mobility

If the samples from the whole drill core are derived from the same protolith, it is possible to establish which elements have been depleted and which elements have been enriched during the mineralization process. To do this, averages for the mineralized part and the unmineralized part has been calculated. Samples 77-86 (29,5m – 35,5m) are the mineralized part, while the remaining samples are considered as the unmineralized part.

From the results given in table 5.1 below, it is easily seen a big difference between the two parts. The largest compositional differences are observed for Al_2O_3 and CaO. Al_2O_3 is depleted in the mineralized zone by 1.97 Wt. % while CaO is elevated in the mineralized zone by 2.23 Wt. %. A thing to keep in mind is the relative change between the elements, Al_2O_3 change by 13.53 % while CaO change by 61.64 %. So the relative change for CaO is enormous. SiO_2 also has a notably decrease in the mineralized zone (1.37 Wt. %), but the relative change is very low (2.31 %). Trace elements which show a notable change in the mineralized zone are for the most part so-called immobile elements (which will be discussed in the next section) and As. As is unquestionably the element which has the most drastic enrichment (4267.63 %), the same can also be said about Au, but only the XRF-data is reviewed here. In the ICP-MS analysis Sb and Ag also show enrichment in the mineralized zone. There are some base metals (Cu and Pb) which have a great percentage change in the mineralized zone, but this is mainly due to the low concentration of these metals, and even the smallest change will have a great impact on the result.

When the results are reviewed a second time, but without sample 80 and 81 (heavily carbonatized) (table 5.2), the big changes in CaO and Al_2O_3 are almost completely gone. The change for CaO is 5.68 % and 1.79 % for Al_2O_3. Thus the big difference in Al_2O_3 and CaO observed in table 5.1 is mainly due to the heavily carbonization in sample 80 and 81, where carbonates has replaced Al minerals (micas). The change in the immobile elements however, is still present is still present after removing sample 80 and 81 (see section below).

	SiO2	TiO2	Al2O3	Fe2O3	MnO	MgO	CaO	Na2O	K2O	P2O5	H2O	
unmineralized	59,28	0,75	14,58	6,58	0,07	2,89	3,62	1,78	3,49	0,18	6,74	
mineralized	60,65	0,76	12,61	5,57	0,11	2,74	5,85	1,90	2,87	0,27	6,63	
difference in Wt. %	1,37	0,00	-1,97	-1,00	0,03	-0,15	2,23	0,12	-0,61	0,09	-0,11	
difference in %	2,31	0,20	-13,53	-15,26	47,79	-5,19	61,64	6,65	-17,59	49,67	-1,58	
	Ag	Cu	As	Bi	Sb	Se	S	Zn	Pb	Sn	Sc	V
unmineralized	3,03	0,01	32,75	0,50	6,24	0,13	0,55	0,01	0,00	4,94	15,67	120,69
mineralized	2,15	0,00	1430,40	2,30	6,95	0,00	0,89	0,01	0,00	4,88	10,46	90,07
difference in Wt. %	-0,88	-0,01	1397,65	1,80	0,71	-0,13	0,34	0,00	0,00	-0,06	-5,21	-30,62
difference in %	-28,93	-80,65	4267,63	360,00	11,42	-100,00	60,72	-13,30	860,00	-1,16	-33,24	-25,37
	Ga	Rb	Sr	Y	Zr	Nb	Cs	Ba	La	Ce	Th	
unmineralized	18,01	138,76	153,69	22,06	137,58	9,53	4,20	693,37	26,56	64,17	8,72	
mineralized	15,57	112,88	221,92	15,05	168,52	5,61	4,03	571,81	28,05	103,13	1,03	
difference in Wt. %	-2,44	-25,88	68,23	-7,01	30,95	-3,92	-0,17	-121,56	1,49	38,96	-7,69	
difference in %	-13,56	-18,65	44,40	-31,77	22,49	-41,10	-4,05	-17,53	5,62	60,72	-88,19	

Table 5.1: The table is showing the difference in concentration of various elements in the mineralized and unmineralized part of the core. The difference row in the table is given by: mineralized – unmineralized. The data is taken from the XRF-analysis.

	SiO2	TiO2	Al2O3	Fe2O3	MnO	MgO	CaO	Na2O	K2O	P2O5	H2O	
unmineralized	59,28	0,75	14,58	6,58	0,07	2,89	3,62	1,78	3,49	0,18	6,74	
mineralized	61,07	0,89	14,84	5,33	0,07	2,72	3,83	2,34	3,28	0,30	5,31	
difference in Wt. %	1,78	0,13	0,26	-1,24	0,00	-0,17	0,21	0,56	-0,21	0,11	-1,43	
difference in %	3,01	17,58	1,79	-18,91	2,41	-5,84	5,68	31,27	-6,08	62,38	-21,16	
	Ag	Cu	As	Bi	Sb	Se	S	Zn	Pb	Sn	Sc	V
unmineralized	3,03	0,01	32,75	0,50	6,24	0,13	0,55	0,01	0,00	4,94	15,67	120,69
mineralized	1,55	0,00	1716,00	2,63	6,74	0,00	0,70	0,01	0,00	4,81	11,23	101,24
difference in Wt. %	-1,48	-0,01	1683,25	2,13	0,50	-0,13	0,15	0,00	0,00	-0,13	-4,44	-19,45
difference in %	-48,76	-80,65	5139,69	425,00	8,02	-100,00	26,84	-14,29	-100,00	-2,53	-28,36	-16,12
	Ga	Rb	Sr	Y	Zr	Nb	Cs	Ba	La	Ce	Th	
unmineralized	18,01	138,76	153,69	22,06	137,58	9,53	4,20	693,37	26,56	64,17	8,72	
mineralized	17,73	125,14	236,26	16,08	202,34	6,43	4,19	685,73	31,55	117,26	1,29	
difference in Wt. %	-0,29	-13,62	82,58	-5,98	64,76	-3,10	-0,01	-7,64	4,99	53,09	-7,43	
difference in %	-1,60	-9,81	53,73	-27,12	47,07	-32,55	-0,30	-1,10	18,80	82,74	-85,23	

Table 5.2: The table is showing the same as table 5.1 above, but without sample 80 and 81 in the data set.

The Harker diagrams described in chapter 4 include some interesting features. The most apparent connection between elements is the one between As and Au. This connection is likely to come from the formation of arsenopyrite, since most of the Au identified (SEM analysis done by Scandinavian Highlands) is found within the arsenopyrites, which is the only mineral identified which holds As (FeAsS). The concentration of As is significant less in the unmineralized zone opposed to the mineralized one, and the arsenopyrites is only observed

within the mineralized zone. Arsenopyrite is also a mineral which is known to often host gold (Nesse, 2000). Sample 86 is the sample with the highest concentration of As (10468 PPM) and has the highest concentration of arsenopyrites and it is also the only sample where arsenopyrite is more abundant than pyrite. The concentration of As in sample 86 is 8 times higher than the sample with the second most (sample 85).

The Harker diagrams and correlation coefficients in chapter 4 also suggest there is a relationship between K and Na. The Harker diagram shows a negative correlation of 0.9, which could indicate a breakdown of a Na mineral into a K mineral. This also infers that there has been fluids present during the alteration, to add or remove elements from the rock. Clear evidence for fluids being present in the rock is seen by a numerous quartz and carbonate veins. A reaction which could describe this is the breakdown of albite ($NaAlSi_3O_{8)}$ into muscovite/sericite ($KAI_8Si_3O_{10}(OH_2)$

$3NaAlSi_3O_8$ (albite) + $K^+ + 2H^+ = KAl_3Si_3O_{10}(OH)_2$ (sericite) + $6SiO_2$ (quartz) + $3Na^+$ (Ishikawa, 1976)

These reactions could also explain why I have not identified plagioclase, but muscovite is abundant in the whole drill core.

The correlation between Mn and Ca are likely to come from the presence of carbonate veins in the samples. Sample 80 and 81 is the two samples with the highest percentage of Mn and Ca and the two samples with the highest amount of carbonates. The carbonates are likely to consist of either calcite ($CaCO_3$) or dolomite ($CaMg(CO_3)_2$), which is known to host Mn. If not, some of the carbonates could be rhodochrosite ($MnCO_3$), which is a mineral that mainly appear in hydrothermal veins (Nesse, 2000) such as the veins present in the drill core.

Therefore the variation in the Mn and Ca values seen in Figure 4.1 is likely to come from the precipitation of carbonates in veins.

Immobile elements

Some elements are considered to be immobile during alteration and metamorphism. Cann (1970) showed that Ti, Zr, and V contents in ocean floor basalts were unchanged during metamorphism and weathering. Winchester and Floyd (1977) also considered Nb, Ce, Ga, Y, and Sc to be immobile when they constructed a range of diagrams to discriminate between different magmatic series. This immobility of the elements mentioned above could help identify the protolith of the altered rock. The immobile elements plots will also help to identify possible different trends in the drill core. Floyd and Winchester (1978) states that when applying the different discrimination diagrams, you have to be sure that the protolith is a volcanic rock or a volcanogenic sedimentary rock. If not, the different geochemical plots are not valid. Even if the protolith isn't volcanic, the ratios between the immobile elements can be used to discriminate between different trends, but no magmatic origin can be established.

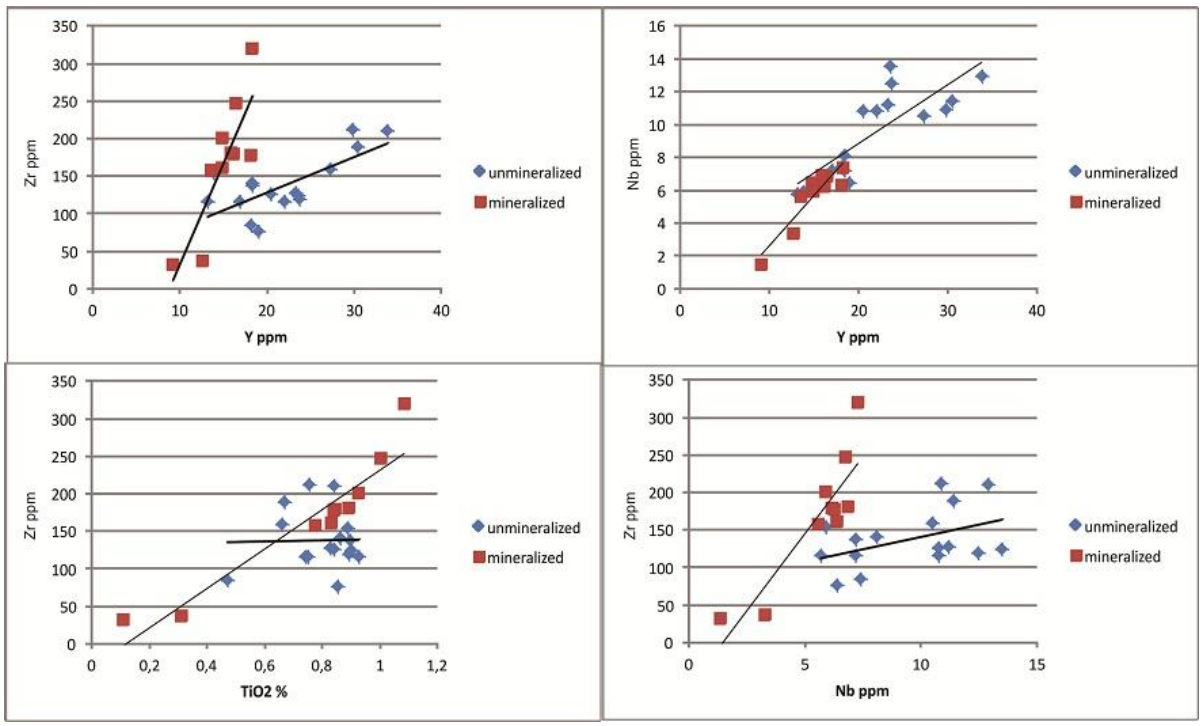

Figure 5.1: Harker diagrams showing the different trends for immobile elements, in the unmineralized and mineralized samples.

	Mineralized part	Unmineralized part	Mineralized + unmineralized
Ti/Zr	0,94	0,02	0,68
Y/Zr	0,84	0,71	0,32
Nb/Zr	0,88	0,44	0,25
Nb/Y	0,91	0,81	0,88

Table 5.3: The table is showing the correlation coefficients for some immobile elements. Note the big difference between the samples from the mineralization and the samples from the unmineralized part.

In Figure 5.1 some selected immobile elements are shown in Harker diagrams. The plots indicate that some of the ratios between the different elements change between the mineralized and unmineralized zone.

The Ti/Zr diagram (Figure 5.1) does not show any big difference in ratio between the elements. It might be better to remove the trend line for the unmineralized samples in the diagram, since they seem to be on the same trend line.

In the ratio between Y and Zr, there is an apparent difference in the ratio of the mineralized and the unmineralized samples. The same can also be seen for the ratios between Zr/Nb and Nb/Y.

The correlation coefficients in table 5.3 show a clear difference between the mineralization and the unmineralized part. All the coefficients from the mineralized part show a correlation (high numbers in table 5.3), while in the samples from the unmineralized part show no correlation. Only Nb/Y (0.81) and Zr/Y (0.71) to some extent show some correlation, while the other two shows no correlation. A problem for calculating the correlation coefficient for

the mineralization and unmineralized part separated and not together, is that the numerical basis is very poor, and single outliers can have a big impact on the result. Sample 80 and 81 are the two outliers in the mineralized part.

Based on the results from the immobile element plots it can be reasonable to assume that the core might not consist of one single lithology, since it shows to distinct trends. It might be more likely that the drill core consist of minimum two different lithologies. The different lithologies would in that case be the Au mineralized part and the unmineralized part. This also fits well with the observations made in the drill core description. Here it was observed two possible breaks in the lithologies, one over the mineralization and one under the mineralization. The breaks in the lithologies were emphasized by veins which cut through the whole core width.

So if the drill core consists of two different lithologies, one possible origin could be that an intrusive intruded the unmineralized part. This might be likely since the lithology above and under the Au mineralization is the same and sharp contacts separates (emphasized by veins) the Au mineralization from the unmineralized part. If this is the case; the samples from the Au-mineralization are magmatic and could be plotted into a diagram to identify a magmatic protolith.

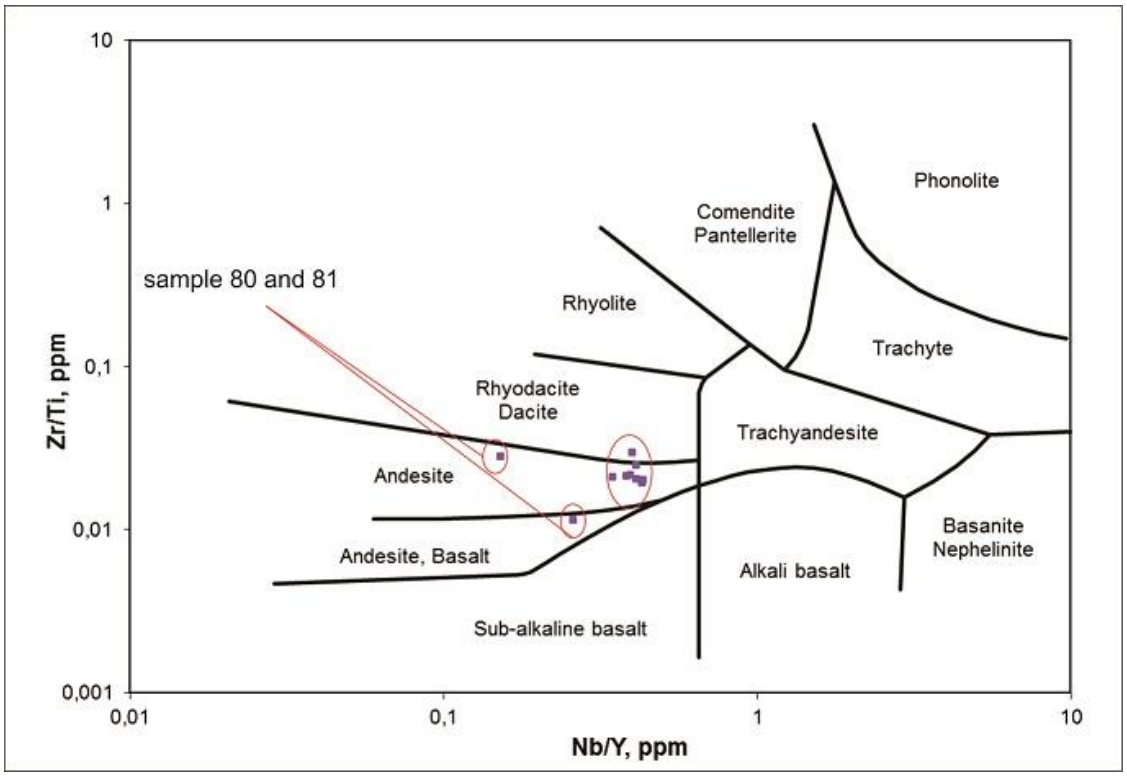

Figure 5.2: The figure shows the XRF data plotted in Winchester and Floyds (1977) diagram for discrimination between different magma series.

In figure 5.2 the XRF data from the Au mineralization is plotted in Winchester and Floyds (1977) discrimination diagram. In the diagram there is a cluster of samples and two outliers. The two outliers are sample 80 and 81 which are subjected to intensive carbonatization. The cluster of samples, plot in the area of andesite and the boundary between rhyodacite/dacite and andesite.

When the samples are plotted in Le Maitre et al (1989) they show the same trend as in the diagram of Cann (1979). Most of the samples plot in the field of andesite, but two samples plot in the field of basaltic andesite. The samples also plot high in the andesite field (except sample 80 and 81), towards trachy andesite. The total alkali vs. silica diagram of Le Maitre is constructed for use on fresh volcanic rocks, since the alkalis tend to be mobilized during metamorphism. In my samples at least silica has been mobilized since numerous quartz veins is identified throughout the core. So the diagram can only be used an indicator for the

magmatic origin, but never the less it gives the same result as the immobile element diagram of Winchester and Floyds (1977).

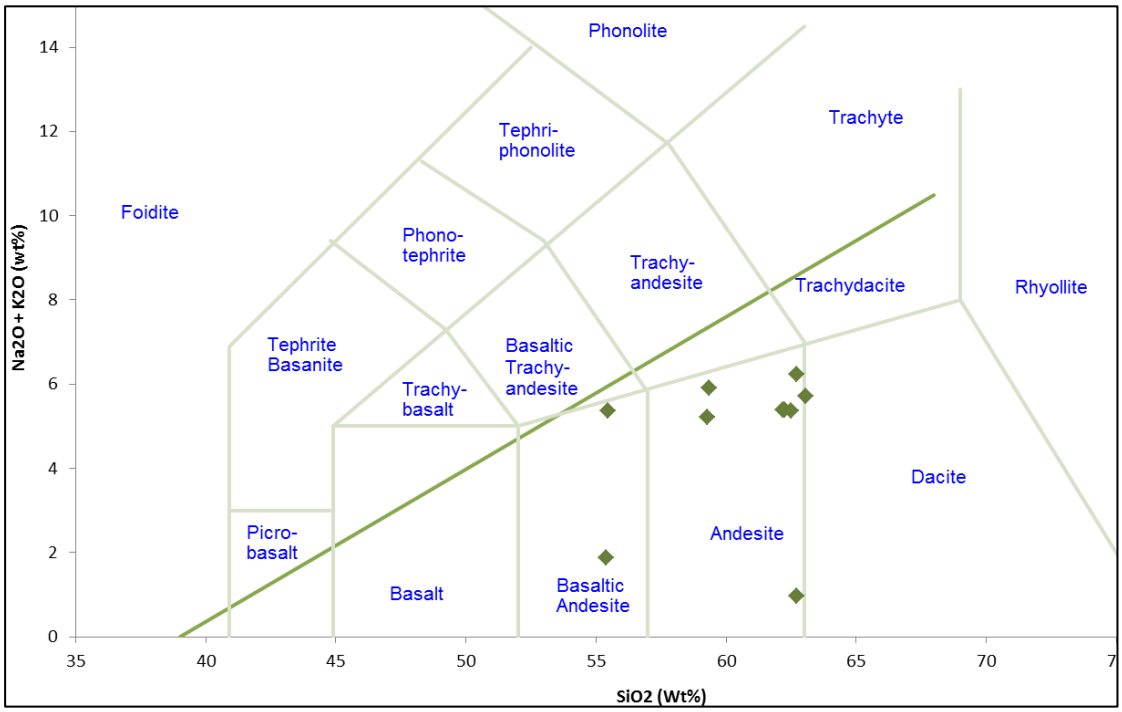

Figure 5.3: XRF data plotted in Le Maitre et al (1989) diagram for discriminating between different magmatic series.

Based on the results from the diagrams presented previous in this section (figure 5.2 and 5.3), a magmatic origin for the Au mineralized part can be inferred. Both diagrams suggest an andesitic composition for the protolith of the Au mineralized zone, but this is only valid if the zone has a magmatic protolith. Andesite is a typical rock of convergent margins e.g. (Blatt, 2006) and often found in subduction zones.

Sedimentary or igneous origin of the rocks hosting the Au mineralized zone?

Based on the investigations done of the drill core it is difficult to establish a certain protolith. The rock could be either a sedimentary or ingenious rock. Either way, the rock has been subjected to metamorphism and the original mineral assemblage has been replaced by other minerals.

The whole drill core has more or less the same mineralogy and chemical composition as shown in the previous sections. So if there have been an intrusion into the unmineralized zone, the chemical composition of the intrusion would need to be similar to the intruded unit, or the metasomatic process taking part in the rocks would need to be extensive.

There are two important facts which point towards an igneous origin. The diagram for the immobile elements in Figure 5.1 show two distinct trends, one for the unmineralized part and one for the Au mineralization. In addition the correlation coefficients in table 5.3 are much higher for the Au mineralization than the unmineralized part. These coefficients could indicate a difference in origin. The unmineralized part shows a lower correlation which could point towards a sedimentary origin with material obtained from different sources. While the Au mineralization has high correlation coefficients in the immobile elements, which would be expected for a igneous protolith (Winchester and Floyd, 1977).

In addition to the immobile plots, the observations done during the core logging suggest a second lithology. There is observed a distinct lithological break both over and under the Au mineralization and the rocks above and below the Au mineralization are similar. So these two indications point towards a magmatic origin for Au mineralized part.

The facts that indicate a non-magmatic origin would be the consistency of the mineral assemblage and consistency of the chemical composition. This indicates that the mineralized zone is a meta-sedimentary rock just like the unmineralized zone.

Based on the data I got available for this thesis it is difficult to establish a protolith for the Au mineralization. The mineralization could either be of magmatic or sedimentary origin.

Alteration during formation of the mineralization

To identify the mineralization type several alteration indexes has been used. The index of Ishikawa (1976) was developed to quantify the alteration in the footwall of volcanic massive sulfides. It is applied here since it also describes the alteration within a hydrothermal system.

$$\mathrm{AI} = \frac{100\ (\mathrm{K2O}\ +\ \mathrm{MgO})}{(\mathrm{K2O}\ +\ \mathrm{MgO}\ +\ \mathrm{Na2O}\ +\ \mathrm{CaO}).}$$

Two of the reactions explaining the equation are:

1) $3NaAlSi_3O_8$ (albite) + K^+ + $2H^+$ =$KAl_3Si_3O_{10}(OH)_2$ (sericite) + $6SiO_2$ (quartz) + $3Na^+$
2) $2KAl_3Si_3O_{10}(OH)_2$ (sericite) + $3H_4SiO_4$ + $9Fe2^+$ + $6Mg2^+$ + $18H_2O$
   =$3Mg_2Fe_3Al_2Si_3O_{10}(OH)_8$ (chlorite) + $2K^+$ + 28H+

The first reaction describes the replacement of albite by sericite, whereas the second one shows the reaction where chlorite becomes the more dominant one on the expense of sericite (Large et al, 2001).

The chlorite-carbonate-pyrite index (CCPI index) measures the increase in FeO and MgO associated with Mg-Fe chlorite development (Large et al, 2001) . This reaction takes place when chlorite replaces albite, K-feldspar or sericite.

$$CCPI = \frac{100\ (MgO\ +\ FeO)}{(MgO\ +\ FeO\ +\ Na2O\ +\ K2O)}$$

Large et al (2001) gives a plot (figure 5.4) to define how altered a rock is and which type of alteration is present. This plot combines the Ishikawa index (x-axis) and the CCPI index (y-axis). The idea is that the further the rock plots from the center, the more altered the rock is. The different arrows in the diagram indicate which type of alteration you have and which mineral assemblage you can expect. The AI values (Alteration Index) and CCPI values used in the thesis are calculated on the basis of the values given in appendix 1 (XRF) and appendix 2 (ICP-MS).

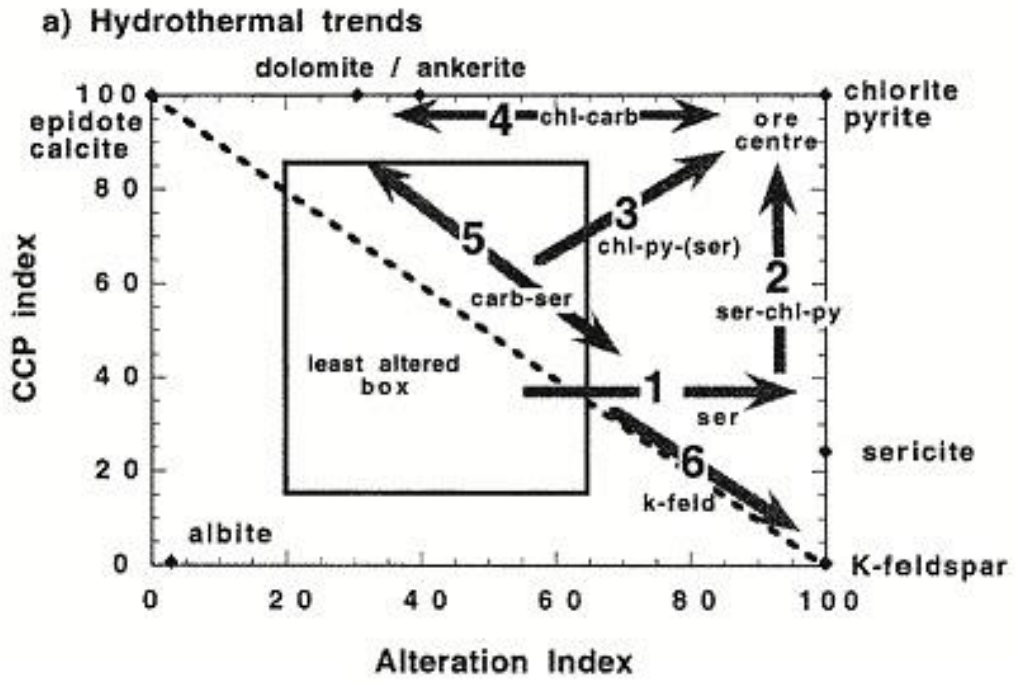

Figure 5.4: The different alteration trends in the box plot (Large et al. 2001).

Figure 5.3 shows values of the CCPI index plotted against the alteration index data from the ICP-analyses. The samples are divided into appropriate intervals. The intervals are decided by their AI values (Ishikawa index).

From the diagram there is one evident trend; there is a cluster of samples which start just outside “the least altered box”. These samples are the ones collected just above the mineralization and the ones straight below. This indicates that the area around the

mineralization is the most altered. There is also one other group which plots outside “the least altered box”, this group is from the interval 66.5 to 73.5. The rest of the data plot within the least altered box. The samples which plot outside the least altered box, plots towards sericitic, pyritic, and chloritic alteration (Figure 5.2). The rest of the samples including the mineralized zone are less altered.

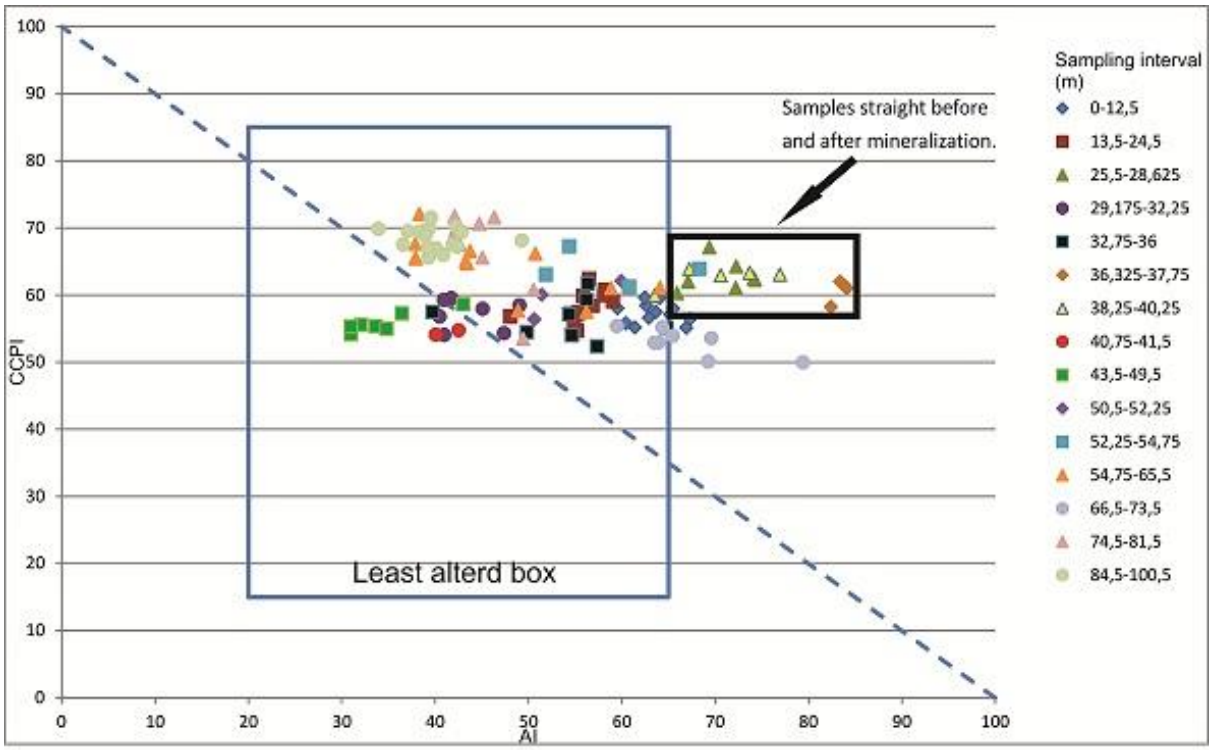

Figure 5.5: Box plot with samples from ICP-analysis showing how altered the rocks are. Notice the samples in the black box which are the samples just over and under the mineralization.

When the XRF-data are plotted in the Box plot (Figure 5.4), they show much of the same trends as the ICP-data in the diagram above. The samples straight below and over the mineralization are the ones which plot furthest towards sericitic, pyritic, and chloritic alteration, while the samples in the mineralized zone are less altered. The data from the XRF-analysis are analysis from a tiny interval (+/- 10 cm) and therefore sample 80 and 81 plot outside the box. They plot away from the center and towards carbonatization. This fits very well with the observations from the thin sections. Sample 80 and 81 are the two samples with the highest percentage of carbonates and therefore they plot away from the other samples and towards carbonatization

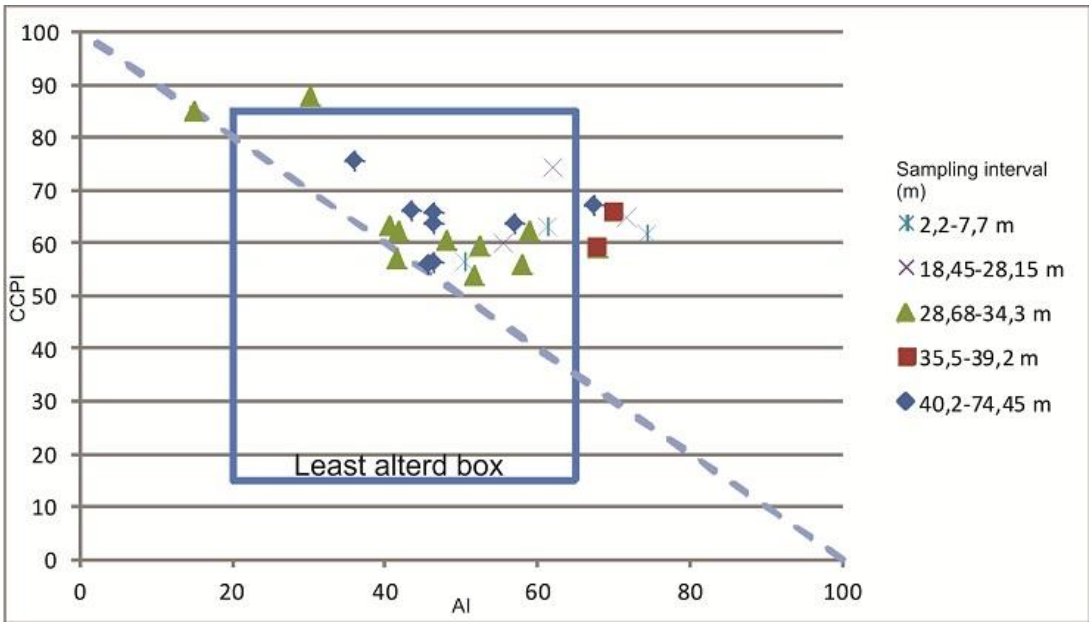

Figure 5.6: Box plot with samples from XRF-analysis showing how altered the rocks are. The two samples in the upper right corner are sample 80 and 81.

After plotting the data in the box plot, the trend of sericitic alteration for the samples around the mineralization was followed up. This was done by taking a closer look at the mineral table in Table 3.1. When plotting the concentration of muscovite and AI along the y-axis, and the sampling interval from the drill core along the x-axis. A connection can be inferred. The samples were only plotted against the AI index since the variation in the CCPI index was very low. Figure 5.5 indicates that there is a connection between the AI and the abundance of muscovite. This connection supports the Box Plot findings, which state that the samples around the mineralization are the samples subjected for the heaviest sericitization. The sericitization is seen in thin sections as a greater amount of muscovite in the samples. Both curves have clear peaks over and under the mineralization.

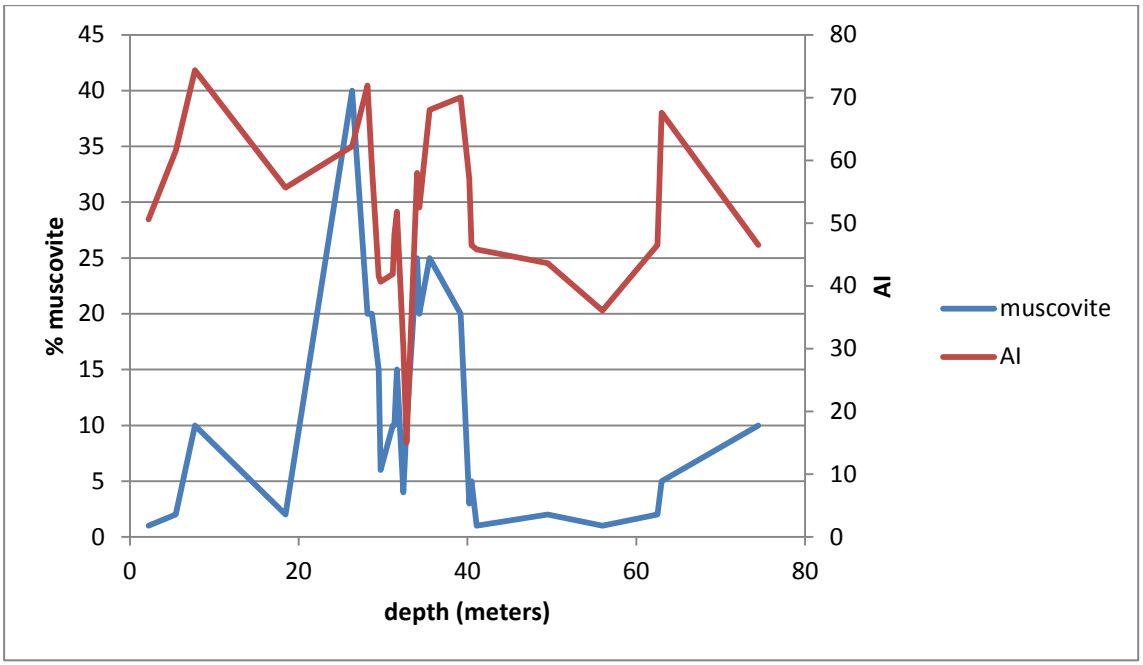

Figure 5.7: Diagram showing the development of the alteration index together with the muscovite concentration in the core.

This connection is only partially seen when plotting chlorite against Ai (Figure 5.8). There are spikes present over and under the Au mineralization, but there are also several other spikes and this could indicate that sericitization is the dominant alteration. Another fact which would emphasis this is that chlorite almost entirely appears as a rim on calcite veins. So when the samples plot towards chlorite and sericite alteration, sericite appears to be the dominant form of alteration.

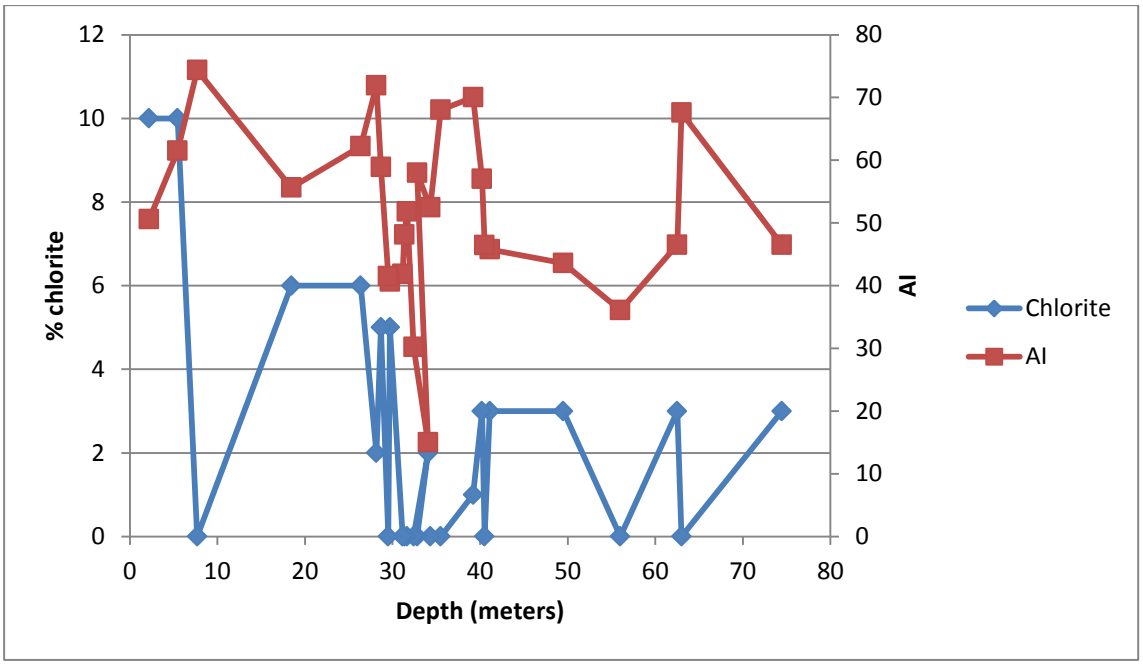

Figure 5.8: Diagram showing the development of the alteration index together with the chlorite concentration in the core.

Presence of indicator minerals

When going through the chemical analysis done for this thesis (XRF-analysis and SEM), there has not been any visualization of gold. The determination of the Au mineralization has been based on previous investigations done by Scandinavian Highlands (ICP-MS analysis and SEM). Only gold indicator minerals have been identified. The telluride minerals identified by SEM is known to be indicator minerals of gold (McClenaghan and Cabri, 2011). Arsenopyrite and pyrite is also known to be an indicator and host mineral for gold (Cook and Chryssoulis, 1990).

Based on those indicators it might be reasonable to suggest there is a potential for good gold grades in this mineralization.

Similarities to the West Troms Basement Complex

The Mauken window is a thought continuation of the WTBC and therefore it might be likely that rocks Mauken have undergone the same metamorphic and tectonic events as the WTBC.

In the WTBC there are several supracrustal belts which are accompanied by steep ductile shear zones (Bergh et al., 2010). The Senja Shear Zone is a assumed part of the Bothnian-Senja Shear zone of Svecofennian age (Doré et al., 1997) and hosts several metasupracrustal belts with NW-SE orientation. This is the same orientation as the shear zone hosting the Au mineralization in Mauken. This could indicate a similar age for the formation of the shear zone in Mauken which host the mineralization. This period is also known to have formed most of the ores in the Fennoscandian shield (Weihed et al., 2005).

The minimum age for the for the Mauken basement rocks was given by intruding granitoids with an age of 1706 +/- 15 and 1768 +/- 49 Ma (Norges geologiske undersøkelse, 2012). The age of these granitoids is somewhat younger than the intrusions found in WTBC. The Ersfjord granite has a U-Pb age of 1792 +/- 5 Ma (Corfu et al., 2003), the norite at Hamn in Senja has been dated to 1802.3 +/- 0.7 Ma (Kullerud et al., 2006).

Type of mineralization

The Au mineralization at Mauken is likely to have formed in relation to the Svecofennian orogeny and at this period the Baltic shield was dominated by convergent tectonics (Gaál and Gorbatschev, 1987).

Groves et al (1998) suggest the term orogenic gold for deposits formed in relation to convergent tectonic. In addition they apply the term mesozonal, for deposits formed at temperatures of 300-475°C and depths of 6-12 km. Metals often found in association with orogenic gold are As, B, Bi, Sb, Te, and W (Groves et al., 2003). In the mineralized zone in Mauken there is an enrichment of As and Sb, and Bi and Te minerals are identified. The mineralization has also been located to a shear zone and if figure 5.9 is applied, the formation of the Mauken mineralization would be in the transpressional environment and the mesozonal Au-As-Te zone.

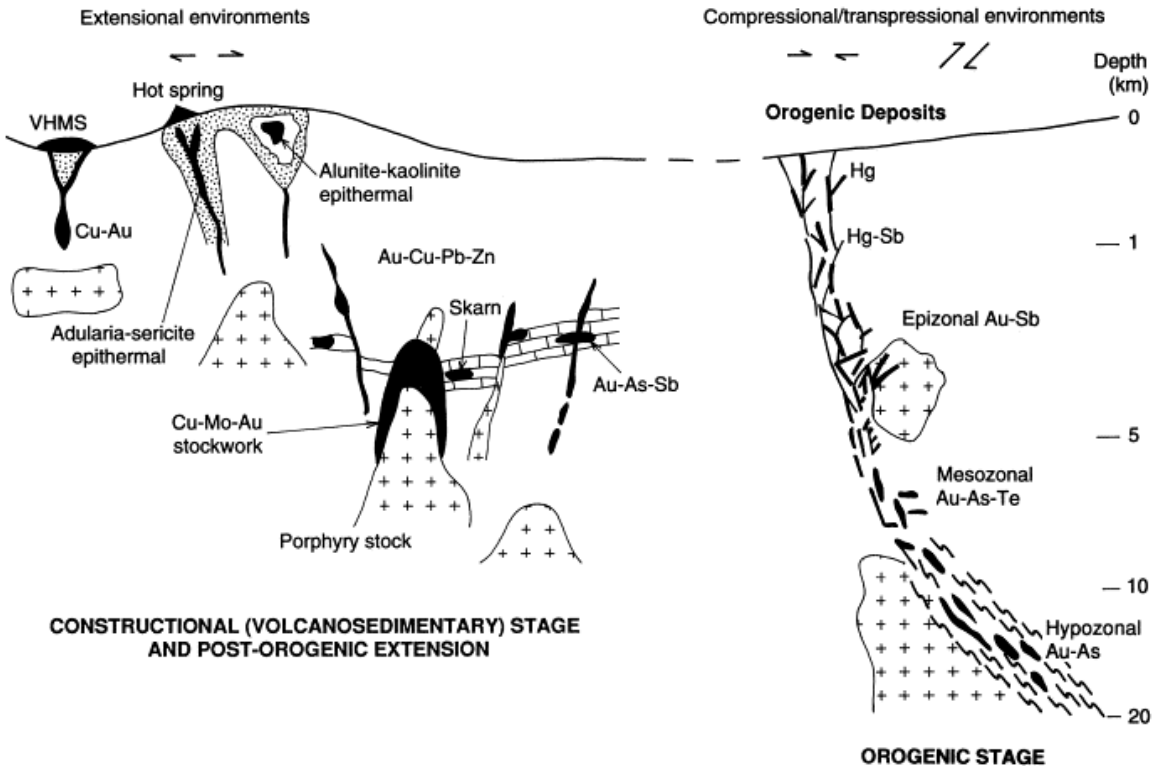

Figure 5.9: Schematic representation of crustal environments of hydrothermal gold deposits in terms of depth of formation and structural setting within a convergent plate margin. From (Groves et al., 1998).

When looking at the tectonic setting for orogenic gold in figure 5.10, it is seen that orogenic gold is found in the vicinity of granitoids. Granitoids are also found as intrusive rocks intruding into the meta-sedimentary unit of the Mauken basement window.

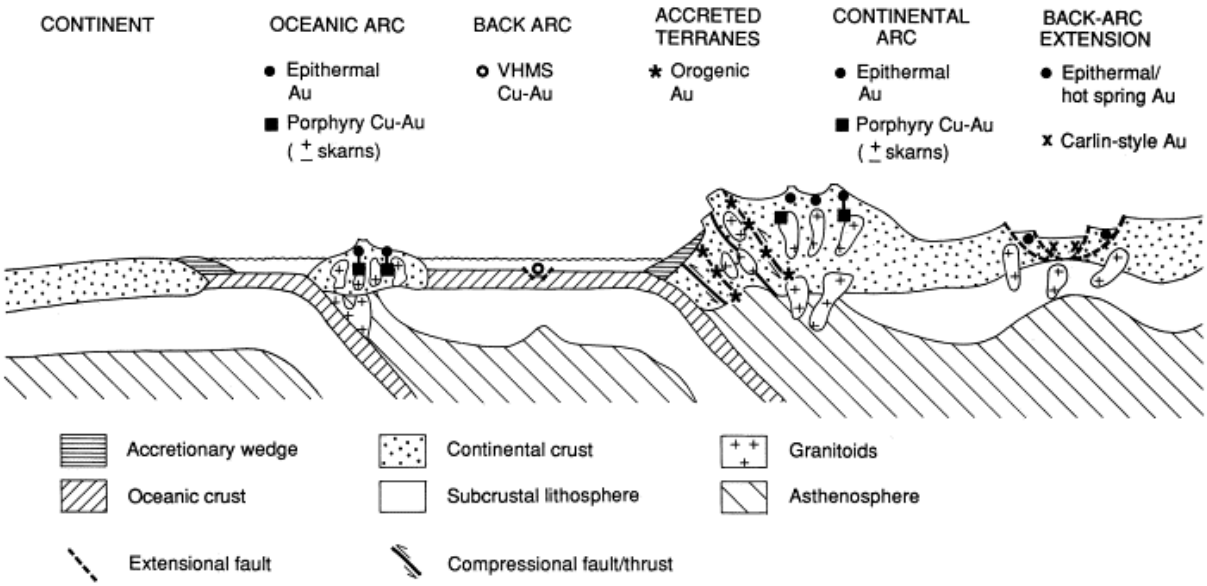

Figure 5.10: Tectonic settings of gold-rich epigenetic mineral deposits. Note that both the lateral and vertical scale of the arcs and accreted terranes have been exaggerated to allow the gold deposits to be shown in terms of both spatial position and relative depth of formation. From (Groves et al., 1998)

6. Conclusions

- Based on similarities to other provinces in the Fennoscandian shield, it is likely that the formation of the Au mineralization at Mauken occurred in relation to the Svecofennian orogeny.
- The rocks which host the Au mineralization have been metamorphosed under greenschist facies conditions.
- The protolith of the mineralization is uncertain and could either be of magmatic or sedimentary origin as the surrounding rocks are.
- The mineralization could be classifies as orogenic gold.
- The Au mineralization is closely linked to the formation of arsenopyrites, which most of the gold is situated within.
- The Au mineralized zone has been enriched in Sb, As, Ag, and P.
- The Au mineralization is surrounded by an alteration halo, which is dominated by sericitization, but also some chloritization is present.
- The Mineral assemblage of the rocks investigated is dominated by quartz, micas, and carbonates. Chlorite and sulfides are also present to some extent, sulfides are mainly pyrite.

7. References

AIRO, M. L. & MERTANEN, S. 2008. Magnetic signatures related to orogenic gold mineralization, Central Lapland Greenstone Belt, Finland. *Journal of Applied Geophysics*, 64(1–2), pp. 14-24. doi: http://dx.doi.org/10.1016/j.jappgeo.2007.10.003.

BERGH S.G., K. K., P.E.B. ARMITAGE, K.B. ZWAAN, F. CORFU, E.J.K. RAVNA, P.I. MYHRE. 2010. Neoarchaean to Svecofennian tectono-magmatic evolution of the West Troms Basement Complex North Norway. *Norwegian Journal of Geology,*, 90 (2010), pp. pp 21-48.

BERTHELSEN, A. 1967. *Geologic and structural studies around two geophysical anomalies in Troms, Northern Norway.,*. Series: Årbok 247, Norges geologiske undersøkelse.

BILLSTRÖM, K., BROMAN, C., JONSSON, E., RECIO, C., BOYCE, A. J. & TORSSANDER, P. 2009. Geochronological, stable isotopes and fluid inclusion constraints for a premetamorphic development of the intrusive-hosted Björkdal Au deposit, northern Sweden. *International Journal of Earth Sciences*, 98(5), pp. 1027-1052. doi: 10.1007/s00531-008-0301-8.

BJØRLYKKE, A., HAGEN, R. & SODERHOLM, K. 1987. Bidjovagge copper-gold deposit in Finnmark, Northern Norway. *Economic Geology*, 82(8), pp. 2059-2075. doi: 10.2113/gsecongeo.82.8.2059.

BLATT, H., TRACY R.J., OWENS, B.E.,. 2006. *Petrology. Igneous, Sedimentary, and Metamorphic*. Third ed. W. H. Freeman and Company.

BUCHER, K., FREY, M.,. 1994. *Petrogenesis of Metamorphic Rocks*. 6th ed. Springer-Verlag Berlin Heidelberg.

CANN, J. R. 1970. Rb, Sr, Y, Zr and Nb in some ocean floor basaltic rocks. *Earth and Planetary Science Letters*, 10(1), pp. 7-11. doi: http://dx.doi.org/10.1016/0012-821X(70)90058-0.

COOK, N. J. & CHRYSSOULIS, S. L. 1990. Concentrations of invisible gold in the common sulfides. *The Canadian Mineralogist*, 28(1), pp. 1-16.

CORFU, F., ARMITAGE, P. E., KULLERUD, K. & BERGH, S. G. 2003. Preliminary U-Pb geochronology in the West Troms Basement Complex, North Norway: Archaean and Palaeoproterozoic events and younger overprints. *NORGES GEOLOGISKE UNDERSOKELSE*, 441, pp. 61-72.

DORÉ, A. G., LUNDIN, E. R., FICHLER, C. & OLESEN, O. 1997. Patterns of basement structure and reactivation along the NE Atlantic margin. *Journal of the Geological Society*, 154(1), pp. 85-92. doi: 10.1144/gsjgs.154.1.0085.

ETTNER, D. C., BJØRLYKKE, A. & ANDERSEN, T. 1993. Fluid evolution and Au・Cu genesis along a shear zone: a regional fluid inclusion study of shear zone-hosted alteration and gold and copper mineralization in the Kautokeino greenstone belt, Finnmark, Norway. *Journal of Geochemical Exploration*, 49(3), pp. 233-267. doi: http://dx.doi.org/10.1016/0375-6742(93)90047-P.

GAÁL, G. & GORBATSCHEV, R. 1987. An Outline of the precambrian evolution of the baltic shield. *Precambrian Research*, 35(0), pp. 15-52. doi: 10.1016/0301-9268(87)90044-1.

GROVES, D. I., GOLDFARB, R. J., GEBRE-MARIAM, M., HAGEMANN, S. G. & ROBERT, F. 1998. Orogenic gold deposits: A proposed classification in the context of their crustal distribution and relationship to other gold deposit types. *Ore Geology Reviews*, 13(1–5), pp. 7-27. doi: http://dx.doi.org/10.1016/S0169-1368(97)00012-7.

GROVES, D. I., GOLDFARB, R. J., ROBERT, F. & HART, C. J. R. 2003. Gold Deposits in Metamorphic Belts: Overview of Current Understanding, Outstanding Problems, Future Research, and Exploration Significance. *Economic Geology*, 98(1), pp. 1-29. doi: 10.2113/gsecongeo.98.1.1.

GUSTAVSON, M. 1974. Geologisk kart over Norge, berggrunnskart Narvik 1:250000. Norges geologiske undersøkelse.

ISHIKAWA, Y., SAWAGUCHI, T., IWAYA, S., AND HORIUCHI, M., . 1976. Delineation of prospecting targets for Kuroko deposits based on modes of volcanism of underlying dacite and alteration halos. *Mining Geology*, 26, pp. 105–117.

KOJONEN, K. & JOHANSON, B. 1999. Determination of refractory gold distribution by microanalysis, diagnostic leaching and image analysis. *Mineralogy and Petrology*, 67(1-2), pp. 1-19. doi: 10.1007/bf01165112.

KRETZ, R. 1983. Symbols for rock-forming minerals. *American Mineralogist*, 68, pp. 277-279.

KRILL, A. G. B., STEFFEN; LINDAHL, INGVAR. 1985. Rb-Sr, U-Pb and Sm-Nd isotopic dates from Precambrian rocks of Finnmark. *Norges geologiske undersøkelse, Bulletin*, 403, pp. 37-54.

KULLERUD, K., CORFU, F., BERGH, S. G., DAVIDSEN, B. & RAVNA, E. K. . 2006. U- Pb constraints of the Archaean and Early Proterozoic evolution of the West Troms Basement Complex, North Norway (Abstract). *Bulletin of the Geological Society of Finland* (Special Issue I,), p. p 79.

LANDMARK, K. 1967. *Description of the geological maps "Tromsø" and "Målselv", Troms*. Series: Årbok 247, Norges geologiske undersøkelse.

LARGE, R. R., J. BRUCE GEMMELL AND HOLGER PAULICK. 2001. The alteration box plot; a simple approach to understanding the relationship between alteration mineralogy and lithogeochemistry associated with volcanic-hosted massive sulfide deposits. *Economic Geology and the Bulletin of the Society of Economic Geologists*, 96 (5), pp. 957-971.

MCCLENAGHAN, M. B. & CABRI, L. J. 2011. Review of gold and platinum group element (PGE) indicator minerals methods for surficial sediment sampling. *Geochemistry: Exploration, Environment, Analysis*, 11(4), pp. 251-263. doi: 10.1144/1467-7873/10-im-026.

MOTUZA, G., MOTUZA, V., BELIATSKY, B., SAVVA, E. 2001. The Ringvassøy greenstone belt (Tromsø, North Norway): implications for a Mesoarchaean subduction zone. *Implication for the Stratigraphy and Tectonic Setting. Journal of Conference (Abstract)*.

NESSE, W. D. 2000. *Introduction to mineralogy*. Oxford University press.

Norge i bilder. 2012. Available at: http://www.norgeibilder.no/ [2012].

Norges geologiske undersøkelse, nasjonal berggrunnsdatabase. 2012. Available at: http://geo.ngu.no/kart/berggrunn/ [2012].

ROBERTS, D. 2003. The Scandinavian Caledonides: event chronology, palaeogeographic settings and likely modern analogues. *Tectonophysics*, 365(1–4), pp. 283-299. doi: 10.1016/s0040-1951(03)00026-x.

RODIONOV ALEXEI, J. K. A. R. L. 2012. *Helicopter-borne magnetic, electromagnetic and radiometric geophysical survey in Mauken area, Målselv, Troms*. NGU Report. NGU.

ROLLINSON, H. 1993. *Using geochemical data: evaluation, presentation, interpretation*. 1 ed. Series: Longman Geochemistry series. Addison Wesley Longman Limited.

SANDSTAD, J. S., NILSSON, L.P. 1998. *Gullundersøkelser på Ringvassøy, sammenstilling av tidligere prospektering og feltbefaring i 1997*. NGU rapport.

WANHAINEN, C., BILLSTRÖM, K., MARTINSSON, O. 2006. Age, petrology and geochemistry of the porphyritic Aitik intrusion, and its relation to the disseminated Aitik Cu-Au-Ag deposit, northern Sweden. *GFF*, 128:4, pp. 273-286.

WEIHED, P., ARNDT, N., BILLSTRÖM, K., DUCHESNE, J.-C., EILU, P., MARTINSSON, O., PAPUNEN, H. & LAHTINEN, R. 2005. Precambrian geodynamics and ore formation: The Fennoscandian Shield. *Ore Geology Reviews*, 27(1–4), pp. 273-322. doi: 10.1016/j.oregeorev.2005.07.008.

WEIHED, P., WEIHED, J. B. & SORJONEN-WARD, P. 2003. Structural Evolution of the Björkdal Gold Deposit, Skellefte District, Northern Sweden: Implications for Early Proterozoic Mesothermal Gold in the Late Stage of the Svecokarelian Orogen. *Economic Geology*, 98(7), pp. 1291-1309. doi: 10.2113/gsecongeo.98.7.1291.

WINCHESTER, J. A. & FLOYD, P. A. 1977. Geochemical discrimination of different magma series and their differentiation products using immobile elements. *Chemical Geology*, 20(0), pp. 325-343. doi: http://dx.doi.org/10.1016/0009-2541(77)90057-2.

ZWAAN, K. B., FARETH, E. & GROGAN, P. W. 1998. Geologisk kart over Norge, berggrunnskart Tromsø 1:250000. Norges geologiske undersøkelse.

Appendix

Appendix 1: Concentrations of elements, from XRF-analysis. Oxides are given in percentage, the rest is given in PPM.

	SiO2	TiO2	Al2O3	Fe2O3	MnO	MgO	CaO	Na2O	K2O	P2O5	H2O	Ag	Cu
568993	60,85	0,67	14,14	4,37	0,08	1,60	5,36	0,38	4,27	0,15	8,12	0,60	0,00
568992	64,44	0,69	13,54	5,45	0,08	2,33	3,11	0,74	3,82	0,15	5,63	5,40	0,00
568991	60,67	0,79	16,56	6,98	0,06	2,61	1,38	1,18	4,82	0,13	4,81	7,60	0,00
568990	62,03	0,77	15,69	5,67	0,08	2,14	2,74	1,75	3,49	0,17	5,46	0,00	0,00
568989	71,24	0,43	9,23	6,53	0,05	1,65	1,99	0,47	2,39	0,10	5,90	4,00	0,01
568988	58,33	0,74	16,87	7,72	0,05	2,90	1,53	1,34	4,44	0,14	5,96	0,90	0,00
568987	59,60	0,87	15,34	5,91	0,07	3,00	3,62	1,32	4,09	0,27	5,89	1,30	0,00
568986	59,52	0,90	15,62	5,40	0,06	2,40	4,09	3,17	2,76	0,31	5,75	0,60	0,00
568985	55,45	0,86	14,47	5,66	0,12	3,57	6,82	2,54	2,84	0,33	7,32	2,60	0,00
568984	59,54	1,02	14,08	5,72	0,11	3,00	5,37	2,57	2,72	0,36	5,50	0,00	0,00
568983	62,15	0,93	14,32	5,59	0,07	2,71	3,54	2,51	2,91	0,30	4,97	1,60	0,00
568982	62,66	0,91	14,94	4,69	0,05	2,55	2,39	3,00	3,25	0,27	5,28	2,70	0,00

568981	55,31	0,33	4,48	9,74	0,24	3,52	12,27	0,04	1,82	0,31	11,92	1,70	0,00
568980	62,72	0,13	2,88	3,34	0,24	2,10	15,65	0,25	0,72	0,05	11,91	7,40	0,00
568979	63,32	0,83	15,39	4,96	0,05	2,36	2,60	1,90	3,84	0,27	4,46	1,40	0,00
568978	63,15	0,79	14,81	5,27	0,07	2,78	3,54	2,08	3,43	0,26	3,81	2,50	0,00
568977	62,76	0,86	15,12	5,39	0,05	2,39	2,28	0,94	4,47	0,29	5,41	1,00	0,00
568976	56,82	0,81	16,96	7,88	0,05	3,59	1,59	1,74	4,20	0,13	6,21	4,30	0,00
568975	54,85	0,84	17,03	7,67	0,06	3,44	3,44	2,24	4,11	0,16	6,13	3,80	0,01
568974	62,70	0,86	14,90	5,02	0,05	2,42	3,04	2,96	2,79	0,33	4,91	2,30	0,00
568973	62,54	0,83	14,77	5,21	0,06	2,46	2,83	3,32	2,74	0,29	4,94	4,30	0,00
568972	57,49	0,86	14,44	7,27	0,07	3,48	3,82	3,42	2,12	0,27	6,75	2,00	0,01
568971	46,56	0,85	12,88	8,38	0,15	5,77	10,13	2,96	1,62	0,17	10,52	0,30	0,01
568970	58,29	0,76	12,60	5,94	0,09	3,48	5,71	1,83	3,09	0,18	8,01	5,20	0,00
568969	54,82	0,68	15,42	10,09	0,04	2,80	1,16	2,17	4,14	0,12	8,54	3,70	0,07
568968	57,33	0,62	13,00	5,21	0,12	2,54	6,53	0,68	3,73	0,15	10,06	2,70	0,01
	As	Bi	Sb	Se	S	Zn	Pb	Sn	Sc	V	Cr	Co	
568993	28,00	0,00	3,90	0,00	0,04	0,01	0,00	5,20	10,70	73,90	159,70	8,60	

568992	31,00	1,00	13,20	0,00	0,04	0,01	0,00	4,80	11,00	84,60	224,90	14,20	
568991	26,00	0,00	5,70	0,00	0,04	0,01	0,00	3,70	17,60	117,70	181,70	18,80	
568990	26,00	0,00	1,30	0,00	0,02	0,01	0,00	2,90	13,50	94,50	216,70	12,20	
568989	17,00	1,00	7,60	0,00	1,57	0,01	0,00	2,70	9,40	75,20	253,40	25,10	
568988	24,00	0,00	4,90	0,00	0,03	0,01	0,00	1,70	11,10	76,30	185,50	8,50	
568987	63,00	0,00	6,00	0,00	0,46	0,01	0,00	11,10	14,30	112,90	202,50	11,60	
568986	10468,00	11,00	7,70	0,00	1,04	0,01	0,00	8,10	13,10	108,60	260,40	12,30	
568985	1272,00	4,00	9,30	0,00	0,59	0,01	0,00	0,00	11,30	99,80	198,60	11,10	
568984	77,00	0,00	3,10	0,00	0,49	0,01	0,00	10,60	10,80	108,80	224,10	12,90	
568983	65,00	0,00	5,20	0,00	0,56	0,01	0,00	4,20	12,60	104,90	236,00	13,20	
568982	520,00	2,00	10,90	0,00	0,52	0,01	0,00	4,00	10,60	101,30	223,60	5,90	
568981	417,00	2,00	7,40	0,00	2,69	0,02	0,00	6,10	9,00	68,40	210,60	16,10	
568980	159,00	0,00	8,20	0,00	0,58	0,01	0,01	4,20	5,80	22,40	225,20	2,70	
568979	54,00	1,00	5,50	0,00	0,74	0,01	0,00	5,20	10,80	96,00	275,10	10,80	
568978	851,00	3,00	8,70	0,00	0,89	0,01	0,00	4,10	10,20	91,50	273,80	10,60	
568977	421,00	0,00	3,50	0,00	0,77	0,01	0,00	2,30	10,40	99,00	219,50	10,60	

568976	32,00	2,00	5,70	0,00	0,90	0,02	0,00	8,20	22,80	165,10	240,80	18,50	
568975	23,00	0,00	3,30	0,00	0,90	0,02	0,00	4,60	20,20	168,80	220,80	19,90	
568974	72,00	1,00	11,80	0,00	0,22	0,01	0,00	3,70	13,00	106,00	235,80	17,10	
568973	22,00	1,00	12,40	0,00	0,05	0,01	0,00	4,70	11,10	93,40	210,40	12,30	
568972	37,00	0,00	4,00	0,00	0,72	0,01	0,00	0,00	16,50	131,70	192,60	24,30	
568971	24,00	1,00	1,30	0,00	0,21	0,01	0,00	8,70	24,80	177,10	267,10	22,80	
568970	54,00	0,00	4,90	0,00	0,13	0,01	0,00	3,90	14,20	124,80	320,20	16,60	
568969	19,00	1,00	7,40	2,00	2,26	0,01	0,00	8,70	20,90	174,10	252,10	46,90	
568968	26,00	0,00	6,40	0,00	1,24	0,01	0,00	4,40	19,60	154,90	214,70	22,10	
	Ga	Rb	Sr	Y	Zr	Nb	Cs	Ba	La	Ce	Th	Ni	
568993	18,10	168,80	70,40	30,50	188,00	11,40	3,40	521,60	23,10	48,10	11,60	43,40	
568992	15,40	172,40	119,70	29,90	211,30	10,90	4,20	566,10	31,70	75,60	19,00	41,80	
568991	21,60	197,20	107,20	23,60	124,30	13,50	4,90	700,90	27,60	63,70	12,60	60,80	
568990	17,60	162,90	127,40	33,90	210,40	12,90	4,60	523,60	35,70	84,80	14,90	47,00	
568989	11,90	83,70	49,50	18,20	84,40	7,40	4,00	485,60	20,80	36,20	3,40	71,00	
568988	15,20	155,40	120,50	27,30	157,80	10,50	3,40	582,20	27,80	70,30	8,90	42,00	

568987	17,00	155,60	164,20	18,40	140,00	8,10	4,00	711,30	28,00	69,00	6,80	42,90	
568986	18,50	104,90	294,70	15,90	180,00	6,90	3,90	555,80	30,30	245,70	0,00	42,60	
568985	18,80	123,50	287,90	18,20	176,10	6,30	3,40	400,60	30,20	126,20	0,00	38,40	
568984	16,50	108,70	252,90	18,30	319,80	7,30	3,70	523,40	39,50	100,60	7,50	35,60	
568983	14,80	111,70	223,30	16,50	246,90	6,80	4,70	590,60	35,90	87,10	2,80	35,20	
568982	18,30	117,30	173,00	15,00	199,70	5,90	4,80	703,70	29,30	104,10	0,00	32,10	
568981	9,30	93,20	163,70	12,70	35,60	3,30	3,40	139,00	11,40	43,10	0,00	50,50	
568980	4,60	34,50	165,40	9,20	30,90	1,40	3,40	93,30	16,70	50,10	0,00	13,10	
568979	20,40	136,50	197,90	14,90	159,60	6,40	4,10	838,80	29,20	77,60	0,00	33,60	
568978	16,80	135,70	289,60	13,60	157,60	5,60	4,30	707,30	28,90	108,20	0,00	35,40	
568977	17,70	162,80	170,80	16,20	179,00	6,20	4,60	1165,60	29,10	88,60	0,00	30,30	
568976	23,60	169,00	121,50	23,80	119,00	12,50	5,70	838,70	29,90	64,30	10,50	66,80	
568975	22,30	165,60	192,40	20,50	124,90	10,80	4,80	855,50	26,20	65,20	14,30	62,10	
568974	16,20	119,20	215,30	18,40	136,90	7,20	4,60	586,30	30,00	83,70	0,00	50,10	
568973	16,90	106,80	140,60	13,90	154,40	5,90	4,20	624,10	27,80	67,10	1,20	39,40	
568972	19,40	80,70	257,90	17,00	115,60	7,20	3,40	608,00	27,10	76,20	2,30	71,60	

568971	19,40	71,10	335,60	19,00	75,10	6,40	3,40	590,90	16,60	55,80	2,60	125,60	
568970	13,10	114,00	173,40	13,20	116,30	5,70	3,40	737,10	18,40	46,60	0,40	69,30	
568969	19,90	126,70	153,20	22,00	115,00	10,80	4,40	1219,20	28,40	62,10	18,20	121,90	
568968	20,60	171,00	110,20	23,30	127,80	11,20	4,80	942,80	25,80	58,00	12,80	58,90	

Appendix 2: Concentrations of elements, from ICP-MS analysis. The following elements are given in percentage: Na, S, Ti, Al, Fe, K, and Mg, the rest is given in PPM.

Depth (m)	Mn	Mo	Na	Ni	P	Pb	S	Sb	Sr	Ti	V	Zn	Au	
1,0	512,0	0,5	0,8	53,0	670,0	13,0	0,1	6,0	110,0	0,4	104,0	80,0	0,0	
2,5	483,0	0,5	0,8	50,0	570,0	14,0	0,1	7,0	111,0	0,4	100,0	83,0	0,0	
3,5	473,0	0,5	1,0	49,0	660,0	23,0	0,1	5,0	194,0	0,4	103,0	120,0	0,0	
4,5	414,0	0,5	0,8	45,0	730,0	21,0	0,1	5,0	153,0	0,4	93,0	107,0	0,0	
5,5	549,0	0,5	0,8	42,0	680,0	20,0	0,1	2,5	162,0	0,4	93,0	110,0	0,0	
6,5	538,0	0,5	0,9	46,0	600,0	20,0	0,1	6,0	168,0	0,4	106,0	119,0	0,0	
7,5	516,0	0,5	1,0	48,0	610,0	18,0	0,0	7,0	161,0	0,4	112,0	108,0	0,0	
8,5	536,0	0,5	1,0	49,0	620,0	21,0	0,0	8,0	166,0	0,4	112,0	114,0	0,0	
9,5	511,0	0,5	1,2	47,0	630,0	21,0	0,0	5,0	170,0	0,4	107,0	109,0	0,0	
10,5	471,0	0,5	1,3	60,0	580,0	20,0	0,2	2,5	144,0	0,5	120,0	113,0	0,0	
11,5	477,0	0,5	1,5	57,0	620,0	23,0	0,1	2,5	154,0	0,4	117,0	120,0	0,0	
12,5	515,0	0,5	1,5	61,0	570,0	22,0	0,1	2,5	162,0	0,5	124,0	122,0	0,0	
13,5	551,0	1,0	1,4	58,0	630,0	20,0	0,1	2,5	156,0	0,4	111,0	108,0	0,0	
14,5	576,0	0,5	1,6	53,0	710,0	21,0	0,1	2,5	181,0	0,5	106,0	116,0	0,0	
15,5	542,0	0,5	1,6	53,0	620,0	17,0	0,0	6,0	165,0	0,5	116,0	114,0	0,0	

16,5	516,0	0,5	1,5	56,0	630,0	10,0	0,0	5,0	149,0	0,4	114,0	99,0	0,0	
17,5	468,0	0,5	1,5	54,0	620,0	7,0	0,0	5,0	127,0	0,4	114,0	96,0	0,0	
18,5	530,0	0,5	1,5	51,0	650,0	6,0	0,0	5,0	137,0	0,4	108,0	86,0	0,0	
19,5	492,0	0,5	1,4	47,0	600,0	6,0	0,0	5,0	120,0	0,4	102,0	81,0	0,0	
20,5	467,0	0,5	1,7	50,0	570,0	9,0	0,0	6,0	143,0	0,4	111,0	94,0	0,0	
21,5	446,0	0,5	1,4	45,0	620,0	8,0	0,1	2,5	147,0	0,4	92,0	80,0	0,0	
22,5	479,0	0,5	1,5	42,0	640,0	7,0	0,1	2,5	149,0	0,4	92,0	83,0	0,0	
23,5	429,0	0,5	1,5	44,0	650,0	7,0	0,0	7,0	148,0	0,4	95,0	82,0	0,0	
24,5	542,0	0,5	1,3	68,0	570,0	8,0	0,1	6,0	140,0	0,5	122,0	101,0	0,0	
25,5	504,0	0,5	1,0	70,0	580,0	10,0	0,1	7,0	136,0	0,5	134,0	118,0	0,0	
26,3	501,0	0,5	0,8	101,0	600,0	20,0	1,5	9,0	91,0	0,4	115,0	128,0	0,0	
26,8	492,0	2,0	0,9	95,0	480,0	10,0	1,3	13,0	103,0	0,4	149,0	140,0	0,0	
Depth (m)	Mn	Mo	Na	Ni	P	Pb	S	Sb	Sr	Ti	V	Zn	Au	
27,3	370,0	4,0	1,0	75,0	520,0	11,0	1,3	13,0	106,0	0,4	147,0	124,0	0,0	
27,8	470,0	1,0	0,9	63,0	540,0	12,0	1,0	11,0	104,0	0,4	141,0	126,0	0,0	
28,3	415,0	6,0	0,8	73,0	530,0	7,0	1,2	11,0	105,0	0,4	150,0	114,0	0,0	
28,7	506,0	9,0	0,8	74,0	740,0	9,0	1,2	14,0	124,0	0,5	154,0	119,0	0,1	
29,2	539,0	0,5	1,4	45,0	1350,0	20,0	0,6	11,0	289,0	0,5	105,0	176,0	0,4	
29,8	605,0	0,5	1,9	41,0	1360,0	21,0	0,8	14,0	293,0	0,5	99,0	100,0	1,1	
30,3	423,0	0,5	2,2	42,0	1410,0	31,0	1,2	33,0	283,0	0,5	106,0	75,0	2,5	
30,8	995,0	0,5	1,7	34,0	1220,0	24,0	0,8	13,0	280,0	0,4	90,0	113,0	1,0	
31,3	973,0	0,5	1,8	37,0	1370,0	14,0	0,4	9,0	269,0	0,5	108,0	81,0	0,1	
31,8	518,0	0,5	2,0	38,0	1240,0	16,0	0,5	11,0	224,0	0,5	110,0	78,0	0,1	
32,3	771,0	0,5	1,9	44,0	1360,0	16,0	1,2	13,0	243,0	0,5	115,0	107,0	0,7	
32,8	486,0	0,5	1,5	44,0	1240,0	12,0	0,9	17,0	257,0	0,4	100,0	91,0	0,9	
33,3	451,0	0,5	1,3	34,0	1210,0	11,0	0,6	7,0	216,0	0,5	98,0	74,0	0,1	
33,8	633,0	0,5	1,3	38,0	1100,0	9,0	0,8	13,0	243,0	0,4	99,0	102,0	0,2	

34,3	853,0	0,5	1,5	34,0	1040,0	18,0	1,1	19,0	274,0	0,4	89,0	83,0	1,5	
34,8	619,0	0,5	1,3	41,0	1140,0	11,0	0,8	15,0	252,0	0,4	94,0	74,0	0,6	
35,3	563,0	0,5	1,0	34,0	1220,0	12,0	0,6	17,0	305,0	0,5	101,0	72,0	0,1	
35,7	475,0	0,5	0,8	35,0	1260,0	11,0	0,8	13,0	208,0	0,5	99,0	78,0	0,1	
36,0	868,0	0,5	0,5	38,0	850,0	12,0	0,9	17,0	107,0	0,3	74,0	112,0	0,8	
36,3	327,0	2,0	0,5	75,0	510,0	7,0	1,9	11,0	61,0	0,4	153,0	89,0	0,4	
36,8	370,0	6,0	0,6	77,0	540,0	8,0	1,5	13,0	80,0	0,4	152,0	109,0	0,0	
37,3	368,0	3,0	0,6	61,0	530,0	8,0	1,3	16,0	85,0	0,4	147,0	128,0	0,0	
37,8	359,0	2,0	0,7	59,0	540,0	9,0	1,0	19,0	83,0	0,5	163,0	124,0	0,0	
38,3	455,0	3,0	0,5	64,0	500,0	8,0	1,0	14,0	106,0	0,4	143,0	142,0	0,0	
38,8	407,0	1,0	0,9	69,0	530,0	15,0	1,0	12,0	146,0	0,4	143,0	136,0	0,0	
39,3	386,0	2,0	1,0	79,0	560,0	17,0	1,3	8,0	111,0	0,5	153,0	131,0	0,0	
39,8	392,0	5,0	1,0	87,0	640,0	16,0	1,4	10,0	155,0	0,4	156,0	139,0	0,0	
Depth (m)	Mn	Mo	Na	Ni	P	Pb	S	Sb	Sr	Ti	V	Zn	Au	
40,3	438,0	7,0	1,3	69,0	680,0	13,0	0,9	9,0	160,0	0,4	154,0	170,0	0,0	
40,8	506,0	0,5	2,2	41,0	1280,0	23,0	0,1	9,0	212,0	0,4	100,0	121,0	0,0	
41,5	580,0	0,5	2,5	42,0	1410,0	15,0	0,1	8,0	195,0	0,5	104,0	94,0	0,0	
43,5	632,0	0,5	2,8	36,0	1250,0	15,0	0,1	2,5	207,0	0,5	97,0	83,0	0,0	
44,5	608,0	0,5	2,7	38,0	1170,0	14,0	0,1	2,5	216,0	0,4	99,0	73,0	0,0	
45,5	586,0	0,5	3,2	47,0	1300,0	12,0	0,2	2,5	273,0	0,5	111,0	88,0	0,0	
46,5	637,0	0,5	3,5	41,0	1300,0	16,0	0,0	2,5	289,0	0,5	98,0	83,0	0,0	
47,5	515,0	0,5	3,6	40,0	1290,0	19,0	0,1	2,5	289,0	0,5	100,0	97,0	0,0	
48,5	625,0	0,5	3,8	57,0	1510,0	22,0	0,2	2,5	360,0	0,5	124,0	116,0	0,0	
49,5	443,0	0,5	3,0	61,0	1230,0	16,0	0,5	5,0	308,0	0,5	128,0	109,0	0,0	
50,5	450,0	0,5	2,7	67,0	1080,0	16,0	0,7	2,5	251,0	0,4	151,0	115,0	0,0	
51,5	459,0	0,5	2,2	56,0	1300,0	16,0	0,3	6,0	245,0	0,5	129,0	105,0	0,0	
52,3	408,0	4,0	2,1	78,0	830,0	10,0	1,5	6,0	132,0	0,4	161,0	118,0	0,0	

52,8	267,0	7,0	1,7	93,0	590,0	12,0	2,1	6,0	114,0	0,4	158,0	101,0	0,0	
53,3	278,0	7,0	2,0	80,0	580,0	17,0	1,7	6,0	145,0	0,4	140,0	98,0	0,0	
53,8	520,0	4,0	1,9	94,0	610,0	15,0	1,7	6,0	154,0	0,4	166,0	127,0	0,0	
54,3	525,0	4,0	2,2	104,0	660,0	12,0	1,0	7,0	202,0	0,4	162,0	122,0	0,0	
54,8	741,0	0,5	2,4	113,0	920,0	11,0	0,1	2,5	332,0	0,5	156,0	144,0	0,0	
55,5	910,0	0,5	2,3	109,0	830,0	13,0	0,2	2,5	269,0	0,4	141,0	140,0	0,0	
56,5	861,0	0,5	2,6	135,0	810,0	10,0	0,4	7,0	338,0	0,5	167,0	141,0	0,0	
57,5	903,0	0,5	3,1	100,0	910,0	15,0	0,2	2,5	337,0	0,5	143,0	134,0	0,1	
58,5	833,0	1,0	2,6	91,0	900,0	13,0	0,3	2,5	304,0	0,4	131,0	99,0	0,1	
59,5	827,0	0,5	2,6	92,0	910,0	11,0	0,3	2,5	308,0	0,4	131,0	102,0	0,0	
60,5	667,0	0,5	2,5	87,0	820,0	11,0	0,2	2,5	259,0	0,4	136,0	101,0	0,0	
61,5	732,0	0,5	2,4	84,0	1030,0	15,0	0,1	2,5	306,0	0,5	144,0	117,0	0,0	
62,3	690,0	1,0	1,2	90,0	690,0	8,0	0,4	2,5	178,0	0,4	142,0	101,0	0,1	
62,8	470,0	6,0	1,4	90,0	860,0	16,0	1,1	2,5	198,0	0,5	158,0	103,0	0,0	
Depth (m)	Mn	Mo	Na	Ni	P	Pb	S	Sb	Sr	Ti	V	Zn	Au	
63,5	627,0	0,5	1,0	52,0	1380,0	13,0	0,2	2,5	188,0	0,5	131,0	110,0	0,0	
64,5	535,0	0,5	1,3	51,0	1470,0	11,0	0,2	2,5	195,0	0,5	122,0	94,0	0,0	
65,5	572,0	0,5	1,3	50,0	1370,0	15,0	0,1	5,0	224,0	0,5	115,0	114,0	0,0	
66,5	504,0	0,5	0,7	38,0	810,0	13,0	0,1	6,0	152,0	0,4	98,0	94,0	0,0	
67,5	378,0	0,5	0,6	46,0	910,0	7,0	0,1	5,0	77,0	0,5	103,0	80,0	0,0	
68,5	473,0	1,0	0,7	38,0	640,0	9,0	0,0	2,5	103,0	0,4	95,0	85,0	0,0	
69,5	459,0	0,5	0,8	38,0	660,0	17,0	0,1	7,0	134,0	0,4	88,0	87,0	0,0	
70,5	422,0	1,0	0,9	42,0	620,0	8,0	0,1	2,5	90,0	0,4	100,0	70,0	0,0	
71,5	395,0	1,0	0,9	41,0	590,0	10,0	0,1	2,5	88,0	0,4	88,0	65,0	0,0	
72,5	406,0	1,0	1,0	44,0	600,0	8,0	0,1	7,0	88,0	0,4	96,0	57,0	0,0	
73,5	454,0	0,5	1,0	47,0	610,0	9,0	0,1	6,0	84,0	0,4	95,0	59,0	0,0	
74,5	615,0	1,0	1,2	45,0	580,0	10,0	0,2	7,0	98,0	0,4	99,0	48,0	0,0	

75,5	686,0	2,0	1,0	87,0	580,0	13,0	0,4	7,0	117,0	0,4	147,0	112,0	0,0	
76,5	879,0	2,0	1,0	112,0	730,0	9,0	0,4	8,0	123,0	0,5	154,0	108,0	0,0	
77,5	830,0	1,0	1,7	112,0	860,0	9,0	0,1	2,5	244,0	0,5	155,0	96,0	0,0	
78,5	696,0	1,0	2,1	116,0	910,0	14,0	0,0	2,5	299,0	0,5	153,0	114,0	0,0	
79,5	795,0	1,0	2,3	115,0	840,0	19,0	0,1	2,5	300,0	0,5	152,0	95,0	0,0	
80,5	668,0	1,0	2,5	101,0	770,0	22,0	0,2	2,5	294,0	0,4	146,0	96,0	0,0	
81,5	713,0	1,0	2,3	109,0	880,0	12,0	0,0	2,5	304,0	0,5	147,0	93,0	0,0	
82,5	792,0	1,0	2,4	109,0	930,0	15,0	0,0	2,5	336,0	0,5	145,0	102,0	0,0	
84,5	721,0	1,0	2,3	109,0	910,0	18,0	0,1	2,5	333,0	0,5	148,0	114,0	0,0	
85,5	738,0	2,0	2,5	102,0	820,0	19,0	0,1	2,5	305,0	0,4	141,0	94,0	0,0	
86,5	646,0	1,0	2,5	105,0	790,0	16,0	0,1	2,5	319,0	0,5	144,0	108,0	0,0	
87,5	819,0	1,0	2,8	122,0	760,0	22,0	0,3	2,5	342,0	0,5	164,0	128,0	0,0	
88,5	904,0	1,0	2,8	128,0	930,0	15,0	0,1	2,5	345,0	0,5	171,0	130,0	0,0	
89,5	799,0	1,0	2,8	95,0	890,0	26,0	0,0	2,5	338,0	0,5	149,0	141,0	0,0	
90,5	701,0	1,0	2,6	93,0	960,0	32,0	0,0	2,5	287,0	0,5	175,0	181,0	0,0	
Depth (m)	Mn	Mo	Na	Ni	P	Pb	S	Sb	Sr	Ti	V	Zn	Au	
91,5	786,0	0,5	2,8	94,0	890,0	16,0	0,0	2,5	296,0	0,5	157,0	125,0	0,0	
92,5	771,0	1,0	2,9	87,0	850,0	13,0	0,0	2,5	304,0	0,5	164,0	114,0	0,0	
93,5	837,0	1,0	2,5	109,0	810,0	18,0	0,1	2,5	236,0	0,5	154,0	174,0	0,0	
94,5	742,0	1,0	2,8	88,0	780,0	19,0	0,1	5,0	317,0	0,5	159,0	169,0	0,0	
95,5	913,0	1,0	2,8	112,0	930,0	10,0	0,0	2,5	309,0	0,5	162,0	121,0	0,0	
96,5	1300,0	1,0	2,9	94,0	850,0	18,0	0,1	2,5	268,0	0,5	147,0	92,0	0,0	
97,5	1030,0	0,5	2,5	124,0	830,0	12,0	0,1	2,5	270,0	0,5	159,0	87,0	0,0	
98,5	879,0	1,0	2,5	115,0	810,0	12,0	0,1	2,5	286,0	0,5	154,0	83,0	0,0	
99,5	818,0	1,0	2,4	113,0	840,0	14,0	0,1	2,5	279,0	0,5	157,0	101,0	0,0	
100,5	720,0	2,0	2,8	105,0	740,0	17,0	0,3	2,5	303,0	0,5	160,0	99,0	0,0	

Depth (m)	Ag	Al	As	Ba	Be	Bi	Ca	Cd	Co	Cr	Cu	Fe	K	Mg
1,0	0,3	8,0	38,0	530,0	2,1	1,0	1,9	0,3	20,0	179,0	39,0	4,4	3,4	1,3
2,5	0,3	7,9	31,0	570,0	1,8	1,0	2,1	0,3	16,0	183,0	40,0	3,9	3,4	1,3
3,5	0,3	8,5	34,0	590,0	2,2	1,0	1,8	0,3	17,0	190,0	41,0	4,2	3,3	1,4
4,5	0,3	8,2	26,0	590,0	2,0	1,0	1,5	0,3	16,0	178,0	45,0	4,0	3,4	1,2
5,5	0,3	8,0	21,0	580,0	1,9	1,0	2,1	0,3	17,0	175,0	41,0	3,8	3,2	1,3
6,5	0,3	8,3	29,0	650,0	2,0	3,0	1,9	0,3	17,0	172,0	71,0	4,4	3,2	1,4
7,5	0,3	8,6	23,0	640,0	2,3	2,0	1,5	0,3	18,0	164,0	35,0	4,4	3,5	1,4
8,5	0,3	8,2	17,0	590,0	2,2	1,0	1,5	0,3	18,0	174,0	34,0	4,4	3,3	1,4
9,5	0,3	8,5	20,0	550,0	2,3	1,0	1,8	0,3	18,0	177,0	36,0	4,4	3,0	1,4
10,5	0,3	8,6	16,0	620,0	2,2	3,0	1,2	0,3	19,0	176,0	73,0	4,9	3,3	1,5
11,5	0,3	8,7	20,0	510,0	2,2	3,0	1,2	0,3	22,0	173,0	73,0	5,3	3,2	1,6
12,5	0,3	8,7	20,0	500,0	2,5	1,0	1,4	0,3	21,0	179,0	54,0	5,2	3,2	1,7
13,5	0,3	8,5	21,0	520,0	2,1	3,0	1,6	0,3	18,0	171,0	79,0	4,8	2,9	1,5
14,5	0,3	8,3	24,0	510,0	2,2	1,0	1,5	0,3	21,0	178,0	62,0	5,0	2,7	1,6
15,5	0,3	8,8	16,0	520,0	2,3	2,0	1,5	0,3	18,0	161,0	30,0	4,9	2,7	1,6
16,5	0,3	8,3	24,0	500,0	2,4	1,0	1,7	0,3	18,0	158,0	53,0	4,6	2,6	1,5
17,5	0,3	8,1	20,0	480,0	2,3	1,0	1,5	0,3	19,0	156,0	39,0	4,5	2,6	1,4
18,5	0,3	8,4	19,0	530,0	2,3	1,0	1,8	0,3	19,0	169,0	44,0	4,4	2,8	1,3
19,5	0,3	7,4	23,0	480,0	2,1	1,0	1,8	0,3	18,0	163,0	40,0	3,9	2,7	1,2
20,5	0,3	8,3	29,0	520,0	2,4	1,0	1,5	0,3	19,0	157,0	25,0	4,4	2,6	1,4
21,5	0,3	7,7	19,0	500,0	2,1	1,0	1,6	0,3	17,0	149,0	36,0	3,7	2,6	1,1
22,5	0,3	7,3	25,0	430,0	2,1	1,0	2,3	0,3	17,0	161,0	44,0	3,8	2,3	1,2
23,5	0,3	7,8	17,0	470,0	2,1	1,0	1,6	0,3	16,0	156,0	40,0	3,9	2,4	1,3
Depth (m)	Ag	Al	As	Ba	Be	Bi	Ca	Cd	Co	Cr	Cu	Fe	K	Mg

24,5	0,3	7,9	44,0	460,0	2,1	1,0	2,0	0,3	20,0	180,0	55,0	4,7	2,6	1,7
25,5	0,3	8,3	41,0	640,0	2,3	1,0	1,5	0,3	19,0	180,0	64,0	4,8	3,3	1,7
26,3	0,3	8,3	65,0	690,0	2,2	1,0	1,4	0,3	33,0	172,0	181,0	6,6	3,3	1,7
26,8	0,3	8,9	84,0	830,0	2,3	1,0	1,3	0,3	28,0	171,0	143,0	6,3	3,7	1,9
27,3	0,3	8,4	43,0	810,0	2,2	1,0	0,8	0,3	25,0	178,0	136,0	5,6	3,4	1,6
27,8	0,3	8,7	70,0	820,0	2,4	1,0	1,2	0,3	22,0	159,0	116,0	5,4	3,7	1,7
28,3	0,3	8,3	80,0	870,0	2,4	1,0	1,1	0,3	26,0	191,0	152,0	5,7	3,6	1,7
28,7	0,3	8,3	256,0	750,0	2,3	1,0	1,8	0,3	30,0	173,0	132,0	5,5	3,6	1,8
29,2	0,3	7,6	1005,0	530,0	1,5	1,0	2,9	0,5	17,0	158,0	52,0	4,1	2,6	1,6
29,8	0,6	7,4	2730,0	450,0	1,4	1,0	3,4	0,3	17,0	151,0	32,0	3,7	2,1	1,5
30,3	0,6	7,6	8270,0	520,0	1,5	1,0	2,6	0,3	18,0	169,0	31,0	3,9	2,1	1,3
30,8	0,6	7,1	2850,0	400,0	1,3	1,0	4,6	0,3	15,0	130,0	22,0	3,8	2,4	2,2
31,3	0,6	7,3	280,0	460,0	1,4	1,0	4,2	0,3	15,0	150,0	23,0	3,9	2,2	1,9
31,8	0,3	7,7	534,0	580,0	1,5	1,0	2,3	0,3	15,0	166,0	23,0	3,8	2,4	1,5
32,3	0,8	8,0	1700,0	780,0	1,7	1,0	3,7	0,3	17,0	179,0	35,0	4,7	2,8	1,8
32,8	0,3	7,8	2470,0	890,0	1,6	1,0	2,2	0,3	19,0	157,0	31,0	3,9	3,0	1,4
33,3	0,3	7,9	383,0	850,0	1,6	1,0	2,1	0,3	14,0	165,0	20,0	3,4	3,1	1,4
33,8	0,3	7,3	529,0	720,0	1,5	1,0	2,4	0,3	17,0	144,0	29,0	4,4	2,9	1,8
34,3	0,6	7,1	3770,0	640,0	1,4	1,0	4,5	0,3	16,0	161,0	28,0	3,9	2,5	1,5
34,8	0,5	7,0	2040,0	750,0	1,5	1,0	2,9	0,3	14,0	159,0	20,0	3,3	2,7	1,5
35,3	0,3	7,8	461,0	660,0	1,5	1,0	2,7	0,3	13,0	166,0	21,0	3,7	2,9	1,6
35,7	0,3	7,7	926,0	1000,0	1,7	1,0	1,9	0,3	17,0	170,0	40,0	3,8	3,5	1,4
36,0	0,6	5,8	2250,0	850,0	1,5	1,0	3,2	0,3	22,0	144,0	53,0	4,1	3,1	1,6
36,3	0,3	8,4	346,0	1070,0	2,2	1,0	0,6	0,3	24,0	169,0	104,0	5,8	4,2	1,5
36,8	0,3	8,7	68,0	1090,0	2,5	1,0	0,5	0,3	26,0	169,0	86,0	6,1	4,3	1,7
37,3	0,3	8,2	126,0	1030,0	2,5	1,0	0,6	0,3	25,0	170,0	87,0	5,9	4,1	1,7
37,8	0,3	8,9	144,0	1110,0	2,6	1,0	0,6	0,3	23,0	170,0	73,0	5,2	4,3	1,7
Depth	Ag	Al	As	Ba	Be	Bi	Ca	Cd	Co	Cr	Cu	Fe	K	Mg

(m)														
38,3	0,7	8,4	66,0	900,0	2,4	1,0	1,2	0,3	23,0	159,0	84,0	5,7	3,9	1,9
38,8	0,3	9,1	77,0	850,0	2,3	3,0	1,4	0,3	25,0	187,0	93,0	5,9	3,7	1,9
39,3	0,3	8,8	117,0	830,0	2,3	1,0	1,0	0,3	28,0	194,0	128,0	6,1	3,7	1,9
39,8	0,3	8,9	65,0	970,0	2,2	2,0	1,6	0,3	28,0	207,0	160,0	6,3	3,5	1,8
40,3	0,3	8,9	44,0	820,0	2,2	2,0	1,8	0,3	21,0	194,0	115,0	5,3	3,5	1,9
40,8	0,3	7,2	74,0	500,0	1,1	2,0	2,6	0,3	16,0	184,0	20,0	3,8	2,1	1,5
41,5	0,3	7,6	40,0	550,0	1,0	1,0	3,2	0,3	18,0	173,0	22,0	3,9	2,2	1,6
43,5	0,3	7,4	20,0	500,0	1,1	1,0	4,0	0,3	15,0	160,0	18,0	3,7	1,6	1,5
44,5	0,3	7,1	17,0	510,0	1,2	1,0	3,4	0,3	15,0	151,0	39,0	3,8	1,5	1,4
45,5	0,3	7,9	25,0	600,0	1,4	1,0	3,3	0,3	19,0	171,0	36,0	4,2	1,6	1,7
46,5	0,3	7,7	25,0	460,0	1,1	1,0	3,1	0,3	17,0	162,0	16,0	3,9	1,1	1,8
47,5	0,3	7,8	33,0	440,0	1,1	1,0	2,4	0,3	17,0	169,0	22,0	3,9	1,2	2,0
48,5	0,3	8,9	69,0	510,0	1,3	1,0	3,0	0,3	21,0	199,0	50,0	4,7	1,5	2,4
49,5	0,3	8,0	64,0	610,0	1,6	2,0	2,2	0,3	23,0	202,0	102,0	4,8	1,9	2,1
50,5	0,3	8,0	72,0	890,0	2,1	1,0	1,9	0,3	24,0	216,0	114,0	5,4	2,5	2,3
51,5	0,3	7,7	79,0	870,0	1,4	1,0	2,1	0,3	19,0	199,0	36,0	4,2	2,5	1,9
52,3	0,3	8,5	90,0	1110,0	1,8	1,0	1,5	0,3	29,0	200,0	176,0	6,2	3,1	2,2
52,8	0,3	8,6	92,0	1220,0	2,0	1,0	0,8	0,3	38,0	195,0	206,0	6,9	3,4	2,0
53,3	0,3	8,7	22,0	980,0	2,0	2,0	1,2	0,3	30,0	188,0	179,0	6,0	3,0	2,0
53,8	0,3	8,1	48,0	790,0	1,8	3,0	2,5	0,3	35,0	238,0	179,0	6,8	2,7	2,6
54,3	0,3	8,0	114,0	760,0	1,6	1,0	2,7	0,3	31,0	258,0	151,0	5,8	2,7	2,6
54,8	0,3	7,7	63,0	500,0	1,0	1,0	3,9	0,3	24,0	317,0	59,0	5,5	1,9	3,0
55,5	0,3	7,1	30,0	380,0	0,8	1,0	4,9	0,3	25,0	266,0	128,0	5,7	1,2	3,3
56,5	0,3	7,7	37,0	580,0	1,2	1,0	4,7	0,3	32,0	263,0	218,0	6,3	1,7	3,6
57,5	0,3	7,8	51,0	360,0	1,0	4,0	3,8	0,3	25,0	292,0	74,0	5,6	1,1	3,1
58,5	0,3	7,3	34,0	380,0	0,9	1,0	4,0	0,3	22,0	270,0	82,0	5,0	1,4	2,7
59,5	0,3	7,2	35,0	360,0	0,9	1,0	4,0	0,3	25,0	283,0	81,0	5,0	1,4	2,7

Depth (m)	Ag	Al	As	Ba	Be	Bi	Ca	Cd	Co	Cr	Cu	Fe	K	Mg
60,5	0,3	7,5	76,0	460,0	1,2	2,0	3,1	0,3	24,0	251,0	71,0	5,0	1,7	2,6
61,5	0,3	7,9	104,0	410,0	1,2	2,0	3,6	0,3	24,0	302,0	40,0	5,2	1,8	2,8
62,3	0,3	6,9	150,0	690,0	1,2	1,0	3,8	0,3	27,0	237,0	83,0	5,2	2,7	2,4
62,8	0,3	8,7	44,0	1000,0	1,7	1,0	2,0	0,3	30,0	208,0	282,0	6,4	4,0	2,0
63,5	0,3	8,1	90,0	820,0	1,4	1,0	3,1	0,3	18,0	191,0	42,0	5,2	3,7	2,3
64,5	0,3	7,8	62,0	680,0	1,4	2,0	3,6	0,3	19,0	189,0	56,0	4,5	3,1	1,6
65,5	0,3	7,7	86,0	870,0	1,4	1,0	2,7	0,3	20,0	189,0	28,0	4,5	3,4	1,8
66,5	0,3	8,4	214,0	920,0	1,8	2,0	1,7	0,3	13,0	181,0	15,0	3,6	4,2	1,4
67,5	0,3	9,0	73,0	880,0	2,1	1,0	1,0	0,3	16,0	200,0	50,0	3,9	4,6	1,2
68,5	0,3	7,5	37,0	760,0	2,2	1,0	1,6	0,3	14,0	157,0	15,0	3,8	3,9	1,4
69,5	0,3	7,7	48,0	630,0	2,0	1,0	1,8	0,3	15,0	168,0	32,0	3,7	3,5	1,4
70,5	0,3	7,3	27,0	560,0	2,1	1,0	1,7	0,3	15,0	164,0	40,0	3,7	3,5	1,2
71,5	0,3	6,9	25,0	480,0	2,0	1,0	1,6	0,3	14,0	155,0	43,0	3,8	3,2	1,2
72,5	0,3	7,3	25,0	520,0	1,9	1,0	1,6	0,3	18,0	163,0	30,0	3,7	3,4	1,3
73,5	0,3	7,1	19,0	470,0	1,8	1,0	2,0	0,3	17,0	160,0	31,0	3,9	3,2	1,3
74,5	0,3	7,1	134,0	460,0	1,8	1,0	2,9	0,3	16,0	177,0	56,0	3,6	2,9	1,1
75,5	0,3	7,5	58,0	570,0	1,8	1,0	3,4	0,3	23,0	224,0	74,0	4,8	3,0	1,5
76,5	0,3	7,6	61,0	570,0	1,4	1,0	5,2	0,3	29,0	234,0	79,0	5,6	3,0	2,1
77,5	0,3	7,4	58,0	480,0	1,2	1,0	4,9	0,3	28,0	251,0	82,0	5,7	1,8	3,0
78,5	0,3	7,4	51,0	400,0	1,0	1,0	3,6	0,3	28,0	272,0	67,0	5,7	1,5	3,4
79,5	0,3	7,8	35,0	510,0	1,2	1,0	3,9	0,3	29,0	235,0	97,0	5,6	1,5	3,1
80,5	0,3	7,6	16,0	580,0	1,5	1,0	3,1	0,3	26,0	245,0	130,0	5,3	1,4	2,8
81,5	0,3	7,3	33,0	430,0	1,0	1,0	3,3	0,3	28,0	259,0	62,0	5,6	1,3	3,2
82,5	0,3	7,6	22,0	400,0	1,0	3,0	4,1	0,3	26,0	261,0	69,0	5,4	1,2	3,0
84,5	0,3	7,4	19,0	630,0	1,1	1,0	3,4	0,3	28,0	266,0	88,0	5,4	1,2	2,9
85,5	0,3	7,5	15,0	660,0	1,1	1,0	3,5	0,3	25,0	243,0	81,0	5,2	1,0	2,9

86,5	0,3	7,2	15,0	650,0	1,1	2,0	3,4	0,3	26,0	281,0	75,0	5,1	0,9	2,7
Depth (m)	Ag	Al	As	Ba	Be	Bi	Ca	Cd	Co	Cr	Cu	Fe	K	Mg
87,5	0,3	7,8	15,0	770,0	1,2	1,0	3,8	0,3	29,0	261,0	116,0	5,7	1,0	2,9
88,5	0,3	7,9	20,0	680,0	1,0	2,0	4,0	0,3	31,0	278,0	111,0	6,2	1,1	3,4
89,5	0,3	7,3	13,0	500,0	1,0	2,0	4,4	0,3	25,0	272,0	53,0	5,2	1,2	3,0
90,5	0,3	7,2	8,0	690,0	0,9	2,0	2,7	0,3	25,0	326,0	30,0	5,9	1,8	3,4
91,5	0,3	7,3	8,0	510,0	0,9	1,0	3,8	0,3	24,0	292,0	43,0	5,4	1,4	3,1
92,5	0,3	7,2	11,0	510,0	1,1	1,0	3,6	0,3	24,0	299,0	48,0	5,1	1,3	2,9
93,5	0,3	7,1	9,0	550,0	0,8	2,0	3,9	0,3	28,0	269,0	57,0	5,8	1,5	3,4
94,5	0,3	7,1	5,0	630,0	1,0	1,0	3,4	0,3	23,0	293,0	68,0	5,2	1,4	2,9
95,5	0,3	7,6	12,0	620,0	1,1	1,0	3,9	0,3	27,0	292,0	69,0	5,7	1,5	3,3
96,5	0,3	7,1	25,0	290,0	0,9	1,0	4,6	0,3	26,0	263,0	54,0	5,2	0,7	3,1
97,5	0,3	7,5	20,0	460,0	1,0	1,0	3,9	0,3	27,0	269,0	83,0	5,8	1,5	3,3
98,5	0,3	7,6	21,0	520,0	1,1	1,0	3,8	0,3	27,0	278,0	70,0	5,4	1,6	3,0
99,5	0,3	7,4	16,0	530,0	1,0	2,0	4,4	0,3	27,0	288,0	70,0	5,5	1,4	3,0
100,5	0,3	7,8	6,0	650,0	1,3	1,0	3,6	0,3	27,0	249,0	139,0	5,7	1,4	2,8


UNIVERSITY
OF TROMSØ